REDUCTION OF IRON OXIDES IN A COUNTER-FLOW REACTOR

LABORATORY REDUCTION TESTS ON PREREDUCED PELLETS UNDER BLAST FURNACE CONDITIONS WITH A COUNTER-FLOW REACTOR

By

MICHEL ROBERT HONE, B.A., B.Sc.A.

A Thesis

Submitted to the Faculty of Graduate Studies

in Partial Fulfilment of the Requirements

for the Degree

Master of Science

McMaster University

October 1966

MASTER OF SCIENCE (1966) McMaster University
(Metallurgy) Hamilton, Ontario

TITLE: Laboratory Reduction Tests on Prereduced Pellets under Blast Furnace Conditions with a Counter-flow Reactor

AUTHOR: Michel Robert Hone, B.A. (Université de Montréal)
B.Sc.A. (Université de Montréal)

SUPERVISOR: Professor R. G. Ward

NUMBER OF PAGES: xiv, 50

SCOPE AND CONTENTS:

An experimental investigation has been conducted into the reduction of iron oxides under blast furnace conditions. The necessary equipment has been designed, constructed and tested, and a program of study on two types of prereduced ore materials has been completed.

ACKNOWLEDGEMENTS

The author expresses his gratitude to his research director, Dr. R. G. Ward, and to other members of the Department of Metallurgy and Metallurgical Engineering, and of the Department of Chemical Engineering, for valuable discussions of the problems encountered during the course of the present investigation. He is also indebted to the members of the Department of Research and Development of the Steel Company of Canada Limited for their assistance.

The author is pleased to acknowledge the tenure of a McMaster Graduate Research Scholarship and a Steel Company of Canada Limited Graduate Research Fellowship in Metallurgy, as well as the financial support of the investigation in the form of research grants from the Steel Company of Canada Limited.

TABLE OF CONTENTS

LIST OF SYMBOLS

C_s	total carbon in solid phase	wt %
CO	carbon monoxide	vol %
CO_2	carbon dioxide	vol %
C/Fe	carbon to iron ratio	at C/at Fe
C_s/Fe	solid carbon to iron ratio	at C/at Fe
D_A	distance between the point at which the temperature is 300°C at the solids inlet of the reactor and the bottom of the reaction tube.	cm
d_b	distance between a point above 300°C on the recorder trace and the 300°C point corresponding to the solids inlet of the recorder.	cm
D_B	distance between a point of known O/Fe ratio and the bottom of the reaction tube.	cm
d_c	distance between points at 300°C on the recorder trace	cm
D_C	distance between the thermocouple junction and the bottom of the reaction tube	cm
e_r	reduction efficiency	
Fe	total iron in sample of material	wt %
Fe^o	metallic iron in sample of material	wt %

Fe^{2+}	ferrous iron in sample of material	wt %
Fe^{3+}	ferric iron in sample of material	wt %
$FeO_{1.50}$	hematite	
$FeO_{1.33}$	magnetite	
$FeO_{1.05}$	wustite	
n_c	carbon deposition rate	at C/min
n_{Fe}	flow rate of iron	at Fe/min
n_g	flow rate of carbon	at C/min
n_o	number of oxygen atoms transferred per unit time	at O/min
O/C	oxygen to carbon ratio	at O/at C
O/Fe	oxygen to iron ratio	at O/at Fe
P_g	absolute metering pressure of gas	atm
r	subscript used to designate the reactor	
r_a	flow rate of air at 21.11°C and 1 atm, or flowmeter reading	liter/min
r_{Fe}	flow rate of iron through the reactor	at Fe/min
r_g	flow rate of gas at 21.11°C and 1 atm	liter/min
s_g	specific gravity of gas mixture at standard temperature and pressure referred to air at standard temperature and pressure of 21.11°C and 1 atm	
t_1, t_2, t_3	iron oxide reaction zones	hr

T_g	absolute metering temperature of gas	^oK
T_r	temperature of isothermal zone in reactor	^oC
t_s	residence time of solids in reactor	hr
t_s^*	critical residence time of solids in reactor	hr
U_s	velocity of the solids	cm/min
U_c	chart speed	cm/min
U_f	furnace speed	cm/min
U_g	gas velocity through the bed	cm/min
U_s	solids velocity in the reactor	cm/min
v	subscript used to designate the reaction vessel	
V_i	velocity of interface i	cm/min
X_A	O/C ratio of the gas at the gas outlet to the reactor	at O/at C
X_B	O/C ratio of the gas at the gas inlet to the reactor	at O/at C
X_H	O/C ratio of the gas in equilibrium with hematite and magnetite	at O/at C
X_M	O/C ratio of the gas in equilibrium with wustite and magnetite	at O/at C
X_W	O/C ratio of the gas in equilibrium with wustite and iron	at O/at C

Y_A	O/Fe ratio of solids at the solids inlet to the reactor	at O/at Fe
Y_B	O/Fe ratio of solids at the solids outlet to the reactor	at O/at Fe
Y_H	O/Fe ratio of hematite	at O/at Fe
Y_M	O/Fe ratio of magnetite	at O/at Fe
Y_W	O/Fe ratio of wustite	at O/at Fe
α	ratio of metallic to total iron in the solids	
ρ_{Fe}	linear density of iron in the reactor	at Fe/cm
ρ_s	linear bulk density of the solids	g/cm

LIST OF TABLES

9. Carbon Deposited at Solids Outlet of Reactor, Determined from C_g/Fe Profiles of Figure 20

LIST OF FIGURES

CHAPTER 1

Introduction

The production of pig iron in the blast furnace is an extremely complex process. Researchers confronted with the task of understanding the process in order to increase its efficiency and output have dissected it into sub-processes and initiated mathematical and experimental studies of chemical, thermal, aerodynamical, physical and mechanical phenomena occurring within the boundaries of each sub-process.

Although mathematically feasible, at least in principle, the rigorous simultaneous reproduction of the above-mentioned phenomena is impossible on a laboratory scale. Cognizant of this fact, experimentalists have strived for an accurate simulation of various individual phenomena. In recent years, a technique which simulates the reduction chemistry of iron oxides in the upper part of the blast furnace stack has been developed by IRSID (Institut de la Recherche de la Sidérurgie). Experimentally sound and backed by an elegant theoretical structure, this technique was employed in the present investigation to study the reduction of iron oxides under simulated blast furnace conditions.

CHAPTER 2

Literature Survey

The reduction of iron oxides has been the subject of a prodigous amount of research as attested by the literature reviews of Specht and Zapffe (1), Themelis and Gauvin (2), and Dutilloy, Ghosh and Rist (3).

The bulk of attention has been focused on the reduction of single particles of iron oxide, in which case the experimental procedure is straightforward. Reducing gas of a fixed composition is admitted to an isothermal reactor containing a particle suspended from a gravimetric device. By the method of trial and error, a critical flow rate of reducing gas is established, at which the rate of reduction is negligibly affected by a further increase in the flow rate of gas. Effectively, at flow rates equal or superior to the critical flow rate, the gas at the surface of the particle has, throughout the course of reduction, the composition of the gas admitted to the reactor. The rate of reduction, which is determined from the loss in weight of the particle with time, is then a function of the rates of two processes: chemical reactions at gas-solid interfaces, and mass transfer by solid or gas phase diffusion within the particle.

A good exposition of single particle reduction, which is of background interest only in this investigation, has been given by Dutilloy, Ghosh and Rist (3).

The reduction of iron oxides in a fixed isothermal bed has also been studied but, perhaps because of the increased complexity of the system, has been accorded less attention. Wetherill and Furnas (4), Udy and Lorig (5), Schurmann, Beer and Willems (6) and Beeton (7) have deliberately utilized gas flow rates greater than the critical flow rate, with the result that the gas composition at the surface of each particle of the bed was equal to that entering the reactor and reduction proceeded simultaneously throughout the whole bed. In these tests, the reduction rate is determined effectively by the reduction kinetics of the single particle.

Other investigators, Ilschener (8) and El-Mehairy and Philbrook (9), have allowed a gas composition profile to exist along the length of the bed by admitting to the reactor reducing gas at flow rates below the critical value. Then, in addition to the chemical reaction and diffusion kinetics inside individual particles, external factors such as the structure of the bed and the flow rate of gas come into play and affect the rate of reduction. Privalov, Timofeev and Bokovikov (10) and Rist and Bonnivard (11, 12, 13), have made theoretical studies of this case.

Attempts to classify ore materials for the blast furnace in terms of reducibility, that is, the ease of oxygen removal, have been reviewed by Thibaut (14) and Ispas (15). Some investigators, among whom may be mentioned Korotich and Gruzinov (16) and Shkodin (17), have utilized variations of the isothermal single particle and packed bed reduction tests briefly examined above. However, there is a considerable dissimilarity between the reduction conditions of the experiments and those observed in

the blast furnace.

Von Bogdandy et al. (18) have developed a temperature programmed reduction test, and Linder (19), a combined temperature and gas composition programmed test. In both tests, a vessel containing ore material is enclosed in a furnace controlled to follow a time-temperature program. In the Linder test, the composition of the reducing gas admitted to the vessel is changed in steps. Schenk et al. (20) have refined the approach of Von Bogdandy et al. and Linder: the temperature, gas composition, quantity and pressure, and the burden pressure are programmed in a continuous fashion. Sophisticated instrumentation is required to carry out these programs.

In the apparatus of Ramm and Svintsov (21), which is also described by Privalov, Timofeev and Bokovikov (10), the ore material actually descends through a column in counter-flow to a preheated reducing gas. In order to effect a continuous descent of materials in the column, the reduced products are removed by means of a rotating table. Experiments can be performed under isothermal conditions and also with the temperature varying up the length of the bed. It is thus possible for reduction conditions in the shaft of the blast furnace to be closely reproduced. The disadvantage of this approach lies in the complexity of the solids conveying equipment.

In the technique of Klemantaski (22), ore material is fed to a container through which gas is passed at the same rate, temperature, pressure and composition as at the stock-line of the furnace. By continuously adjusting the gas admitted to the container inlet, conditions

at the gas outlet are kept constant and equal to those at the blast furnace stock-line, until the bed builds up to a suitable height. The ore material feed is arrested and the gas inlet conditions are continuously adjusted so that the outlet conditions lag behind the inlet conditions by the time a charge of equivalent thickness would take to descend through its own height in the blast furnace. The test has been used with some degree of success by Klemantaski and Wild (23) but has not been widely accepted because of the complications arising out of the continuous adjustment and monitoring of the inlet and outlet gas characteristics.

In the reduction tests developed by Kurchatov (24) and Bonnivard and Rist (25), a traveling furnace imposes on part of a long fixed bed of ore material a temperature profile similar to that of the upper part of the blast furnace stack. Reducing gas of blast furnace composition is admitted to the bed in counter-flow to the apparent flow of solids. The difference between the two tests lies in the method of introducing gas to the reaction zone. In the test of Kurchatov, a gas tuyere is dragged immediately behind the reduction zone, through the bed of material. The technique of Bonnivard and Rist circumvents this experimental complication by admitting the gas at the end of the reaction tube and allowing it to heat up in contact with the material leaving the hot zone of the bed.

The approach of Bonnivard and Rist will be further explained in the following chapter.

CHAPTER 3

Theoretical Considerations

3.1 Simulation of Iron Oxide Reduction Chemistry in the Indirect Reduction Zone of the Blast Furnace

3.1.1 Principles of the Simulation

The shaft of the blast furnace may be considered as a steady-state gas-solid counter-flow reactor in which oxygen and heat are transferred as the descending charge encounters the ascending reducing gas, Figure 1-A.

On a laboratory scale, part of the process may be simulated by introducing reducing gas at the bottom of a long vertical tube containing ore material and allowing a concentric furnace to travel up the tube, thus creating a mobile hot zone. As reactions occur solely within the hot zone, the limits of the reactor coincide with those of the zone. The ore material descending through the reactor heats up and reacts with the hot reducing gas ascending in counter-flow.

Although the flow rate of material is proportional to the velocity of the furnace, the flow rate of gas is independent of it as its absolute velocity is approximately three orders of magnitude greater than that of the furnace.

Each slice of material is cycled through a temperature profile comprising:

(a) a heating gradient in the upper half of the reactor, AB, Figure 1-C.

(b) a plateau, in the second half, BC.

(c) an abrupt quenching gradient, CD.

The useful portion of the reactor temperature profile, AC, is similar if considered with respect to time, to the temperature profile of the indirect reduction zone of the blast furnace, $\alpha\gamma$, Figure 1-B. Curve $\alpha\delta$, drawn from measurements effected in the shaft of the furnace (26, 27), represents the mean temperature of gas and solids. Portion CD of the profile does not have a counterpart in the blast furnace.

Each slice of material is also cycled through a gas composition profile. Once the composition and the flow rates of the gas and solids admitted to the reactor have been fixed, the shape of the profile is dictated by the stoichiometric, thermodynamic and kinetic factors of the reactions.

When tests are conducted with hydrogen as a component of the reducing gas, the water vapor produced by oxygen transfer condenses in the cooler regions of the reaction vessel above the reaction zone. Under the force of gravity, the water trickles down into the reactor, where it may influence the chemical reactions under consideration. For this reason, the gas and material flows in the actual laboratory model are reversed with respect to those of the blast furnace. As the furnace travels down, the ore material "ascends" while the gas descends in counter-flow.

Following the anlaysis of Bonnivard and Rist (25), a certain number of parameters can control the steady-state reduction chemistry of a packed bed in a reactor. These are:

1. the chemical and physical nature of the ore material.
2. the inlet reducing gas composition.
3. the total pressure of the gas.
4. the ratio of the mass flow rates of reducing gas and solids flow rates; that is, the specific consumption of carbon.
5. the residence time of the solids in the reactor.
6. the thermal profile with respect to time of the reactor.
7. the gas velocity through the bed.

An adequate simulation of the indirect reduction process in the blast furnace by a laboratory reactor requires that the values of the parameters enumerated above be similar in both cases. Although it is a simple matter to reproduce the first six parameters, it is physically impossible to reproduce simultaneously the seventh parameter. In effect, the gas velocity varies with the length of the laboratory reactor, for a given set of values for parameters 1 to 6. However, Bonnivard and Rist (25) and El-Mehairy and Philbrook (28) have shown that transport phenomena in the gas phase between the particles of the bed do not affect the reduction rate of the bed, even at gas velocities that are very low in comparison to those encountered in the stack of the blast furnace. Hence the gas velocity is not a fundamental factor in the simulation of the blast furnace reduction conditions, provided the laboratory reactor is of reasonable length; for example, of the order of two feet.

3.1.2 Counter-flow Reduction of a Column of Iron Oxides

Four cases of counter-flow reduction of iron oxides are enumerated below, in order of increasing complexity:

(i) isothermal reduction with infinite reaction rates

(ii) isothermal reduction with finite reaction rates

(iii) non-isothermal reduction with infinite reaction rates

(iv) non-isothermal reduction with finite reaction rates

Excellent studies of the first three cases have been made by Bonnivard and Rist (11, 12, 13), but a study of the last case has yet to appear in the literature.

For the present investigation, the theoretical paraphernalia of the first two cases are required and are therefore summarized in the following sub-sections.

3.1.2.1 Infinite Reaction Rates

If reducing gas is admitted to an isothermal counter-flow reactor initially containing hematite, reaction interfaces are formed. Assuming that the solids descend through the reactor in an ascending stream of gas, certain reaction interfaces will progress upward in the reactor, while others will be entrained downward by the flow of solids. This transition-state reduction gives way to a steady-state reduction when the interfaces have reached their stable positions at the top and bottom of the reactor.

On the hypothesis of instantaneous reaction rates, it is possible to predict the steady-state location of each reaction interface. An oxygen balance for a reaction i occurring at an interface i gives:

$$(n_o)_i = n_g\,(\Delta X)_i = n_{Fe}\,(\Delta Y)_i \qquad 3.1$$

where: $(n_o)_i$ = number of oxygen atoms transferred from the solids to the gas per unit time

$X = \dfrac{CO_2}{CO + CO_2}$, the mole fraction of CO_2

$Y = \dfrac{O}{Fe}$, the number of oxygen atoms per iron atom in the solids

$(\Delta X)_i$, $(\Delta Y)_i$ = variation of X and Y at the reaction interface i

n_g, n_{Fe} = number of moles of gas and atoms of iron involved in reaction i per unit time

Assuming the iron density, ρ_{Fe}, is not changed by the reaction, n_{Fe} is proportional to the instantaneous rate of progression of the reaction interface. It is thus possible to define, from Equation 3.1, a specific gasified carbon consumption rate for each reaction i:

$$\left(\frac{n_g}{n_{Fe}}\right)_i = \left(\frac{\Delta Y}{\Delta X}\right)_i$$

which is inversely proportional to the progression rate of interface i, V_i.

In a similar manner, it is possible to define an overall specific gasified carbon rate, for the reactor;

$$\left(\frac{n_g}{n_{Fe}}\right)_r = \left(\frac{\Delta Y}{\Delta X}\right)_r$$

to which the velocity of the solids in the reactor, U_s, is inversely proportional.

In relation to a fixed point on the wall of the reactor, it

follows that:

(i) if $(n_g/n_{Fe})_r > (n_g/n_{Fe})_i$, interface i has a net upward velocity, which is the resultant of velocities V_i and U_s.

(ii) if $(n_g/n_{Fe})_r = (n_g/n_{Fe})_i$, interface i has a null velocity.

(iii) if $(n_g/n_{Fe})_r < (n_g/n_{Fe})_i$, interface i has a net downward velocity.

The specific gasified carbon consumptions for various reactions occurring at 900°C are calculated in Table 2 for the equilibrium mole fractions of the oxidized gas, X_W, X_M and X_H given in Table 1 (29). In Table 2, X_B is the oxidized mole fraction of the inlet gas which, for simplicity in this study, is set equal to zero. Therefore, if

$$0.657 < (n_g/n_{Fe})_r < 3.33 \qquad 3.2$$

interface 1 descends while interface 2 ascends in the reactor. Interface 3 progresses at a slower rate than interface 2 , but as reaction 2 occurs before reaction 3 , interface 2 carries interface 3 upwards. In other words, reaction 4 is operative.

Once the reduction system has attained a steady-state, reaction 4 occurs at the solids inlet to the reactor, reaction 1 at the solids outlet, and a zone of wustite, $FeO_{1.05}$, exists throughout the reactor, as shown in Figure 2-A.

The reduction configuration of Figure 2-A is of considerable importance as it applies, within the restriction of infinite reaction rates, to the stack of the blast furnace. In effect, the specific gasified carbon consumption of an actual furnace is always between the

limits given by relation 3.2.

3.1.2.2 Finite Reaction Rates

If the restriction of infinite reaction rates is lifted, a new parameter, the residence time of the solids in the column of oxides, t_s, must be taken into consideration, in addition to the stoichiometric and equilibrium relationships. In effect, because the step-wise reactions $FeO_{1.50} \rightarrow FeO_{1.05}$ and $FeO_{1.05} \rightarrow Fe$ proceed at finite rates, it is possible for them to overlap. A critical residence time, t_s^*, may be defined at this point, as the shortest residence time sufficient to avoid any overlapping between the reduction steps. The critical residence time may be considered as a measure of the reducibility of the iron oxides, for the particular conditions of reduction.

Four cases of residence times are of interest:

(a) $t_s \rightarrow \infty$: (Figure 2-A) the case of an infinite residence time is equivalent to the hypothetical case of infinite reaction rates. The wustite zone occupies the whole column, and the $FeO_{1.50} \rightarrow FeO_{1.05}$ and $FeO_{1.05} \rightarrow FeO$ reactions occur at the solids inlet and outlet planes of the reactor.

(b) $\infty > t_s > t_s^*$: (Figure 2-B) when the residence time of the solids is greater than the critical residence time, but finite, the two reduction steps occur over a finite distance in the column but a wustite zone still exists in the middle. The reducing potential of the gas is completely exhausted with respect to wustite.

(c) $t_s = t_s^*$: (Figure 2-C) as the residence time of the solids becomes equal to the critical residence time, the wustite zone vanishes.

The reduction potential of the gas is exhausted as in the previous case.

(d) $t_s < t_s^*$: (Figure 2-D) when the residence time of the solids is less than the critical residence time, the reaction zones overlap. Higher oxides like hematite and magnetite coexist with wustite and iron in the middle of the column and the gas utilization is incomplete.

3.1.3 Graphical Representation of Reduction Effects

3.1.3.1 Oxygen Transfer Diagram

The oxygen transfer diagram, Figure 3, is a convenient representation of the chemical performance of the reactor. The co-ordinates are the O/Fe and O/C ratios of the iron oxide and reducing gas, respectively, at various levels in the reactor. The O/Fe ratio, on the Y axis, is the number of oxygen atoms in the iron oxides, per atom of iron and it varies from 0 for pure iron to 1.5 for hematite. The O/C ratio, or equivalently the $CO_2/(CO+CO_2)$ ratio, on the X axis represents the number of oxygen atoms removed from the oxides by one mole of reducing gas and varies from 0 to 1.

The course of the reduction process is followed by an operating line, AB. The solids enter and the gases leave the reactor at point A; the solids leave and the gases enter at point B. The slope of the line is the C/Fe ratio; that is, the number of carbon atoms utilized in the production of one iron atom.

The diagram is divided into two regions, clear and dark. The operating line, for a reduction process, translates in the clear region. The common boundary of the regions represents the equilibria between the reducing gas and the iron oxides. It is drawn from the Iron-Oxygen phase diagram (29) to the left, and the Carbon Monoxide-Carbon Dioxide-Iron Oxide equilibrium diagram (29) to the top.

When the residence time of the solids in the reactor, t_s, is greater than or equal to the critical residence time t_s^*, the reducing gas comes to equilibrium with the wustite in the middle zone of the reactor and the operating line, Figure 4-A, goes through the wustite corner which represents the reducing gas-wustite-iron equilibrium. In this case, the reactor operates at unit chemical efficiency. When the residence time of the solids is less than the critical residence time, the operating line is located to the left of point W.

A quantitative measure of the reduction efficiency, e_r, is given by the ratio:

$$e_r = \frac{Y_A - Y_B'}{Y_A - Y_B}$$

that is, the ratio of oxygen atoms actually removed during reduction, to the oxygen atoms theoretically removable, per atom of iron.

3.1.3.2 Reduction Path Diagram

The reduction path diagram, Figure 4-B, is constructed by plotting in triangular coordinates the Fe^o/Fe, Fe^{2+}/Fe and Fe^{3+}/Fe ratios of the iron oxides at successive levels in the column. On this diagram, the atomic fractions of metallic, ferrous and ferric iron are designated by Fe^o, Fe^{2+} and Fe^{3+}.

When the residence time of the solids, t_s, is greater than or equal to the critical residence time, t_s^*, the three states of iron evolve on the diagram as follows: 100% Fe^{3+} → 10% Fe^{3+} - 90% Fe^{2+} → 100% Fe^o.

When the residence time of the solids is less than the critical residence time, the reduction proceeds along a path located in the right-

hand section of the diagram, such as the one indicated by the broken line.

In principle, the reduction path should not traverse the 0.1 Fe^{3+} - Fe^{o} line into the left-hand region of the diagram. In effect, a point in this region represents a mixture of iron and unstable wustite of some composition between that of FeO and $FeO_{1.05}$ according to the data of Darken and Gurry (29).

3.1.3.3 Residence Time Diagram

In order to calculate the residence time of the solids in the reactor, the boundaries of the latter must be known. The solids inlet of the reactor is defined as the point at which the temperature of the solids first reaches 300°C, and the solids outlet as the point at which the temperature of the solids begins to decrease at the end of the isothermal zone.

The residence time diagram is a plot of various parameters versus the residence time of the solids in the reactor; in particular, the O/Fe and C_s/Fe ratios and the reactor temperature. As will be seen in section 5.6, the C_s/Fe ratio is defined as the ratio of carbon atoms to iron atoms of the solid phases in the reactor. Typical profiles, on which the instantaneous rates of the iron oxide and carbon reactions, and of solids heating, $d(O/Fe)/dt_s$, $d(C_s/Fe)/dt_s$ and dT/dt_s, appear as slopes, are shown in Figure 4-C.

If the residence time of the solids is greater than the critical residence time, two iron oxide reaction zones, t_1 and t_3, separated by a zone of chemical inactivity, t_2, at the Y_w level,

Figure 5-A, are distinguishable on the O/Fe profile. The critical residence time is calculated from this profile by:

$$t_s^* = t_s - (t_1 + t_3)$$

If the residence time is equal to the critical residence time, zone t_2 does not exist and the O/Fe profile, Figure 5-B, although similar to the previous, exhibits an inflection point in lieu of a plateau at the Y_W level. This mode of operation, unlike the previous, combines maximum throughput of solids with maximum chemical reduction efficiency.

If the residence time is less than the critical residence time, zones t_1 and t_2 overlap. The O/Fe profile differs markedly from the previous two profiles: it does not exhibit an inflection point at the Y_W level and the outlet O/Fe ratio is greater.

3.2 Reduction of Prereduced Pellets

A theoretical study by Meysson, Maaref and Rist (30) has outlined the advantages of the utilization of prereduced ore material in the blast furnace, advantages which vary considerably with the mode of prereduction.

The operation of the blast furnace may be graphically represented on the overall oxygen transfer diagram of Figure 6-A, as proposed by Rist and Bonnivard (25). The left half of the diagram is an extension of the oxygen transfer diagram of the indirect reduction zone of the furnace in which the reducing gas is utilized, Figure 4-A, to the direct reduction zone in which the gas is produced. Salient features of this diagram are point W, the wustite-iron-reducing gas

equilibrium constraint, which was discussed in previous sections, and the pivot point of the operating line, P, which is the thermal constraint of the direct reduction zone of the furnace (31, 32, 33)

Operation of the furnace on ore burdens in which prereduction of the higher iron oxides to wustite has been effected, results in a top gas richer in CO and H_2 than that normally produced in classical practice. The decrease in the amount of reduction performed by the gases in the stack is graphically depicted on the oxygen transfer diagram of Figure 6-B as a decrease in the length of the operating line, AE, and consequently, in the projection of the line on the abcissa, which, in the indirect reduction region, represents the $(CO_2 + H_2O/(CO + CO_2 + H_2 + H_2O)$ ratio of the top gas.

Greater rewards can be expected, however, from the operation of the furnace on burdens containing metallic iron. At constant wind rate, the pig iron production rate increases with the amount of metallization, α, of the burden. The parameter α is defined as the ratio of metallic to total iron in the burden:

$$\alpha = \frac{\% \ Fe^{o}}{\% \ Fe}$$

The coke rate, on the other hand, is a decreasing function of α, as well as Y_W, the ordinate of the wustite-iron equilibrium:

$$Y_W = 1.05 \ (1 - \alpha)$$

An increase in α causes a change in the constraint ordinate from Y_W to Y_W' and a clockwise rotation of the operating line about P. These particular effects are explained graphically in Figure 6-C. Consequently,

the fuel rate, which is proportional to the slope of the line, decreases and the production rate, an inverse function of the length of segment OE on the ordinate, increases.

While recognizing the merits of metallized burdens, ironmakers have been concerned over the possibility of oxidation of the metallic iron in contact with gases or phases of high oxygen potential in the upper part of the furnace stack. Oxidation decreases the value of α, and, as graphically put forth in Figure 6-D, lengthens the constraint ordinate Y_W' to Y_W'', and forces the operating line to rotate counter-clockwise. Anticipated gains in fuel and production rates are thus offset by the oxidation of metallic iron.

The counter-flow reactor is well suited for a laboratory investigation into the possible occurrence of oxidation. The latter manifests itself on the oxygen transfer diagram as an apparent lack of reactor efficiency, Figure 7-A. If the metallization of the bed entering the reactor is decreased, the wustite-iron constraint Y_W' shifts to Y_W'', but in this case, the operating line translates vertically. The reactor operating line, unlike the blast furnace line which is coupled to an elaboration zone pivot point, cannot rotate. In effect, the slope of the line is a function of the carbon, hydrogen and iron flow rates only, and remains fixed, regardless of shaft efficiency or oxidation phenomena.

On the reduction path diagram, oxidation of metallic iron shows up as a deviation of the path away from the Fe^{o} corner, as exemplified by the hypothetical path of Figure 7-B, and on the residence

time diagram, Figure 7-C, as a chemical reserve zone plateau located at level Y''_W instead of Y'_W.

CHAPTER 4

Experimental Considerations

4.1 Description of Apparatus

Photographs showing the essential features of the apparatus are given in Figures 8 and 9. The reaction vessel, furnace, furnace power control unit and gas train are non-standard equipment and are described in the following sub-sections.

4.1.1 Reaction Vessel Design

A diagram of the reaction vessel is shown in Figure 10.

The top cap, which connects the vessel to the gas input line, comprises a brass connecting piece and two stainless steel flanges bolted together and sealed with a rubber O-ring. The brass connecting piece of the upper flange is fitted with a gas pressure tap. The lower flange is welded to the reaction tube.

The reaction tube is welded 18-8 stainless steel, 9.5 ft. long, with a 2 1/16 in. I.D. and a wall thickness of 5/16 in.

The bottom cap which connects the vessel to the gas output line, comprises a stainless steel tightening ring, a Teflon ring seal and a brass connecting T-piece. The latter is fitted with a gas analysis and pressure tap, and also holds in place a 1/4 in. O.D. stainless steel thermocouple well by means of a Teflon plug.

4.1.2 Furnace Design

Construction details of the furnace shell are given in Figures 11 and 12. It comprises a 24 in. long, 18 in. I.D. asbestos pipe capped at the top by a 1/8 in. steel plate and at the bottom by a 1/4 in. plate. These parts are held together by three 3/8 in. rods which also serve as furnace suspension rods. Three spring loaded guide-pulleys, which maintain the mobile furnace aligned concentrically with the reaction tube, are attached to each cap.

The furnace is suspended by three 1/4 in. steel cables passing through pulleys in the top plate of the apparatus structure, Figure 12, and counterbalanced by three cylindrical weights. It is chain-driven by a 1/12 hp variable speed electric motor coupled to a demultiplying device with a 20940:1 reduction ratio. The furnace speed ranges from 1.6 cm./min. to 0.09 cm./min., corresponding to solids residence times of 40 min. to 11 hr.

Construction details of the heating unit are shown in Figure 13. It is made up of three independent heating elements, constructed from 2 1/2 x 4 1/2 x 9 in. insulation bricks and Kanthal strip rated at 0.0756 ohm/ft., affixed to the brickwork by Kyanex cement.

The windings are designed to radiate directly onto the reaction tube but are insulated from it by a 1/4 in. air gap. The bottom and middle heating elements each comprise two 6.6 ft. Kanthal strips wound in parallel, and the top element, a 3.3 ft. strip. The resistance of each element is 0.25 ohm. The winding leads are built up by helium arc-welding additional Kanthal strips. They are connected

to the power input cables anchored on the asbestos shell of the furnace by means of stranded copper conductors.

Four chromel-alumel thermocouples, useful for adjusting and stabilizing the reactor temperature profile, are located along the heating unit.

4.1.3 Furnace Power Control Unit

The wiring diagram of the furnace power control unit is given in Figure 14. It comprises three delta-connected autotransformers operating off the 220 volt, 3-phase main line, with each side of the delta connected to a furnace winding through a voltage 10:1 stepdown transformer. The input lines and the autotransformer sliders are fused. The power input to each winding is determined approximately from the readings of a voltmeter and ammeter located between the autotransformer and the transformer. The circuitry of the unit ensures an independent regulation of power in each winding. Maximum power output to each winding is 2500 watts.

4.1.4 Gas Train

The gas train of the apparatus is depicted schematically in Figure 15. High pressure cylinders of CO, CO_2, H_2 and N_2 are connected in pairs to the system. The gas from a cylinder flows through a regulator, an on-off valve and a variable-area flowmeter before converging with the other gases in a mixing chamber. At the exit of the chamber, the pressure, temperature and volume flow rate of the gas are measured by a differential inclined mercury manometer, a gas stream thermocouple and a variable-area flowmeter. Samples of gas are obtained, upstream

and downstream from the reaction vessel, by diverting small amounts of gas through sampling lines leading to a gas chromatograph equipped with a sampling valve. The pressure at the inlet and outlet of the vessel is measured by a differential inclined mercury manometer. The gas continues on through a throttling valve, a three-way valve, the reaction vessel and another three-way valve. The throttling valve ensures that the minimum operating pressure requirements of the upstream flowmeters can be met and buffers gas pulsations generated downstream. The three-way valves provide a means of reversing the gas flow at the end of a reduction test to quench the material in the hot zone of the vessel. If the gas flow is not reversed, the heavy nitrogen flow carries an excessive amount of heat to the vulnerable Teflon fittings at the gas outlet of the reactor. The path of the quenching gas through the system is indicated by broken arrows. The gas is then cooled in a heat exchanger and dust particles and condensed water, if any, are collected in a trap. The gas is further cleaned in a fiberglass packed tube, and dried in a silica gel column. Its pressure, temperature and volume flow rate are again measured. It is then exhausted to the atmosphere through a throttling valve, which serves to adjust the reactor pressure and provide a minimum working pressure in the outlet flowmeter. At this point, the gas may be shunted through a calibration device, such as a flow nozzle or a wet test meter, for the purpose of calibrating the flowmeters.

4.2 Measurement Technique

4.2.1 Gas Analysis

The composition of the gas is determined by a Fisher Model 25V

Gas Partitioner coupled to a Honeywell Millivolt Recorder.

The partitioner has an integral gas sampling valve which is connected to the gas train at points upstream and downstream from the reaction vessel, Figure 15.

The chromatographic system comprises a 30 in. Hexamethylphosphoramide column and a 6 1/2 ft. molecular sieve column. With helium as a carrier gas flowing at a rate of 80 ml./min., a conductivity cell current of 6.8 ma and a temperature of 50°C, the gases are separated and eluted in the order: carbon dioxide; hydrogen; nitrogen and carbon monoxide. Satisfactory peak heights are obtained at 2% of full sensitivity, for carbon dioxide, nitrogen and carbon monoxide. Under the aforementioned conditions, hydrogen, which has a thermal conductivity very close to that of helium, gives on the recorder chart a weak blip of qualitative value only. The instrument's sensitivity for hydrogen can be increased momentarily as the hydrogen peak is recorded or by substituting argon for helium. The latter technique would require the injection of another sample into the system.

A calibration chart for the instrument is established by injecting different gas mixtures of known composition, supplied by Matheson (Canada) Ltd., and plotting the height of the peak for each component against its known concentration. Reproducibilities of approximately 0.5% are obtained.

4.2.2 Solids Analysis

A comprehensive analysis is performed on the lot of ore material to be used for a test series. The material is grab sampled,

crushed to 14 mesh and split with an Otto sample splitter. It is then pulverized to 100 mesh, split and analysed for total, metallic and ferrous iron, and for alumina, lime, magnesia, silica, sulphur and carbon.

Upon completion of a reduction test, the bottom cap of the reaction vessel is removed and the material extracted by tapping it with a steel rod. Samples are taken throughout the lower 100 cm. of the reaction bed, each sample consisting of material collected over an interval of approximately 5 cm. The material is prepared as explained above and analysed for total, metallic and ferrous iron, and for carbon.

The analytical methods of the Steel Company of Canada Ltd. are described in Appendix A.

4.2.3 Gas Flow Rate

Variable area flowmeters manufactured by Fischer and Porter Co. Ltd. are utilized to measure the gas volumetric flow rate at the inlet and outlet of the reaction vessel. The metering pressure is measured by differential mercury manometers inclined 14° to the horizontal, and the metering temperature by thermocouples located at the outlet of the flowmeters.

4.2.4 Linear Bulk Density of Ore

The linear bulk density of the ore material, ρ_s, is determined by weighing the amount of material contained in a 75 cm. length of tube, which has an internal diameter equal to that of the reaction tube. A rod of diameter equal to that of the thermocouple well is located concentrically within the tube. The packing of the ore material in

the reactor is closely reproduced by this method. Five determinations are averaged to give the final value of density.

4.2.5 Furnace Speed

The furnace speed, U_f, is determined using a cathetometer and a stopwatch.

4.2.6 Reactor Temperature Profile

The temperature profile of the reactor is determined with a 1/8 in. diameter chromel-alumel thermocouple, magnesia insulated and inconel sheathed, manufactured by Thermo Electric (Canada) Ltd. The thermocouple slides within a well located along the axis of the reaction tube, as shown in Figure 10, making it possible to read the temperature at any level.

The temperature as measured by this technique, is an average temperature of the gas and solids.

Two methods are used to determine the reactor profile. The first method is applied during the initial stages of a test to adjust and stabilize the profile. It consists of sliding the thermocouple to one point, allowing the bead to achieve equilibrium with its surroundings, noting the temperature and repeating this procedure at intervals of 10 cm. until the complete profile is established. The second method, applied during the terminal stage of a test, consists of setting the thermocouple at a point ahead of the descending furnace. The profile is then automatically registered on the recorder chart. If the system is in thermal steady state, the profiles determined by these two methods are identical.

4.3 Experimental Procedure

The success of an experiment hinges on obtaining a stable temperature profile of satisfactory configuration and an outlet gas of constant composition. Under these conditions, a steady-state heat exchange between gas, ore material and surroundings, and a steady-state oxygen transfer are achieved. The regulation of the temperature profile is the most delicate part of the experiment. The following procedure has been found to give satisfactory results.

Heating-up Period (Figure 16-A)

The furnace is positioned at the upper end of the reaction vessel and is brought up to temperature in approximately six hours.

Transition Period (Figure 16-B)

At the end of the heating-up period, the reducing gas is admitted to the reactor and the furnace set in motion. The temperature profile is determined at frequent intervals during this period and the power input to the furnace adjusted until the required profile is obtained. The gas composition and flow rate are also adjusted by means of the gas partitioner and the flowmeter which is located downstream from the gas mixer, Figure 15.

Steady-state Period (Figure 16-C)

Fluctuations in the gas composition and temperature profile are gradually attenuated, and when the steady-state period is attained, the thermocouple bead is fixed at approximately the 100 cm. level from the bottom of the reaction tube. As the hot zone moves down, the final temperature profile is recorded, from 300°C at the solids inlet

of the reactor to 300°C at the gas inlet.

Quench Period (Figure 16-D)

At the end of the test, the hot zone must be quenched as quickly as possible in order to preserve the high temperature phases of the material for chemical analysis and microscopic examination. The furnace is raised to the upper end of the reaction vessel, the flow of the reducing components of the gas arrested, the nitrogen flow reversed and increased, and the tube quenched on the outside with water. The quenching rate is approximately 100°C/min.

CHAPTER 5

Calculation Methods

5.1 Carbon Flow Rate

The volume flow rate corresponding to full-scale (100%) deflection of the float in the flowmeters is reported by the manufacturer as 49.27 liter/min of air at 21.11°C and 1 atm. When a gas other than air is metered, or when gas flow occurs under different conditions of pressure and temperature, a correction factor (34) must be applied to the flowmeter reading. The corrected flow rate is given by:

$$r_g = r_a \left[\frac{s_g}{1} \cdot \frac{1}{P_g} \cdot \frac{T_g}{294.27} \right]^{1/2}$$

where: r_g = flow rate of gas at 21.11°C and 1 atm $\left[\frac{\text{liter}}{\text{min}}\right]$

r_a = flowmeter reading $\left[\frac{\text{liter}}{\text{min}}\right]$

s_g = specific gravity of gas mixture at standard temperature and pressure referred to air at standard temperature and pressure of 21.11°C and 1 atm

P_g = absolute metering pressure of gas [atm]

T_g = absolute metering temperature of gas [°K]

The specific gravity of the gas mixture is calculated from:

$$s_g = 0.009671\ (CO) + 0.01529\ (CO_2) + 0.009672\ (N_2) \qquad 5.1$$

where: CO = carbon monoxide [vol %]

CO_2 = carbon dioxide [vol %]

N_2 = nitrogen [vol %]

The coefficients of Equation 5.1 are the specific gravity, divided by 100, of the gas components (35).

The carbon rate at the inlet or outlet of the reaction vessel is calculated from the volumetric flow rate and composition of the gas:

$$n_g = \frac{r_g}{24.160} \cdot \frac{CO + CO_2}{100}$$

where: n_g = carbon flow rate $\left[\frac{\text{at C}}{\text{min}}\right]$

24.160 = molar volume of gas at $\left[\frac{\text{liter}}{\text{mole}}\right]$ $21.11^{\circ}C$ and 1 atm

If carbon deposition occurs at the reactor gas inlet, the carbon flow rate at the vessel outlet is lower than that at the vessel inlet since the carbon deposition reaction:

$$2CO = C + CO_2$$

results in a decrease in gas volume.

Because the iron oxide reactions are equimolar in the gas phase, the carbon rate measured at the vessel gas outlet is the true reactor carbon rate. Another method of obtaining the reactor carbon rate, $(n_g)_r$, is to calculate the carbon deposition rate, n_c, and to

subtract it from the carbon rate at the gas inlet of the vessel, $(n_g)_{v_{in}}$:

$$n_c = \left[\left(\frac{C_s}{Fe}\right)_{v_{in}} - \left(\frac{C_s}{Fe}\right)_{r_{in}}\right] \cdot n_{Fe}$$

and

$$(n_g)_r = (n_g)_{v_{in}} - n_c$$

where: n_c = carbon deposition rate at gas inlet of the reactor $\left[\frac{\text{at C}}{\text{min}}\right]$

$(n_g)_{v_{in}}$ = carbon rate at the gas inlet of the vessel $\left[\frac{\text{at C}}{\text{min}}\right]$

$(n_g)_r$ = carbon rate of the reactor $\left[\frac{\text{at C}}{\text{min}}\right]$

5.2 Iron Flow Rate

The iron flow rate is calculated by the following equation:

$$r_{Fe} = U_f \cdot \frac{\rho_s}{55.85} \cdot \frac{Fe}{100}$$

where: r_{Fe} = iron flow rate through the reactor $\left[\frac{\text{at Fe}}{\text{min}}\right]$

ρ_s = linear bulk density of the ore material $\left[\frac{g}{cm}\right]$

U_f = furnace speed $\left[\frac{cm}{min}\right]$

Fe = total iron in the input ore material [wt %]

5.3 Oxygen to Carbon Ratio

The oxygen to carbon ratio, O/C, is defined as the mole or volume fraction of carbon dioxide in the gas phase. The notation O/C is justified if the "O" is taken as the number of oxygen atoms transferred from the iron oxides to the CO molecules to form CO_2. The "C" represents the total number of carbon atoms in the gas phase.

The O/C ratio is calculated from the gas analysis by:

$$\left(\frac{O}{C}\right) = \frac{CO_2}{CO + CO_2}$$

where: $\left(\frac{O}{C}\right)$ = oxygen to carbon ratio $\left[\frac{\text{at O}}{\text{at C}}\right]$

CO_2 = carbon dioxide [vol %]

CO = carbon monoxide [vol %]

5.4 Oxygen to Iron Ratio

The oxygen to iron ratio, O/Fe, is defined as the ratio of oxygen atoms to iron atoms associated with the iron oxides in the material. It is calculated from:

$$\left(\frac{O}{Fe}\right) = \frac{1.05\ (Fe^{2+}) + 1.50\ (Fe^{3+})}{Fe}$$

where: $\left(\frac{O}{Fe}\right)$ = oxygen to iron ratio $\left[\frac{\text{at O}}{\text{at Fe}}\right]$

Fe^{2+} = ferrous iron in the ore material [wt %]

Fe^{3+} = ferric iron in the ore material [wt %]

Fe = total iron in the ore material [wt %]

The amount of ferric iron in the sample is calculated by:

$$Fe^{3+} = Fe - (Fe^{o} + Fe^{2+})$$

where: Fe^{o} = metallic iron in the ore material [wt %]

5.5 Carbon to Iron Ratio

The carbon to iron ratio, C/Fe, also referred to as the specific carbon consumption of the reactor , is defined as the ratio

of the carbon flow rate to the iron flow rate:

$$\left(\frac{C}{Fe}\right) = \frac{n_g}{n_{Fe}}$$

where: $\left(\frac{C}{Fe}\right)$ = carbon to iron ratio $\left[\frac{\text{at C}}{\text{at Fe}}\right]$

n_g = flow rate of carbon atoms in gas phase $\left[\frac{\text{at C}}{\text{min}}\right]$

n_{Fe} = flow rate of iron atoms $\left[\frac{\text{at Fe}}{\text{min}}\right]$

5.6 Solid Carbon to Iron Ratio

The solid carbon to iron ratio, C_s/Fe, is defined as the ratio of carbon atoms to iron atoms in the ore material. The subscript s of "C_s" indicates that the carbon atoms involved are present in the material as solid carbon and as carbon dissolved in the iron. The ratio is calculated by:

$$\left(\frac{C_s}{Fe}\right) = \frac{55.85}{12.01} \cdot \frac{C_s}{Fe}$$

where: $\left(\frac{C_s}{Fe}\right)$ = solid carbon to iron ratio $\left[\frac{\text{at C}}{\text{at Fe}}\right]$

C_s = total carbon in the ore material $\left[\text{wt \%}\right]$

Fe = total iron in the ore material $\left[\text{wt \%}\right]$

5.7 Calculation of Fe, Fe^o, α and O/Fe for Mixtures of Ore Materials

Because of the difficulty of obtaining representative samples in beds composed of two or more ore materials, it is preferable to calculate values of Fe, Fe^o, α and O/Fe from the chemical analyses of the separate components rather than from the analyses of the mixtures.

If a, b, c ... n represent the weight fractions of ore materials A, B, C ... N, then:

$$(Fe)_{mix} = a.(Fe)_A + b.(Fe)_B + \ldots n.(Fe)_N$$

$$(Fe^{o})_{mix} = a.(Fe^{o})_A + b.(Fe^{o})_B + \ldots n.(Fe^{o})_N$$

$$(Fe^{2+})_{mix} = a.(Fe^{2+})_A + b.(Fe^{2+})_B + \ldots n.(Fe^{2+})_N$$

$$(Fe^{3+})_{mix} = a.(Fe^{3+})_A + b.(Fe^{3+})_B + \ldots n.(Fe^{3+})_N$$

$$O_{mix} = 1.05\,(Fe^{2+})_{mix} + 1.50\,(Fe^{3+})_{mix}$$

$$\alpha_{mix} = \frac{(Fe^{o})_{mix}}{(Fe)_{mix}}$$

$$\left(\frac{O}{Fe}\right)_{mix} = \frac{O_{mix}}{Fe_{mix}}$$

5.8 Residence Time Correlations

In the analysis of the results, the O/Fe ratio of each sample of ore material is plotted against its residence time in the reactor. The temperature throughout the reactor is also plotted in terms of residence time. Before the latter can be calculated however, the limits of the reactor must be defined. The most convenient way of assigning limits to the reactor is in terms of temperature levels. For the purpose of constructing these diagrams, the reactor limits are defined as the points at which the ore material first and last exceeds 300°C. These points are designated A and B in the schematic diagram of the reaction tube, and a and b in the diagram of the recorder chart trace of the temperature profile, Figures 17-A and 17-B.

The nomenclature is given below:

U_c = chart speed $\left[\frac{cm}{min}\right]$

U_f = furnace speed $\left[\frac{cm}{min}\right]$

D_A = distance between the point at which the temperature is 300°C at the solids inlet of the reactor, and the bottom of the tube. [cm]

D_B = distance between a point of known O/Fe ratio and the bottom on the tube. [cm]

D_C = distance between the thermocouple junction and the bottom of the tube. [cm]

d_b = distance between a point above 300°C on the recorder trace and the 300°C point corresponding to the solids inlet of the reactor [cm]

d_c = distance between points at 300°C on the recorder trace [cm]

Temperature versus Residence Time

The residence time, t_{ab}, of point b on the temperature trace of Figure 17-B is given simply by:

$$t_{ab} = \frac{d_b}{U_c}$$

O/Fe Ratio versus Residence Time

The residence time, t_{AB}, of sample B of the ore material in the reactor, Figure 17-A, is given by:

$$t_{AB} = \frac{D_B - D_A}{U_f} \qquad 5.8.1$$

The distance, D_A, however, is not readily measureable. By adding to and subtracting from the right side of Equation 5.8.1, the quantity D_C/U_f:

$$t_{AB} = \frac{D_C - D_A}{U_f} + \frac{D_B - D_C}{U_f} \qquad 5.8.2$$

where: $$\frac{D_C - D_A}{U_f} = \frac{d_c}{U_c} \qquad 5.8.3.$$

Substitution of the right-hand term of Equation 5.8.3. into Equation 5.8.2. gives:

$$t_{AB} = \frac{d_c}{U_c} + \frac{D_B - D_C}{U_f} \qquad 5.8.4.$$

The residence time t_{AB} is now given by Equation 5.8.4. in terms of the easily measured variables d_c, D_C, D_B, U_c and U_f.

CHAPTER 6

Reduction Tests

6.1 Purpose of Reduction Tests

The purpose of the reduction tests to be described in the following sections was twofold:

(a) To check the operation of the apparatus and establish a working procedure for conducting reductions tests.

(b) To investigate the possibility of metallic iron oxidation in homogeneous beds of partly metallized pellets and in heterogeneous beds of highly metallized pellets and normal oxide pellets, at various levels of metallization and under thermal and chemical conditions similar to those existing in the indirect reduction zone of the blast furnace.

6.2 Test Materials

6.2.1 Ore Materials

Three lots of ore material were obtained from the Steel Company of Canada, Ltd.

The first lot consisted of pellets balled from Hilton concentrates, simultaneously indurated and partly metallized by the Stelco-Lurgi process (36); the second, of indurated Hilton oxide pellets highly metallized by the Stelco-Lurgi process.

Comprehensive chemical analyses of the three lots, performed by the Steel Company of Canada, Ltd., are reported in Table 3.

The pellets were screened on a Dillon vibrating screen, and the - 1/2 + 3/8 in. fraction was retained for the experiments. Approximately one half of the pellets in the retained fraction of the first lot were broken and the rest were deeply cracked, spalled and non-spherical. The pellets in the other lots were fairly spherical and generally in good condition.

The linear bulk density, ρ_s, of the three ore materials was determined as 31.2, 41.1 and 33.9 g/cm, respectively.

6.2.2 Gases

Reducing gas for the tests was produced by mixing 98% grade CO, obtained from Matheson of Canada Co. Ltd., and 99.6% grade N_2 and 99% grade CO_2, obtained from Canadian Liquid Air Co. Ltd.

6.3 Operating Conditions

6.3.1 Tests on Partly Metallized Pellets

Test series "A" consisted of two reduction tests on beds of Hilton partly metallized pellets.

For both tests, a reducing gas mixture composed of approximately 40 vol% CO and 60 vol% N_2 was fed to the reaction vessel.

For test A-1, the gasified carbon flow rate was 0.198 at C/min and the iron flow rate, 0.105 at Fe/min, giving a specific carbon consumption of 1.897at C/at Fe. The isothermal zone temperature was 954°C and the residence time of the solids, 3.75 hours.

For test A-2, the gasified carbon flow rate was increased 0.357 at C/min and the iron flow rate, to 0.138 at Fe/min, resulting in a higher specific carbon consumption of 2.595at C/at Fe and a shorter residence time of 3.00 hr. The isothermal zone temperature was 900°C.

The conditions of tests A-1 and A-2 are summarized in Table 4.

6.3.2 Tests on Mixtures of Highly Metallized and Normal Oxide Pellets

Test series "B" consisted of four reduction tests on beds composed of 100-0, 75-25, 50-50, and 25-75 wt % mixtures of Hilton oxide and Hilton highly metallized pellets, designated B-1 to B-4, respectively.

From B-1 to B-4, the operating conditions were chosen to simulate the clockwise rotation of the operating line of the blast furnace about the elaboration zone pivot point, on the oxygen transfer diagram, Figure 6, as the amount of metallic iron in the burden is increased. In particular, the specific carbon consumption was decreased from a value of 1.792 atC/at Fe for B-1 to 0.678 at C/at Fe for B-4. The pivot point chosen for these reduction tests was a typical blast furnace elaboration zone pivot point, P(-0.65, -0.25), in the direction reduction zone of the oxygen transfer diagram.

A temperature profile with an isothermal zone in the vicinity of 900°C was established for all four tests.

The solids velocity, that is, the furnace speed, was fixed at 0.29 cm/min. This resulted in a three hour residence time

for the solids in the reactor.

The conditions of tests B-1 to B-4 are summarized in Table 4.

6.4 Presentation of Results

Initial and derived results of the reduction tests are presented in Tables 4, 5, 6, and 7, from which the oxygen transfer, reduction path and residence time diagrams of Figures 18, 19, and 20, have been constructed.

CHAPTER 7

Discussion of Results

In the following sections, the apparatus and experimental procedure, the iron analyses, the occurrence of carbon deposition, and finally the question of metallic iron oxidation are discussed in the light of the experimental results.

7.1 The Apparatus and Experimental Procedure

No furnace alignment problems, distortion, nor excessive oxidation of the reaction tube were encountered during the experiments. The low-voltage three-phase furnace proved to be reliable, and gave the required shape of the temperature profile. However, fluctuations in the line voltage affected both the power input to the furnace and the speed of the furnace. Hence, the installation of voltage stabilizing devices upstream of the furnace power control unit and the furnace motor is recommended.

A reasonable mass balance closure is obtained attesting to the accuracy of such measurements as furnace speed, gas flow rates and analyses and bulk density of the ore material. In effect, for a given experiment, the value of the solids outlet O/Fe ratio, Y_B, which is calculated from the values of X_A, X_B, Y_A and the slope of the operating line, C/Fe, Table 5, is close to the value of Y_B calculated solely from the iron analyses and appearing on the residence time diagrams of

Figures 4-C and 20.

El-Mehairy and Philbrook (28) have shown that transport phenomena in the gas phase between particles of the bed do not affect the reduction rate of the bed, even at gas flow rates dictated by pressure drops as low as 0.01 in. H_2O/in. of bed for 3/16 in. diameter pellets. In this investigation, the pressure drop in the bed corresponding to the lowest flow rate used was approximately 0.025 in. H_2O/in. of bed. Moreover, the pellets were of diameter between 1/2 and 3/8 in. The gas velocities were therefore much greater and the gas more turbulent than in the experiments of El-Mehairy and Philbrook. It can then be concluded that no reagent starvation occurred in the boundary layer around the particles of the bed and that the rate of reduction was not affected by the gas velocity. As explained in section 3.1.1, this was one of the conditions to be satisfied for an adequate simulation of the blast furnace reduction process.

7.2 Iron Analyses

Two techniques, described in Appendix A, were utilized for the iron analysis of the solids over the length of the reactor. The solids of tests A-1 and A-2 were analyzed by Technique I, and those of tests B-1 to B-4 by Techniques I and II. In the case of tests B-1 to B-4, there was a considerable discrepancy between the results of analyses performed by the two techniques on a given sample of material, particularly in the poorly reduced samples. Subsequent calculations revealed that the Fe^{2+} analyses obtained by Technique I were low, so that for tests B-1 to B-4, only the analytical results of Technique II were retained.

The considerable scatter in the points on the O/Fe profiles of tests B-2, B-3, and B-4, Figure 20, is due to the fact that these experiments were conducted on mixtures of very different pellets. This scatter is not present in the O/Fe profiles of tests A-1, A-2 and B-1 which were conducted on beds containing only one type of pellet. This suggests that the main error occurs in sampling rather than in chemical analysis. In effect, the sample of material extracted at 5 cm intervals in the reacted bed contained approximately 50 pellets, and hence was not necessarily representative of the overall proportions of metallized and oxide pellets in the mixture.

Many of the experimental points in the reduction path diagrams of Figure 19 are in a seemingly forbidden zone, that is, to the left of the $FeO_{1.05}$ - Fe^{o} line. Indeed, the reduction path follows a $FeO_{1.025}$ - Fe^{o} line in most of the diagrams. No systematic investigation of this anomaly has been undertaken; however, several explanations are suggested:

(i) Iron bearing compounds such as hercynite, $FeAl_2O_4$ and fayalite, Fe_2SiO_4, may be present in the ore material and the Fe^{2+} in these compounds is included in the analysis of the iron oxide Fe^{2+}. A correction for this effect would shift the reduction paths towards the unforbidden zone.

(ii) A systematic error may be present in the analyses of Fe, Fe^{o} and Fe^{2+}.

(iii) As shown by the data of Darken and Gurry (29), stable wustite containing the least amount of oxygen at the temperatures of the reduction tests has the composition $FeO_{1.05}$. The presence of

impurities in the natural oxides of the pellets, however, could alter the composition of stable wustite to a point somewhere between the FeO and $FeO_{1.05}$ compositions.

7.3 Carbon Deposition Effects

As evidenced by the C_s/Fe profiles of the residence time diagrams of Figure 20, carbon deposition by the reaction:

$$2CO = CO_2 + C$$

occurred in the temperature gradient at the solids outlet of the reactor. The number of carbon atoms deposited, per atom of iron, is equal to the difference between the plateaus of the C_s/Fe profiles. Values for the reduction experiments are given in Table 9. The variation in carbon deposition from one experiment to the next is due mainly to the variation in the flow rate of reducing gas. In terms of composition changes in the inlet gas, which before the occurrence of carbon deposition is a mixture of CO and N_2 only, the effect is small but not negligible. This is indicated by the X_B values of Table 5 which are the $CO_2/(CO+CO_2)$ ratios of the inlet gas. In particular, for test B-1, about 4% CO_2 enters the reactor proper.

The value of the carbon rate determined from the gas inlet flowmeter was corrected by subtracting from it the carbon deposition rate, Table 8, determined from the solids analyses and the iron flow rates. The values of n_g in Table 4 were calculated in this manner. As carbon deposition did not occur downstream of the gas inlet to the reactor, it appears that it would have been simpler to calculate the carbon rate from the gas outlet flow rate. However, oscillations of

the float in the gas outlet flowmeter during some experiments made readings difficult and possibly less accurate so that the former method was favored.

The carbon deposition rates for tests B-1 to B-4, calculated from the carbon analyses of the solids, are in good agreement with those calculated from the difference in volume flow rate of the gas at the inlet and outlet of the reaction vessel, as shown in Table 8. This is an indication that the flowmeters are sensitive and accurate enough for the purpose of the tests. In the case of tests A-1 and A-2, the disagreement between the two methods of calculating the carbon deposition rates is explained by the fact that floats of a greater capacity, inherently less accurate and sensitive, were used in the flowmeters.

7.4 Discussion of Metallic Iron Oxidation

Two conditions are necessary for an oxygen potential ($X_A - X_W$) to exist in the gas leaving the reactor with respect to the metallic iron entering the reactor: first, oxides of higher oxygen content than wustite must be present in the starting material, that is, Y_A must be greater than Y_W; secondly, the reactor efficiency must be sufficiently high, that is, the operating line must lie close enough to the wustite-iron constraint in order that X_A be greater than X_W.

The question of metallic iron oxidation during the reduction of the ore materials employed during the experiments is discussed in the following sub-sections in the light of these conditions.

7.4.1 Reduction Tests A-1 and A-2

As shown in the chemical analyses of Table 3, the ore material

employed for tests A-1 and A-2 contains only a small amount of Fe^{3+}, 2.6%. As shown in Table 5, the Y_A values, 0.842 and 0.856, for the ore materials are only slightly greater than their Y_W value, 0.835. Therefore, large oxygen potentials cannot be expected.

For test A-1, it is seen on the oxygen transfer diagram of Figure 18 and in Table 5, that the X_A value, 0.309, exceeds only slightly the X_W value, 0.298. The oxidation potential is small in this case, and little, if any, oxidation of metallic iron has occurred, as shown by the high reactor efficiency of 97.8% reported in Table 5.

The reactor efficiency for test A-2 was much lower, 80.3%, because of the relatively shorter residence time of the solids in the reactor and the lower temperature of the isothermal zone. The reactor efficiency was calculated for an isothermal zone temperature of 900°C. However, the temperature profile of test A-2, Figure 20, reveals that there is a temperature maximum at approximately 950°C. As the gas would tend to achieve equilibrium with wustite and iron at this temperature rather than at 900°C, the efficiency value quoted above may be slightly in error. A correction would shift the X_W point from 0.315 to 0.298 resulting in a higher efficiency of 85%. However, the X_A value for the outlet gas, 0.259, is considerably less than either of the values for the wustite-iron equilibrium constraint. Therefore, the outlet gas had a negative oxidation potential, that is, a reduction potential, and did not oxidize the metallic iron in the incoming material.

Comparison of the experimental reduction paths and O/Fe profiles for tests A-1 and A-2 in Figures 19 and 20, with the hypothetical

paths and profiles of Figures 7-B and 7-C, reveals that oxidation of metallic iron did not occur. In particular, oxidation would show up an an increase in the Y_W value of the O/Fe profiles to Y'_W. In the present case, in fact, the wustite plateau of test A-1 and the inflection point of test A-2 on the O/Fe profiles have Y_W values of approximately 0.77, considerably lower than the Y_W values of the wustite-iron constraints, both equal to 0.835. The latter values have been calculated from the chemical analyses of the material at the inlet of the reactor. The reason for this apparent anomaly is that some wustite in the ore material is reduced to iron while heating up to the temperature of the isothermal zone. This effect occurs between levels 4 and 6 in test A-1 and levels 3 and 6 in test A-2. The reactor efficiencies, based on a Y_W value of 0.77, are lower than those previously calculated: 87% for test A-1 and 74% for test A-2.

To summarize, the partly metallized pellets utilized for tests A-1 and A-2 contained too little Fe^{3+}, as shown in the chemical analysis of Table 3, for metallic iron oxidation to occur.

7.4.2 Reduction Tests B-1, B-2, B-3 and B-4

The reduction efficiencies, e_r, of tests B-1 to B-4 reported in Table 5 are very high, decreasing from 98.0% for test B-1 to 95.9% for test B-4. These high reduction efficiencies are expressed graphically in the oxygen transfer diagram of Figure 18, in which the operating lines are close to their respective wustite points. It can thus be concluded that oxidation of metallic iron, if any, is negligible, despite the sizeable oxidation potential of the gas with respect to

the metallic iron. In effect, the oxidation potential is proportional to the difference of the X_A and X_W values reported in Table 5.

Offroy (37), has conducted similar experiments using the IRSID counter-flow reactor on a mixture of 42% Hilton pellets highly metallized by the Stelco-Lurgi process, 38% Hilton oxide pellets and 20% Erie pellets, corresponding to an overall metallization 46.3%. He showed that the Hilton metallized pellets, chemically and physically similar to the ones employed in the present experiments, were not oxidized by the gas produced by the reduction of the oxidized Hilton and Erie pellets.

As indicated by the reduction path and residence time diagrams of test B-1, Figures 19 and 20, the Hilton pellets exhibit an almost ideal reduction pattern under these conditions. During the initial stages of reduction, points 1 to 7, the reduction path follows very closely the Fe^{2+} - Fe^{3+} boundary of the diagram. Also, as seen on the residence time diagram and in Table 7, reduction to metallic iron did not occur in the temperature gradient at the solids inlet of the reactor, as was the case in tests A-1 and A-2.

The reduction paths and O/Fe profiles for tests B-2 to B-4 follow the same general trend, although, for the reasons given in section 7.2, they are not as clear-cut as in the case of test B-1.

CHAPTER 8

Summary and Conclusions

1. A counter-flow reactor has been constructed, tested, and found satisfactory for the study of the reduction chemistry of packed beds of iron oxides. It is believed that chemical conditions in the indirect reduction zone of the blast furnace are adequately simulated by this laboratory model.

2. The apparatus is similar in principle to that of Bonnivard and Rist. However, certain components of the present apparatus are original: the bed temperature probe; the self-aligning, three-phase, low-voltage furnace; the power control unit; and the reverse-flow system. These have proved valuable in the course of experimentation.

3. The installation of voltage stabilizing devices upstream of the furnace power control unit and the furnace motor is recommended.

4. A good mass balance over the reactor was obtained in the reduction experiments, attesting to the accuracy of the measuring techniques.

5. Carbon deposition has been found to occur in the temperature gradient at the gas inlet to the reactor. It has been accounted for by two independent methods: one method is based on the carbon and iron analyses of the material as well as the iron flow rate; the other on the determination of the gas composition and flow rate at the inlet and outlet of the reaction vessel.

6. An experimental investigation has been conducted into the possibility of metallic iron oxidation in two types of prereduced ore materials during reduction under conditions similar to those encountered in the indirect reduction zone of the blast furnace.

7. In the two experiments on homogeneous beds of partly metallized pellets, the oxidation potential was small in one and non-existent in the other, so that no oxidation of metallic iron occurred. An investigation into homogeneous beds of pellets containing an appreciable amount of ferric iron is suggested.

8. In the experiments on heterogeneous beds of oxidized and highly metallized pellets, there existed a definite oxidation potential with respect to metallic iron. No oxidation occurred, however, presumably because of the compactness of the highly metallized pellets.

9. It is believed that the conclusions drawn from this investigation may be extended to the operation of an actual blast furnace on similar ore materials.

APPENDIX A

Determination of Total, Metallic, Ferrous and Ferric Iron (38)

A.1. Reagents

Potassium dicromate (0.0895 N):

Dissolve 4.389 grams of the salt in water and dilute to one litre. Standardize against a standard iron ore, and adjust, if necessary, so that I ml.= 0.005 grams of Fe.

(Note: Potassium dicromate (Reagent grade) may be regarded as a primary standard after the following treatment:- grind crystals in agate mortar to a fine powder; heat at I40-I50'C for about an hour and cool in desiccator)

Titration mixture (and indicator):

To about 300mls. of water (in a I litre boiling flask) add: I50 mls. of sulphuric acid (conc.): cool cold
I50 mls. of phosphoric acid (conc.)
I2 mls. of a 0.3% aqueous solution (0.3 gm/I00 mls.) of p-Diphenylaminesulphonic acid, sodium salt.
Dilute to I litre and use 30 mls. per determination.

Stannous chloride:

Dissolve 25 gm. of $SnCl_2 \cdot 2H_2O$ in 50 mls. of hydrochloric acid (conc.). Boil for five minutes. Cool. Add 5 gm of mossy tin metal, and 50 mls. of water. Shake and transfer to dropping bottle.

Mercuric chloride:

A saturated aqueous solution of $HgCl_2$.

Sulphuric Acid I/4.

Add 500mls. H_2So_4(conc.) to 2 litres of water. Cool.

Copper sulphate:

Dissolve 100 gm. of $CuSO_4.5H_2O$ in about 300 mls. of water, in a I litre boiling flask. Add 3-4 gm. of cupric oxide. Allow to stand in a warm place for several hours, with occasional shaking.

Filter and dilute filtrate to I litre.

<u>Reactions</u> $Fe_2O_3(S) + 6H^+ = 2Fe^{+3} + 3H_2O$

$2Fe^{+3} + Sn^{++} = 2Fe^{++} + Sn^{+4}$

$Sn^{++} + 2HgCl_2 = Sn^{+4} + Hg_2Cl_2(S) + 2Cl^-$

$6Fe^{++} + Cr_2O_7^{--} + I4H^+ = 6Fe^{+3} + 2Cr^{+3} + 7H_2O$

diphenylamine + $Cr_2O_7^{--}$ = diphenylbenzidine violet + Cr^{+3}

A.2. <u>Technique I</u>

Technique I is the standard technique for the determination of total, metallic, ferrous and ferric iron.

Total iron:

Weigh 0.25 gm. of sample (0.50 gm. if the iron content is less than 50%) into a 500 ml. Berzelius beaker. Add I0-I5mls. of water and bring just to the boil while swirling. Add 20 ml of hydrochloric acid (conc.) Cover and digest at below boiling.

As the iron yellow colour develops add stannous chloride solution dropwise to completely decolorize the solution. This

is repeated as long as the colour reappears(except silica or free carbon). Remove from heat, add a dilute solution of potassium permanganate dropwise to restore the iron yellow colour and boil for 4-5 minutes. While still hot, wash off cover glass and sides of beaker, reduce with stannous chloride solution, dropwise, until all yellow is destroyed, and two drops in excess. Cool cold, quickly. Add IO mls of mercuric chloride solution quickly, and allow to stand with occasional swirling for not less than 3 or more than 5 minutes. Dilute to about 350 mls, add 30 mls of titration mixture and titrate immediately with potassium dichromate to violet.

Calculate percent of total iron from titration

mls. of titrant x 2 = %Fe(T). (on 0.25 g sample)

Metallic iron:

Weigh 0.25 gm. of sample into a 250 ml. beaker. Add 90 mls. of copper sulphate solution. Leave sit for 2 hours with occasional stirring until samle has desolved completely. Cover with watch glass.

Filter through a #40 Whatman paper retaining the filtrate in a 500 ml. Berzelius beaker. Police the 250 ml. beaker twice and also wash 3 times. Wash paper and residue thoroughly with could water about 8 times. Reserve residue for Fe^{++}. Dilute the filtrate to about 300 mls. with cold distilled water; add 30 mls. of titration mixture and titrate with potassium dichromate as before. mls. of titrant x 2 = %Fe(M). (on 0.25 gm. sample)

Ferrous iron:

Place paper and residue, from metallic iron determination, to a stoppered 250 ml. Erlenmeyer flask: Add 50 mls. of sulphuric acid (I:4). Replace stopper and shake vigorously until the paper is disintegrated. Allow to stand for one hour, with occasional shaking. Filter through #4I paper, retaining the filtrate in a 500 ml. Berzelius beaker. Wash mouth of flask after each pour.

Wash filter about 6 times. Dilute filtrate to 150 mls., add 30 mls. of titration mixture and titrate with potassium dichromate as before. mls. of titrant x 2 = $\%Fe^{++}$. (on 0.25 gm. sample)

Ferric iron:

Total iron - (metallic + ferrous iron) = $\%Fe^{+++}$.

A.3. Technique II

Technique II is utilized for the determination of total iron if the material fails to dissolve completely by the other technique.

Weigh 0.25 gm. of sample into a 250 ml. beaker. Add 10-15 mls. of water. Swirl, and heat to almost boiling. Add 30 mls. of hydrochloric acid (conc.), cover the beaker and digest at just below boiling for about an hour. Bring to incipient boiling for about 10 minutes. Wash off cover glass and sides of beaker with warm water bringing the volume to about 50 mls. Filter the insoluble through a #40 filter paper into a 500 ml. beaker and wash the paper and residue with warm hydrochloric acid (1:10) until free from yellow colour and then 6-8 times with warm water.

Place the paper and residue in a platinum crucible, dry and ignite. Cool; moisten with two or three drops of sulphuric acid (1:1); add about 5 mls of hydrofluoric acid and heat gently to dryness. Increase the temperature to dull redness for a few to remove all fumes of sulphuric. Cool; add 2 gms of potassium pyrosulphate, heat gently at first and then to redness with swirling to fuse the insoluble. Place the crucible in a 250 mls beaker containing about 100 mls of warm water. Add 5 mls of hydrochloric acid and heat gently to dissolve the melt. Remove and wash off crucible.

Make slightly alkaline with ammonium hydroxide and boil gently for a few minutes; allow to settle but filter while still warm through a #541 paper and wash 6-8 times with warm water (discard the filtrate).

Dissolve the precipitate from the paper with hot hydrochloric acid (I:2) and then wash well with hot water. Add this solution to the main filtrate (which in the meantime has been boiled down to low volume). Evaporate the combined solutions to about 30 mls; reduce with stannous chloride and proceed to titration with potassium dichromate as described before.

The procedure for metallic and ferrous iron is exactly as described before.

REFERENCES

1. O. G. Specht and G. A. Zapffe, "The Low Temperature Gaseous Reduction of Magnetite Ore to Sponge Iron", Transactions AIME, 167, 237 - 280 (1946).

2. N. J. Themelis and W. H. Gauvin, "Mechanism of Reduction of Iron Oxides", Canadian Mining and Metallurgical Bulletin, 55, 444 - 456 (1962).

3. D. Dutilloy, P. C. Ghosh and A. Rist, "La Réduction d'un Echantillon d'Oxyde de Fer par un Gaz", Revue de Métallurgie, 61, 1043 - 1060 (1964); 62, 15 - 35 (1965).

4. W. H. Wetherill and C. C. Furnas, "The Rate of Reduction of Iron Ores With Carbon Monoxide", Industrial Engineering and Chemistry, 26, 983 - 991 (1934).

5. M. C. Udy and C. H. Lorig, "Low Temperature Gaseous Reduction of a Magnetite", Transactions AIME, 154, 162 - 181 (1943).

6. E. Schurmann, H. Beer and J. Willems, "Die Sauerstoffabbaugeschwindigkeit bie der Reduktion von Eisenerzen mit einem Gasgemisch aus Kohlenmonoxyd, Wasserstoff und Stickstoff", Archiv fur das Eisenhuttenwesen, 31, 509 - 519 (1960).

7. T. B. Beeton, "Reducibility Measurement of Blast Furnace Burdens", Journal Iron and Steel Institute, 201, 913 - 922 (1963).

8. B. Ilschner, "The Reduction Kinetics of Iron Ores By Hydrogen and Hydrogen - Methane Mixtures", Technische Mitteilungen Krupp, 17, 318 - 329 (1959).

9. A. E. El-Mehairy and W. O. Philbrook, "Reduction of Iron Ore Particles In Fixed Beds", Blast Furnace, Coke Oven and Raw Materials Conference, AIME, 20, 280 - 291 (1961).

10. S. I. Privalov, V. N. Timofeev, and B. A. Bokovikov, "Reduction Process In An Ore Bed", Stal in English, No. 1, 4 - 11 (1960).

11. A. Rist and G. Bonnivard, "Réduction d'un Lit d'Oxydes de Fer par un Gaz. 1ère Partie. Etude Théorique dans l'Hypothèse de Vitesses Infinies de Réaction", Revue de Métallurgie, 60, 23 - 37 (1963).

12. A. Rist and G. Bonnivard, "Réduction d'un Lit d'Oxydes de fer par un Gaz. 2ème Partie. Etude à priori dans le Cas Réel de Vitesses Finies de Réaction", Revue de Métallurgie, 63, 197 - 210 (1966).

13. G. Bonnivard and A. Rist, "Réduction a Contre-Courant dans un Gradient de Temperature", BRGM - IRSID Report R-4 (1963).

14. C. G. Thibaut, "Reducibility of Iron Ores", Centre Documentation Sidérurgique, Circulaire Informations Techniques No. 5, 1191 - 1241 (1964).

15. M. Ispas, "Laboratory Apparatus and Calculation Methods used for Reduction of Ores, Agglomerates, and Pellets", Metalurgia, 17, 33 - 35 (1965).

16. V. I. Korotich and V. K. Gruzinov, "Standard Apparatus for Determining Reducibility of Iron - Ore Sinters", Stal in English, No. 8, 560 - 561 (1960).

17. K. K. Shkodin, "Reducibility of Sinters at Works In The USSR", Stal in English, No. 1, 4 - 8 (1961).

18. L. von Bogdandy, P. Dickens, W. vor dem Esche and J. Willems, "Testing Methods For The Reducing of Iron Ores", Troisièmes Journées Internationales Sidérurgie, Luxemburg, 142 - 156 (1962).

19. R. Linder, "A Programme-Controlled Reduction Test for Blast Furnace Burdens", Journal Iron and Steel Institute, 189, 233 - 243 (1958).

20. H. Schenk, W. Wenzel, H. W. Theisges and F. Block, "Determination of Reducibility of Iron Ores with Programmed Blast Furnace Conditions", Stahl und Eisen, 85, 963 - 970 (1965).

21. A. N. Ramm and Yu. P. Svintsov, "Investigation of the Gaseous Reduction of Iron Ores under Counter-Current Conditions For Ore and Gas", Trudy LPI im. Kalinina No. 179 (1955).

22. S. Klemantaski, "A New Experimental Technique For Studying the Blast Furnace Process", Journal Iron and Steel Institute, 185, 237 - 239 (1957).

23. S. Klemantski and R. Wild, "Blast Furnace Reactions and Burden Properties", Troisièmes Journées Internationales Sidérurgie, Luxemburg, 127 - 141 (1962).

24. M. S. Kurchatov, "Laboratory Installation for Determining the Reducibility of Metal Oxides and Ores", Stal in English, No. 3, 177 - 179 (1964).

25. G. Bonnivard and A. Rist, "Etude Expérimentale de la Réduction d'Agglomérés de Minerais de Fer par un Gaz a Contre-Courant", Revue de Métallurgie, 59, 401 - 415 (1962).

26. E. Bonnaure, "Results of Campaigns Performed in 1958 at the Low Shaft Blast Furnace of Liege", Blast Furnace, Coke Oven, Raw Materials Conference, AIME, 18, 75 - 91 (1959).

27. J. Michard, P. Danscoisne and G. Chanty, "Blast Furnace Practice With 100% Low-Grade Self-Fluxing Sinter", Blast Furnace, Coke Oven, Raw Materials Conference, AIME, 20, 329 - 351 (1961).

28. A. E. El-Mehairy and W. O. Philbrook, "The Reduction of Single Particles of Iron Oxide in Inert Fixed Beds", Transactions AIME, 224, 1280 - 1282 (1962).

29. L. S. Darken and R. W. Gurry, "The System Iron - Oxygen. Part I. The Wustite Field and Related Equilibria", Journal American Chemical Society, 67, 1398 - 1412 (1945).

30. N. Meysson, A. Maaref and A. Rist, "Emploi de Boulettes Prérèduites au Haut Fourneau. Etude Graphique", Revue de Métallurgie, 62, 1161 - 1179 (1965).

31. A. Rist and N. Meysson, "Etude Graphique de la Marche du Haut Fourneau Avec Vent Humide et Injections aux Tuyères", Revue de Métallurgie, 62, 995 - 1039 (1965).

32. A. Rist and N. Meysson, "Etude Graphique de la Mise au Mille Minimale de Haut Fourneau a Faible Temperature de Vent", Revue de Métallurgie, 61, 121 - 145 (1964).

33. N. Meysson, J. Weber and A. Rist, "Representation Graphique de la Décomposition des Carbonates dans le Haut Fourneau", Revue de Métallurgie, 61, 623 - 634 (1964).

34. Fischer and Porter Company Limited, Convertible Indicating Flow-rator Meters 3000 Series, Specification 10A1/10A3500, Warminster, Pennsylvania (1963).

35. C. D. Hodgman, ed., "Handbook of Chemistry and Physics", 43rd Edition, Chemical Rubber Publishing Company, Cleveland, Ohio, p. 2141 (1961).

36. J. G. Sibakin, "Development of the SL Direct Reduction Process", Blast Furnace and Steel Plant, 50, 977 - 989 (1962).

37. C. Offroy, "Essai de Réoxydation de Boulettes Stelco - Lurgi dans les Conditions d'Utilisation de ces Boulettes dans un Haut Fourneau", IRSID, Report No. LM.65-N.62-CO/MS (1965).

38. The Steel Company of Canada, Research and Development Department, "Determination of Total, Metallic, Ferrous and Ferric Iron in Reduced Iron Pellets, Sponge Iron Ores, Slag, etc." (1965).

Table 1 Variation of the Oxidized Fraction of CO-CO_2 Mixtures in Equilibrium with Iron and Wustite, Wustite and Magnetite, and Magnetite and Hematite (29)

T	X_W	X_M	X_H
°C	Mole fraction of CO_2		
700	0.400	0.648	1.000
800	0.347	0.719	1.000
900	0.315	0.776	1.000
1000	0.285	0.822	1.000
1100	0.274	0.860	1.000

Table 2 Stoichiometric Calculations for Various Iron Oxide Reductions at 900°C

Index i	Reaction i	$(n_g/n_{Fe})_i = (\Delta Y/\Delta X)_i$
1	$\frac{1}{1.05}\,FeO_{1.05} + CO \rightarrow \frac{1}{1.05}\,Fe + CO_2$	$\frac{1.05}{X_W - X_B} = 3.33$
2	$\frac{1}{0.28}\,FeO_{1.33} + CO \rightarrow \frac{1}{0.28}\,FeO_{1.05} + CO_2$	$\frac{0.28}{X_M - X_W} = 0.607$
3	$\frac{1}{0.17}\,FeO_{1.5} + CO \rightarrow \frac{1}{0.17}\,FeO_{1.33} + CO_2$	$\frac{0.17}{X_H - X_M} = 0.759$
4	$\frac{1}{0.45}\,FeO_{1.5} + CO \rightarrow \frac{1}{0.45}\,FeO_{1.05} + CO_2$	$\frac{0.45}{X_H - X_W} = 0.657$

Table 3 Chemical Composition of Ore Materials used in Reduction Tests

	Hilton Partly Metallized	Hilton Oxide	Hilton Highly Metallized
	wt%	wt%	wt%
Fe	71.8	67.7	92.8
Fe^{o}	15.0	0.2	91.3
Fe^{2+}	54.2	1.0	0.9
Fe^{3+}	2.6	66.4	0.6
Al_2O_3	0.44	0.38	0.79
SiO_2	3.22	1.98	2.76
CaO	0.80	0.18	0.40
MgO	2.98	1.08	1.56
C	0.050	0.052	0.077
S	0.02	0.006	0.009

Table 4 Initial Conditions and Results of Reduction Experiments

Variable	Units	*	A-1	A-2	B-1	B-2	B-3	B-4
SOLIDS								
ρ_s	g/cm	r_{in}	31.2	31.2	41.1	39.3	37.5	35.7
U_f	cm/min	-	0.259	0.346	0.291	0.294	0.294	0.297
Fe	wt %	r_{in}	72.2	71.2	67.7	74.0	80.2	86.5
α	-	"	0.205	0.204	0.003	0.310	0.570	0.792
n_{Fe}	at Fe/min	-	0.105	0.138	0.145	0.153	0.158	0.164
t_s	hr	-	3.75	3.00	2.50	3.00	3.00	3.00
T_r	°C	-	954	900	904	954	873	897
GAS								
r_a	liter/min	v_{in}	12.07	21.26	15.08	12.33	9.66	7.25
	"	v_{out}	12.31	21.77	15.77	12.88	10.10	7.34
T_g	°C	v_{in}	30	30	27	27	27	27
	"	v_{out}	30	30	27	27	27	27
Pg	atm	v_{in}	0.993	1.029	1.053	1.029	1.024	1.028
	"	v_{out}	0.991	1.007	1.028	1.024	1.017	1.022
CO	vol %	v_{in}	39.8	40.0	42.0	41.0	39.4	37.0
N_2	"	"	60.2	60.0	58.0	59.0	60.6	63.0
CO	vol %	v_{out}	27.3	29.4	18.7	19.8	19.7	21.0
CO_2	"	"	12.2	10.3	22.8	20.8	19.6	15.9
N_2	"	"	60.5	60.3	58.5	59.4	60.7	63.1
r_g	liter/min	v_{in}	12.05	21.60	15.58	12.58	9.84	7.40
	"	v_{out}	11.86	21.25	15.12	12.39	9.72	7.15
n_g	at C/min	r	0.198	0.357	0.260	0.206	0.158	0.111

* r and v designate reactor and vessel

Table 5 Data for Construction of Oxygen Transfer Diagrams

Variables	Units	A-1	A-2	B-1	B-2	B-3	B-4
X_A	at O/at C	0.309	0.259	0.549	0.512	0.499	0.431
Y_A	at O/at Fe	0.842	0.856	1.489	1.029	0.639	0.307
X_B	at O/at C	0.002	0.002	0.042	0.036	0.014	0.018
Y_B	at O/at Fe	0.260	0.187	0.581	0.389	0.154	0.027
X_W	at O/at C	0.298	0.315	0.314	0.298	0.324	0.318
Y_W	at O/at Fe	0.835	0.835	1.05	0.724	0.451	0.218
C/Fe	at C/at Fe	1.897	2.595	1.792	1.346	1.000	0.678
e_r	-	0.978	0.803	0.980	0.974	0.974	0.959

Table 6 Reactor Temperature, T, as a Function of Solids Residence Time, t.

A-1		A-2		B-1		B-2		B-3		B-4	
T °C	t min	T °C	t min	T °C	t min	T °C	t min	T °C	t min	T °C	t min
300	0.000	300	0.000	300	0.000	300	0.000	300	0.000	300	0.000
455	0.333	450	0.333	396	0.267	450	0.250	462	0.250	426	0.250
656	0.667	716	0.667	585	0.533	614	0.500	602	0.500	544	0.500
817	1.000	837	1.000	739	0.800	756	0.750	721	0.750	661	0.750
914	1.333	881	1.333	842	1.067	866	1.000	805	1.000	787	1.000
961	1.667	896	1.667	891	1.333	929	1.250	842	1.250	866	1.250
961	2.000	898	2.000	904	1.600	948	1.500	860	1.500	897	1.500
954	2.33	926	2.333	904	1.867	954	1.75o	873	1.750	897	1.750
954	2.667	946	2.667	904	2.133	954	2.000	873	2.000	897	2.000
954	3.000	898	3.000	897	2.400	954	2.250	873	2.250	897	2.250
954	3.333	600	3.333	879	2.667	954	2.500	866	2.500	891	2.500
954	3.667	300	3.600	866	2.933	954	2.750	866	2.750	891	2.750
908	4.000			830	3.200	954	3.000	860	3.000	891	3.000
673	4.333			721	3.467	885	3.250	757	3.250	854	3.250
390	4.667			532	3.733	691	3.500	544	3.500	726	3.500
300	4.833			300	4.000	467	3.750	331	3.750	496	3.750
						300	3.938	300	3.781	300	3.969

Table 7 Solids Analyses and Derived Parameters as a Function of Solids Residence Time

Test A-1

Index	Fe	Fe^{o}	Fe^{2+}	Fe^{3+}	C	$\frac{Fe_m}{Fe}$	$\frac{Fe^{2+}}{Fe}$	$\frac{Fe^{3+}}{Fe}$	$\frac{O}{Fe}$	$\frac{C_s}{Fe}$	t_r
	wt%	wt%	wt%	wt%	wt%				$\frac{\text{at O}}{\text{at Fe}}$	$\frac{\text{at C}}{\text{at Fe}}$	hr
1	72.2	14.8	56.2	1.2	0.066	0.205	0.778	0.017	0.842	4.25	-1.569
2	72.4	16.0	54.6	1.8	0.043	0.221	0.754	0.025	0.829	2.76	-0.508
3	72.1	15.4	55.7	1.0	0.038	0.214	0.773	0.014	0.832	2.45	0.007
4	72.3	16.0	54.8	1.5	0.048	0.221	0.758	0.021	0.827	3.09	0.586
5	72.4	16.6	54.4	1.4	0.043	0.229	0.751	0.019	0.818	2.76	1.069
6	73.0	19.4	53.0	0.6	0.043	0.266	0.726	0.008	0.775	2.74	1.391
7	73.2	20.6	51.0	1.6	0.034	0.281	0.697	0.022	0.764	2.16	1.745
8	73.2	21.2	51.2	0.8	0.005	0.290	0.699	0.011	0.751	0.32	2.098
9	73.4	23.2	49.2	1.0	0.010	0.316	0.670	0.014	0.724	0.63	2.420
10	74.2	25.8	46.8	1.6	0.010	0.348	0.631	0.022	0.695	0.63	2.742
11	74.9	30.4	44.0	0.5	0.024	0.406	0.587	0.007	0.627	1.49	3.128
12	75.2	31.8	40.8	2.6	0.005	0.423	0.543	0.035	0.622	0.31	3.482
13	77.8	45.8	30.0	2.0	0.010	0.589	0.386	0.026	0.443	0.60	3.739
14	81.0	65.0	15.2	0.8	0.043	0.802	0.188	0.010	0.212	2.47	4.029
15	82.2	73.1	8.9	0.2	0.076	0.889	0.108	0.002	0.117	4.30	4.319
16	81.4	65.4	14.6	1.4	0.081	0.803	0.179	0.017	0.214	4.63	4.640
17	82.3	66.0	15.6	0.7	0.081	0.802	0.190	0.009	0.212	4.58	4.994
18	81.8	67.0	13.2	1.6	0.076	0.819	0.161	0.020	0.199	4.32	5.284

Test A-2

Index	Fe	Fe^{o}	Fe^{2+}	Fe^{3+}	C	$\frac{Fe_m}{Fe}$	$\frac{Fe^{2+}}{Fe}$	$\frac{Fe^{3+}}{Fe}$	$\frac{O}{Fe}$	$\frac{C_s}{Fe}$	t_r
	wt%	wt%	wt%	wt%	wt%				$\frac{\text{at O}}{\text{at Fe}}$	$\frac{\text{at C}}{\text{at Fe}}$	hr
1	71.2	14.5	53.6	3.1	0.062	0.204	0.753	0.044	0.856	4.05	-0.302
2	71.8	14.8	53.8	3.2	0.043	0.206	0.749	0.045	0.854	2.78	0.060
3	71.6	14.7	51.2	5.7	0.062	0.205	0.715	0.080	0.870	4.03	0.445
4	72.8	16.5	51.6	4.7	0.043	0.227	0.709	0.065	0.841	2.75	0.806
5	72.8	20.0	49.4	3.4	0.034	0.275	0.679	0.047	0.783	2.17	1.047
6	73.1	22.1	46.4	4.6	0.034	0.302	0.635	0.063	0.761	2.16	1.264
7	73.4	23.8	44.0	5.6	0.019	0.324	0.599	0.076	0.744	1.20	1.529
8	74.1	27.1	43.0	4.0	0.029	0.366	0.580	0.054	0.690	1.82	1.794
9	74.7	27.0	42.6	5.1	0.015	0.361	0.570	0.068	0.701	0.93	2.034
10	75.0	31.6	38.4	5.0	0.010	0.421	0.512	0.067	0.638	0.62	2.251
11	76.4	38.1	35.1	3.2	0.005	0.499	0.459	0.042	0.545	0.30	2.540
12	79.0	53.6	24.2	1.2	0.010	0.678	0.306	0.015	0.344	0.59	2.853
13	81.4	65.5	14.6	1.3	0.029	0.805	0.179	0.016	0.212	1.66	3.094
14	81.8	67.6	12.7	1.5	0.043	0.826	0.155	0.018	0.191	2.44	3.359
15	83.0	68.8	11.8	2.4	0.085	0.829	0.142	0.029	0.193	4.76	3.600
16	83.2	74.5	7.9	0.8	0.085	0.895	0.095	0.010	0.114	4.75	3.793
17	83.0	74.7	7.1	1.2	0.081	0.900	0.086	0.014	0.112	4.54	4.058

Test B-1

Index	Fe	Fe^{o}	Fe^{2+}	Fe^{3+}	C	$\frac{Fe_m}{Fe}$	$\frac{Fe^{2+}}{Fe}$	$\frac{Fe^{3+}}{Fe}$	$\frac{O}{Fe}$	$\frac{C_s}{Fe}$	t_r
	wt%	wt%	wt%	wt%	wt%				$\frac{\text{at O}}{\text{at Fe}}$	$\frac{\text{at C}}{\text{at Fe}}$	hr
1	67.7	0.2	1.0	66.4	0.052	0.003	0.016	0.982	1.489	3.57	-0.696
2	68.1	0.2	2.9	64.9	0.026	0.003	0.043	0.954	1.476	1.78	0.535
3	71.0	0.1	33.7	37.2	0.025	0.001	0.474	0.525	1.285	1.64	1.050
4	73.3	0.2	57.6	15.5	0.016	0.003	0.786	0.211	1.142	1.01	1.394
5	73.9	0.3	62.2	11.4	0.019	0.004	0.842	0.154	1.115	1.20	1.680
6	74.5	0.3	64.1	10.1	0.003	0.004	0.860	0.136	1.107	0.19	1.967
7	74.5	0.2	67.4	6.9	0.019	0.003	0.905	0.093	1.089	1.19	2.253
8	75.1	1.4	68.2	5.5	0.022	0.019	0.908	0.073	1.063	1.36	2.540
9	75.7	5.4	66.0	4.3	0.008	0.071	0.872	0.057	1.001	0.49	2.826
10	77.4	15.8	58.2	3.4	0.006	0.204	0.752	0.044	0.855	0.36	3.112
11	79.4	29.2	48.5	1.7	0.030	0.368	0.611	0.021	0.673	1.76	3.399
12	80.7	39.3	40.0	1.4	0.412	0.487	0.496	0.017	0.546	23.74	3.685
13	79.8	41.9	37.9	0.0	1.350	0.525	0.475	0.000	0.499	78.66	3.971
14	79.6	38.4	38.8	2.4	1.330	0.482	0.487	0.030	0.557	77.69	4.258
15	79.7	40.4	37.8	1.5	1.340	0.507	0.474	0.019	0.526	78.18	4.544
16	79.5	39.4	38.1	2.0	1.330	0.496	0.479	0.025	0.541	77.79	4.830
17	80.2	40.9	37.4	1.9	1.420	0.510	0.466	0.024	0.525	82.33	5.117

Test B-2

Index	Fe	Fe^{o}	Fe^{2+}	Fe^{3+}	C	$\frac{Fe_m}{Fe}$	$\frac{Fe^{2+}}{Fe}$	$\frac{Fe^{3+}}{Fe}$	$\frac{O}{Fe}$	$\frac{C_s}{Fe}$	t_r
	wt%	wt%	wt%	wt%	wt%				$\frac{\text{at O}}{\text{at Fe}}$	$\frac{\text{at C}}{\text{at Fe}}$	hr
1	73.8	20.2	15.4	38.2	0.027	0.274	0.209	0.518	0.996	1.70	1.018
2	75.8	23.9	31.4	20.5	0.016	0.315	0.414	0.270	0.841	0.98	1.301
3	77.4	25.1	45.9	6.4	0.030	0.324	0.593	0.083	0.747	1.80	1.585
4	77.9	23.4	51.2	3.3	0.016	0.300	0.657	0.042	0.754	0.96	1.868
5	79.3	30.8	46.6	1.9	0.030	0.388	0.588	0.024	0.653	1.76	2.152
6	80.0	32.8	44.9	2.3	0.016	0.410	0.561	0.029	0.632	0.93	2.435
7	80.2	37.2	42.0	1.0	0.044	0.464	0.524	0.012	0.569	2.55	2.719
8	79.8	30.9	46.7	2.2	0.011	0.387	0.585	0.028	0.656	0.64	2.974
9	81.5	44.3	36.6	0.6	0.016	0.544	0.449	0.007	0.483	0.91	3.229
10	83.1	48.1	33.4	1.6	0.006	0.579	0.402	0.019	0.451	0.34	3.512
11	86.3	66.2	19.2	0.9	0.243	0.767	0.222	0.010	0.249	13.09	3.796
12	83.4	50.5	31.4	1.5	0.744	0.606	0.376	0.018	0.422	41.48	4.051
13	84.1	59.3	23.9	0.9	0.927	0.705	0.284	0.011	0.314	51.25	4.306

Test B-3

Index	Fe	Fe^{o}	Fe^{2+}	Fe^{3+}	C	$\frac{Fe_m}{Fe}$	$\frac{Fe^{2+}}{Fe}$	$\frac{Fe^{3+}}{Fe}$	$\frac{O}{Fe}$	$\frac{C_s}{Fe}$	t_r
	wt%	wt%	wt%	wt%	wt%				$\frac{\text{at O}}{\text{at Fe}}$	$\frac{\text{at C}}{\text{at Fe}}$	hr
1	80.8	46.3	15.5	19.0	0.063	0.573	0.192	0.235	0.554	3.63	0.578
2	79.9	37.7	32.7	9.5	0.041	0.472	0.409	0.119	0.608	2.39	0.890
3	83.1	51.2	29.1	2.8	0.033	0.616	0.350	0.034	0.418	1.85	1.145
4	85.4	57.6	26.4	1.4	0.027	0.674	0.309	0.016	0.349	1.47	1.400
5	80.9	42.4	37.2	1.3	0.046	0.524	0.460	0.016	0.507	2.64	1.684
6	85.2	59.3	24.2	1.7	0.022	0.696	0.284	0.020	0.328	1.20	1.967
7	83.0	50.6	31.5	0.9	0.038	0.610	0.380	0.011	0.415	2.13	2.222
8	86.5	66.2	19.3	1.0	0.014	0.765	0.223	0.012	0.252	0.75	2.477
9	87.5	68.8	17.4	1.3	0.060	0.786	0.199	0.015	0.231	3.19	2.732
10	86.5	65.7	19.8	1.0	0.054	0.760	0.229	0.012	0.258	2.90	2.959
11	89.4	77.6	10.5	1.3	0.245	0.868	0.117	0.015	0.145	12.74	3.186
12	88.7	77.8	9.8	1.1	0.292	0.877	0.110	0.012	0.135	15.31	3.441
13	89.2	73.9	13.2	2.1	0.311	0.828	0.148	0.024	0.191	16.21	3.725
14	89.3	78.6	9.8	0.9	0.311	0.880	0.110	0.010	0.130	16.19	4.008
15	88.6	77.5	10.6	0.5	0.314	0.875	0.120	0.006	0.134	16.48	4.405

Test B-4

Index	Fe	Fe^{o}	Fe^{2+}	Fe^{3+}	C	$\frac{Fe_m}{Fe}$	$\frac{Fe^{2+}}{Fe}$	$\frac{Fe^{3+}}{Fe}$	$\frac{O}{Fe}$	$\frac{C_s}{Fe}$	t_r
	wt%	wt%	wt%	wt%	wt%				$\frac{\text{at O}}{\text{at Fe}}$	$\frac{\text{at C}}{\text{at Fe}}$	hr
1	85.7	64.6	19.2	1.9	0.061	0.754	0.224	0.022	0.268	3.31	1.415
2	88.3	72.0	15.2	1.1	0.065	0.815	0.172	0.012	0.199	3.42	1.780
3	87.6	69.1	17.4	1.1	0.055	0.789	0.199	0.013	0.227	2.92	2.061
4	-	-	-	-	-	-	-	-	-	-	-
5	-	-	-	-	-	-	-	-	-	-	-
6	90.4	81.2	7.9	1.3	0.055	0.898	0.087	0.014	0.113	2.83	2.903
7	89.5	78.3	10.0	1.2	0.065	0.875	0.112	0.013	0.137	3.38	3.183
8	91.2	85.3	5.4	0.5	0.098	0.935	0.059	0.005	0.070	5.00	3.492
9	91.4	87.7	3.0	0.7	0.205	0.960	0.033	0.008	0.046	10.43	3.744
10	92.4	89.2	2.0	1.2	0.270	0.965	0.022	0.013	0.042	13.59	3.997
11	91.3	86.2	4.0	1.1	0.234	0.944	0.044	0.012	0.064	11.92	4.305
12	91.8	87.6	3.8	0.4	0.264	0.954	0.041	0.004	0.050	13.37	4.558
13	92.3	89.5	1.7	1.1	0.256	0.970	0.018	0.012	0.037	12.90	4.782
14	92.2	89.2	2.5	0.5	0.264	0.967	0.027	0.005	0.037	13.31	5.063
15	92.4	89.8	1.8	0.8	0.286	0.972	0.019	0.009	0.033	14.39	5.400

Table 8 Comparison of Carbon Deposition Rates, n_c, calculated from:

(a) Reaction Vessel Inlet and Outlet Reducing Gas Flow Rates

(b) Carbon and Iron Analyses of Solids, and Iron Flow Rates

Test	n_c, at C/min	
	(a)	(b)
A-1	0.0004	0.0046
A-2	0.0006	0.0084
B-1	0.0110	0.0110
B-2	0.0075	0.0053
B-3	0.0022	0.0024
B-4	0.0020	0.0041

Table 9 Carbon Deposited at Solids Outlet of Reactor, Determined from Cs/Fe Profiles of Figure 20

Test	Carbon Deposited at C/at Fe
A-1	0.004
A-2	0.004
B-1	0.076
B-2	0.049
B-3	0.014
B-4	0.012

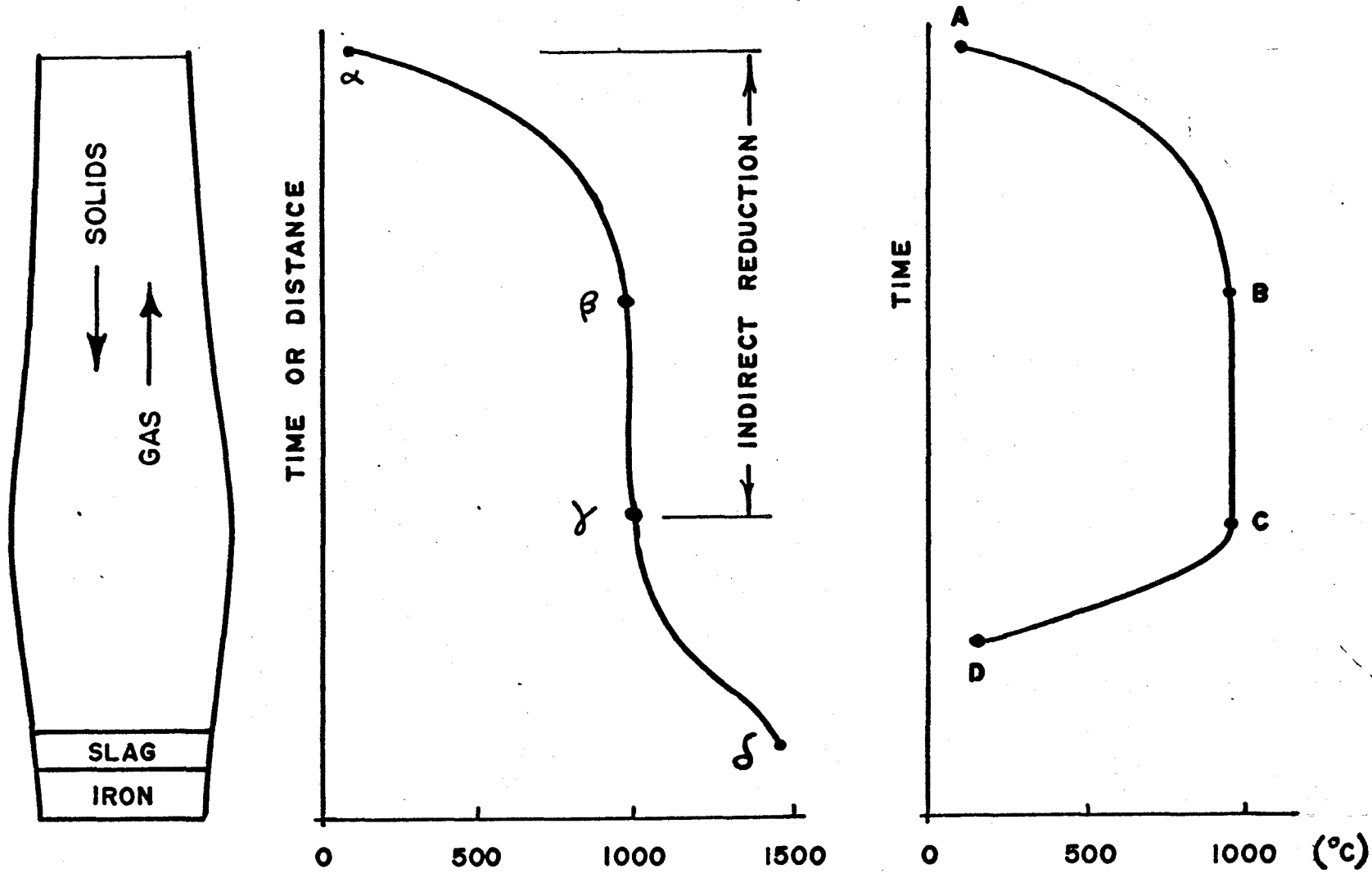

(A)
BLAST FURNACE

(B)
TEMPERATURE PROFILE OF BLAST FURNACE

(C)
TEMPERATURE PROFILE OF LABORATORY REACTOR

FIGURE 1 BLAST FURNACE AND REACTOR TEMPERATURE PROFILES

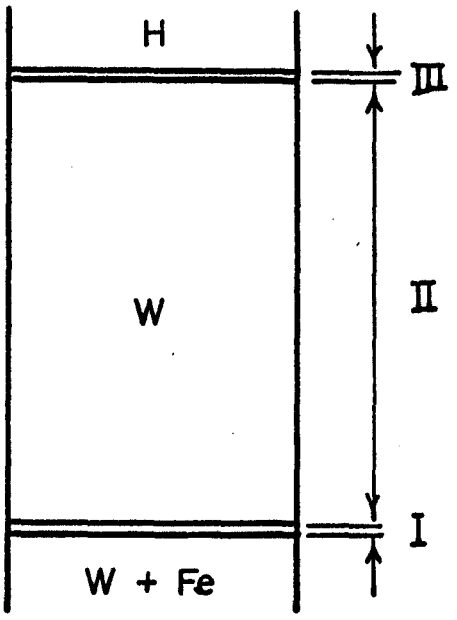

(A) $t_s = \infty$

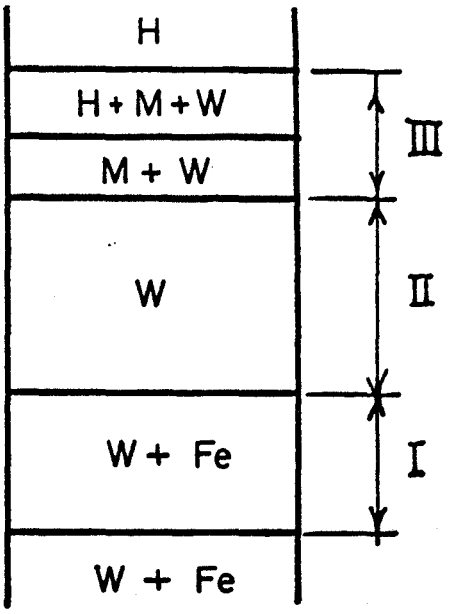

(B) $\infty > t_s > t_s^*$

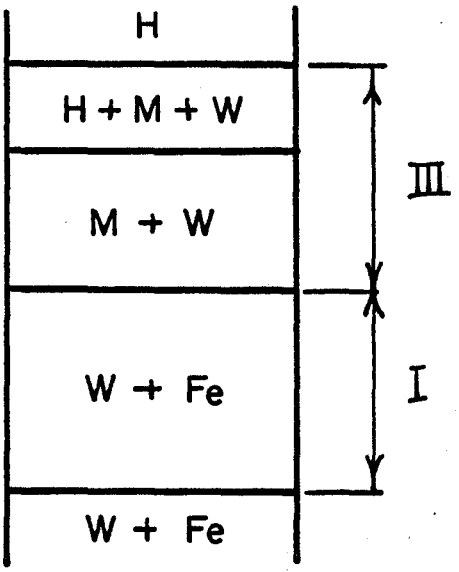

(C) $t_s = t_s^*$

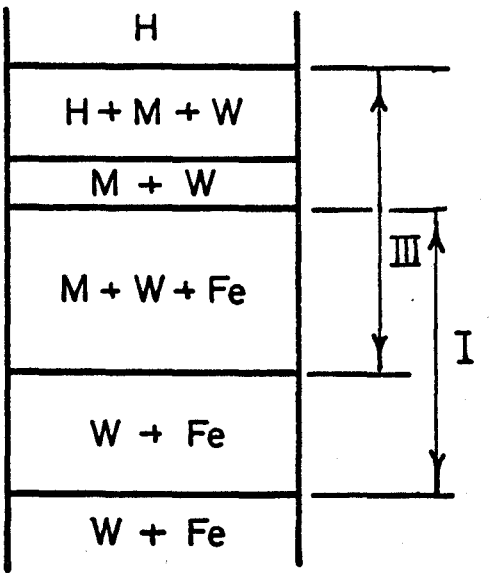

(D) $t_s < t_s^*$

FIGURE 2 DISPOSITION OF IRON OXIDES IN AN ISOTHERMAL COUNTER-FLOW REACTOR FOR VARIOUS SOLIDS RESIDENCE TIMES

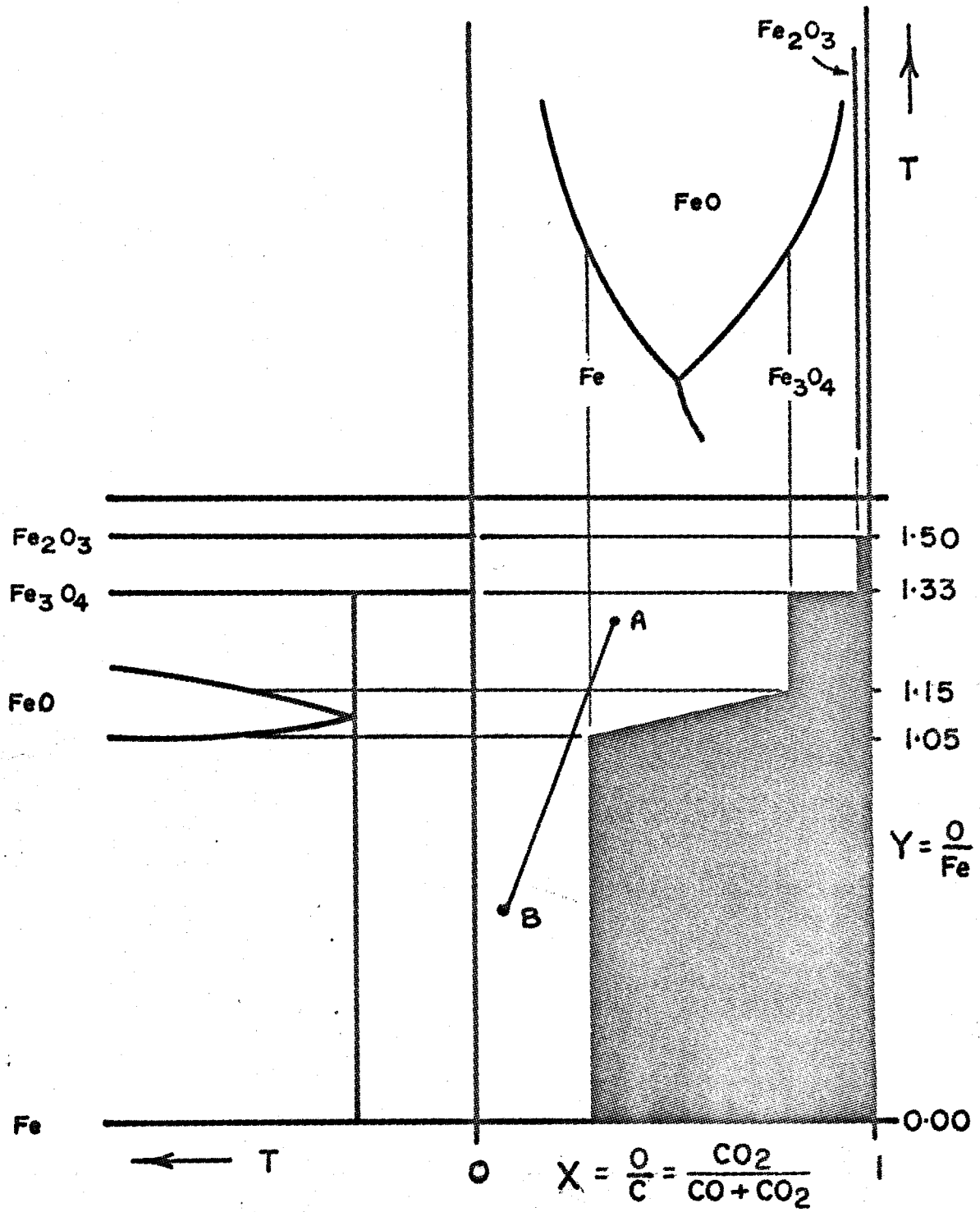

FIGURE 3 CONSTRUCTION OF EQUILIBRIUM CONTOUR IN OXYGEN TRANSFER DIAGRAM

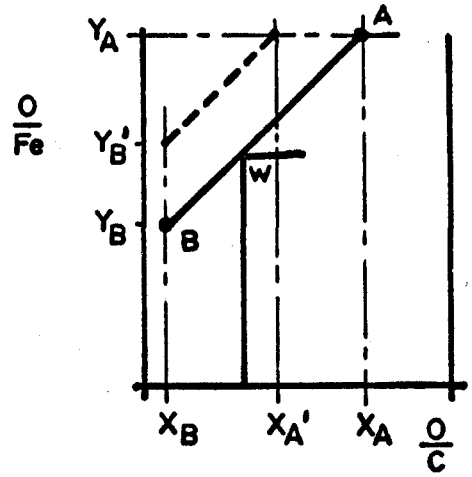

(A) OXYGEN TRANSFER DIAGRAM

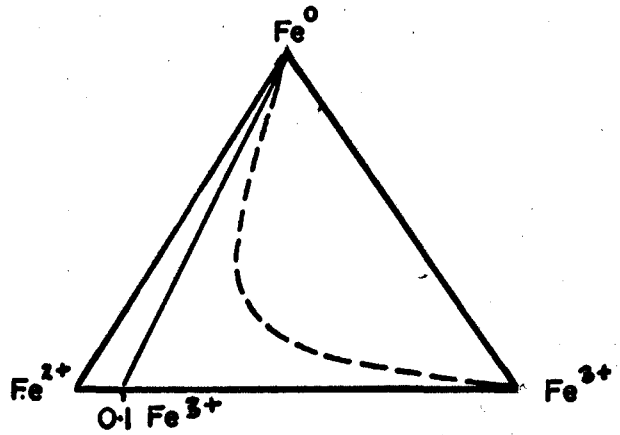

(B) REDUCTION PATH DIAGRAM

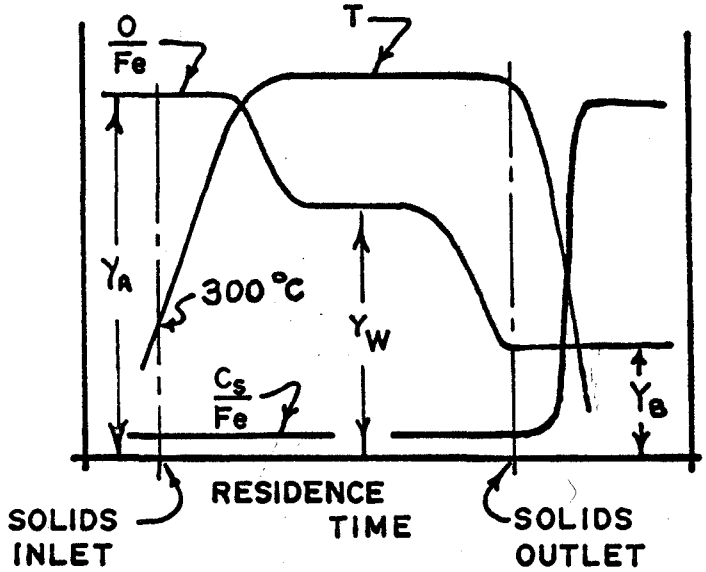

(C) RESIDENCE TIME DIAGRAM

FIGURE 4 GRAPHICAL REPRESENTATION OF CHEMICAL REACTION EFFECTS

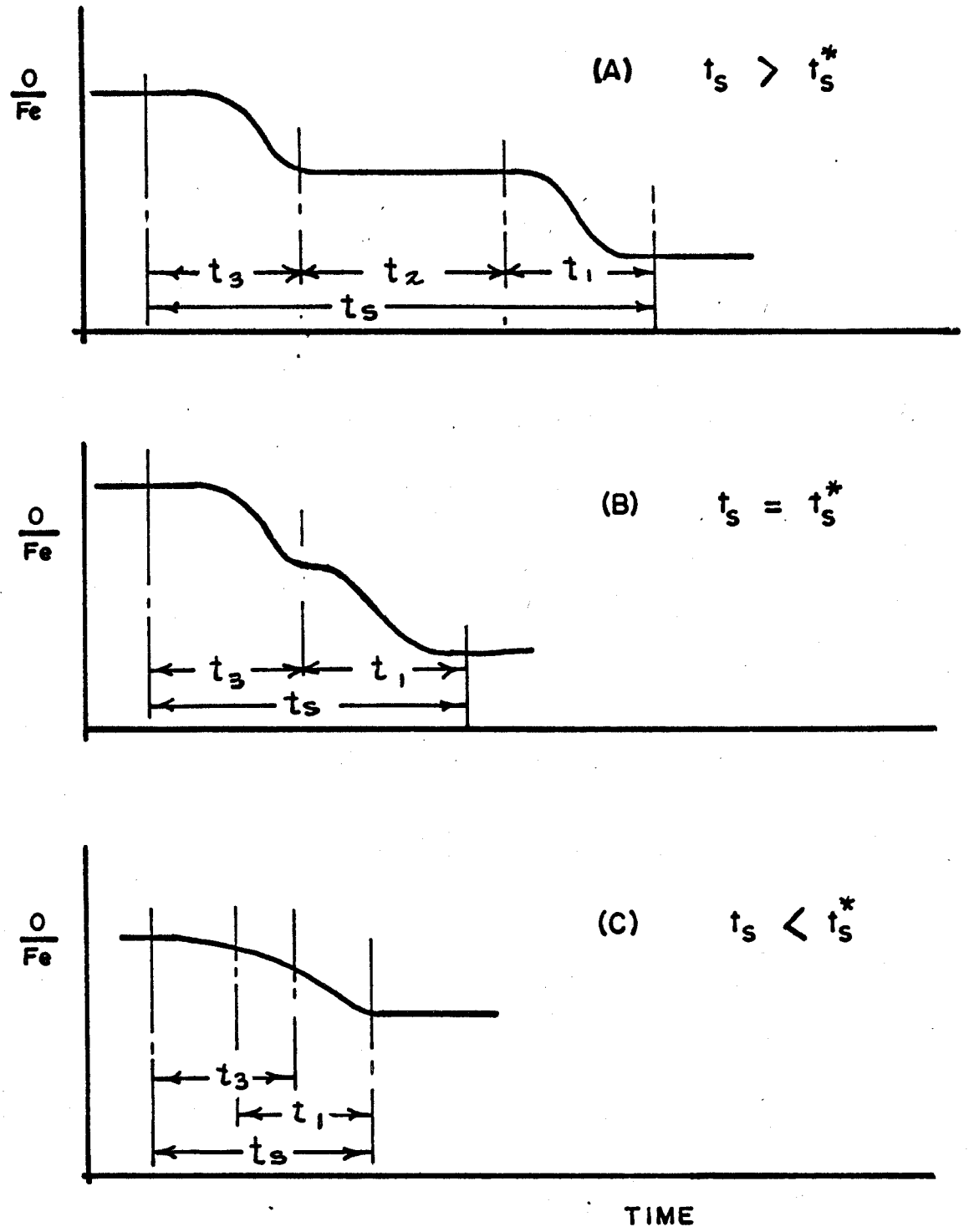

FIGURE 5 TYPICAL VARIATION OF O/Fe PROFILE WITH SOLIDS RESIDENCE TIME IN REACTOR

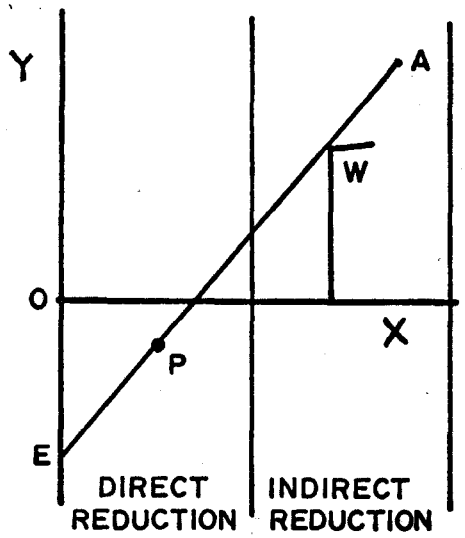

(A) OPERATION WITH OXIDE BURDEN

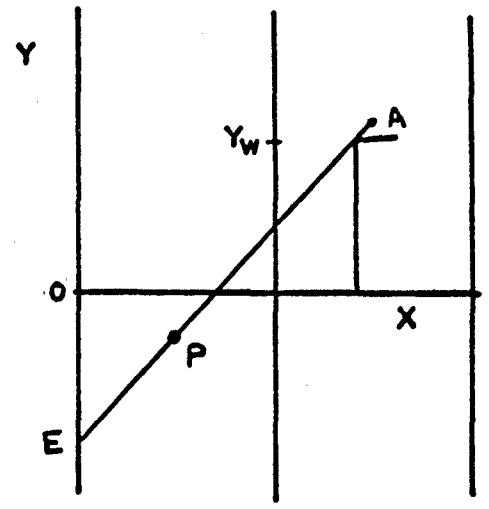

(B) OPERATION WITH ORE BURDEN PARTLY PREREDUCED TO WUSTITE

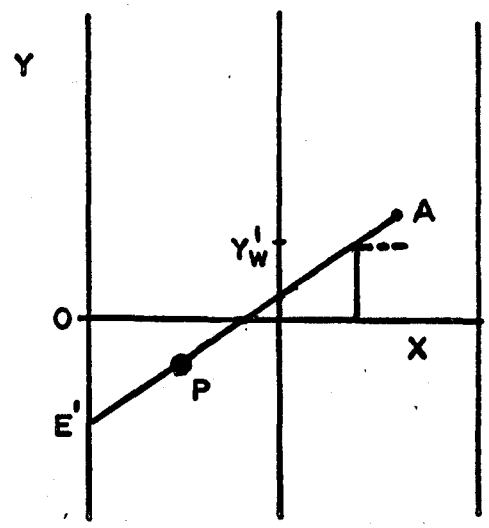

(C) OPERATION WITH ORE BURDEN PARTLY PREREDUCED TO METALLIC IRON

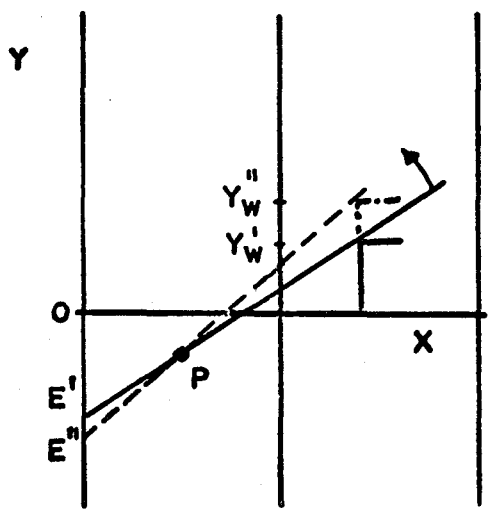

(D) ROTATION OF OPERATING LINE DUE TO METALLIC IRON OXIDATION

FIGURE 6 TYPICAL OXYGEN TRANSFER DIAGRAMS FOR BLAST FURNACE OPERATION

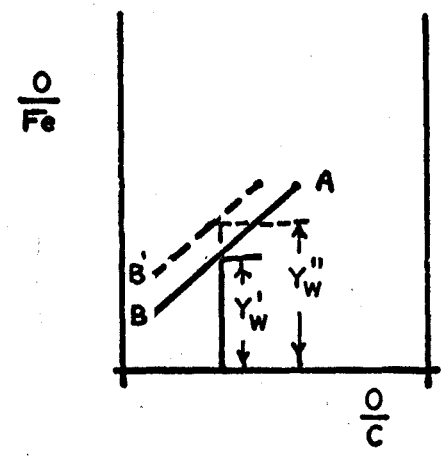

(A) OXYGEN TRANSFER DIAGRAM

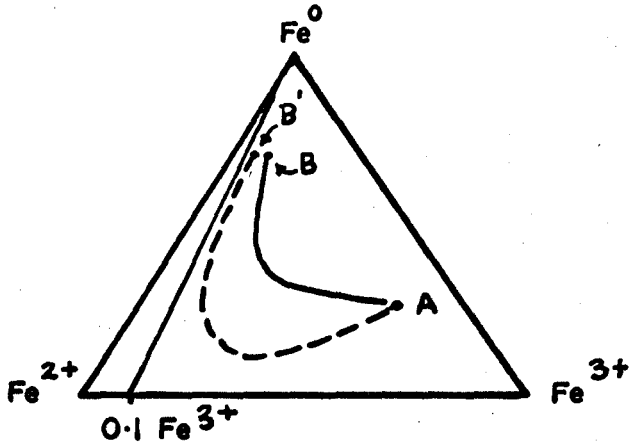

(B) REDUCTION PATH DIAGRAM

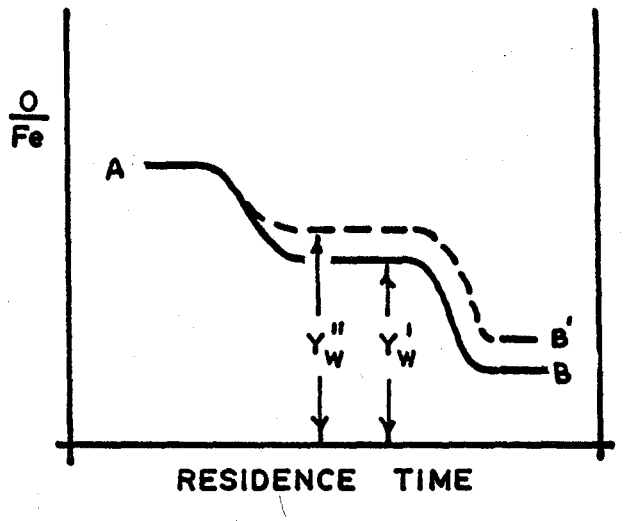

(C) RESIDENCE TIME DIAGRAM

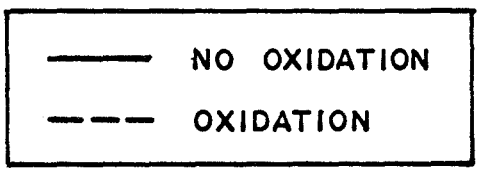

FIGURE 7 GRAPHICAL REPRESENTATION OF METALLIC IRON OXIDATION EFFECTS

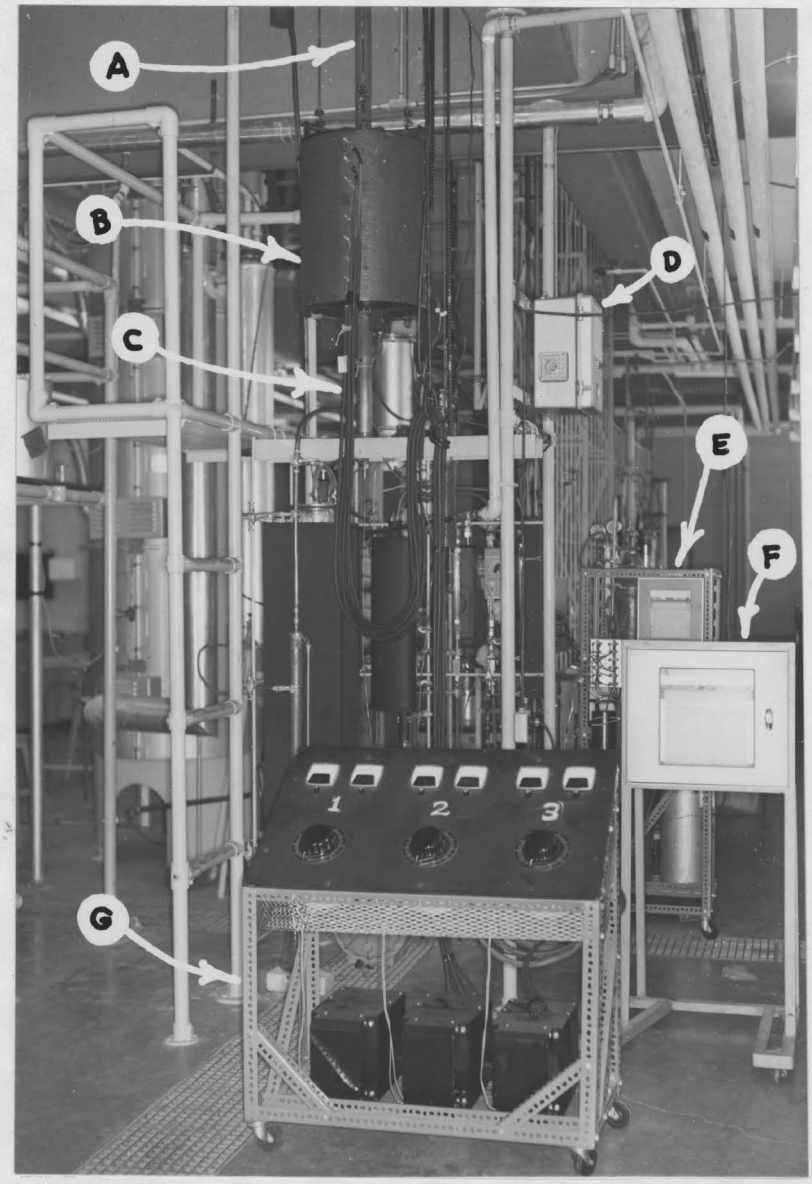

A	REACTION VESSEL
B	FURNACE
C	POWER CABLES
D	CARBON MONOXIDE ALARM
E	GAS CHROMATOGRAPH
F	TEMPERATURE RECORDER
G	FURNACE POWER CONTROL UNIT

FIGURE 8 OVERALL VIEW OF APPARATUS

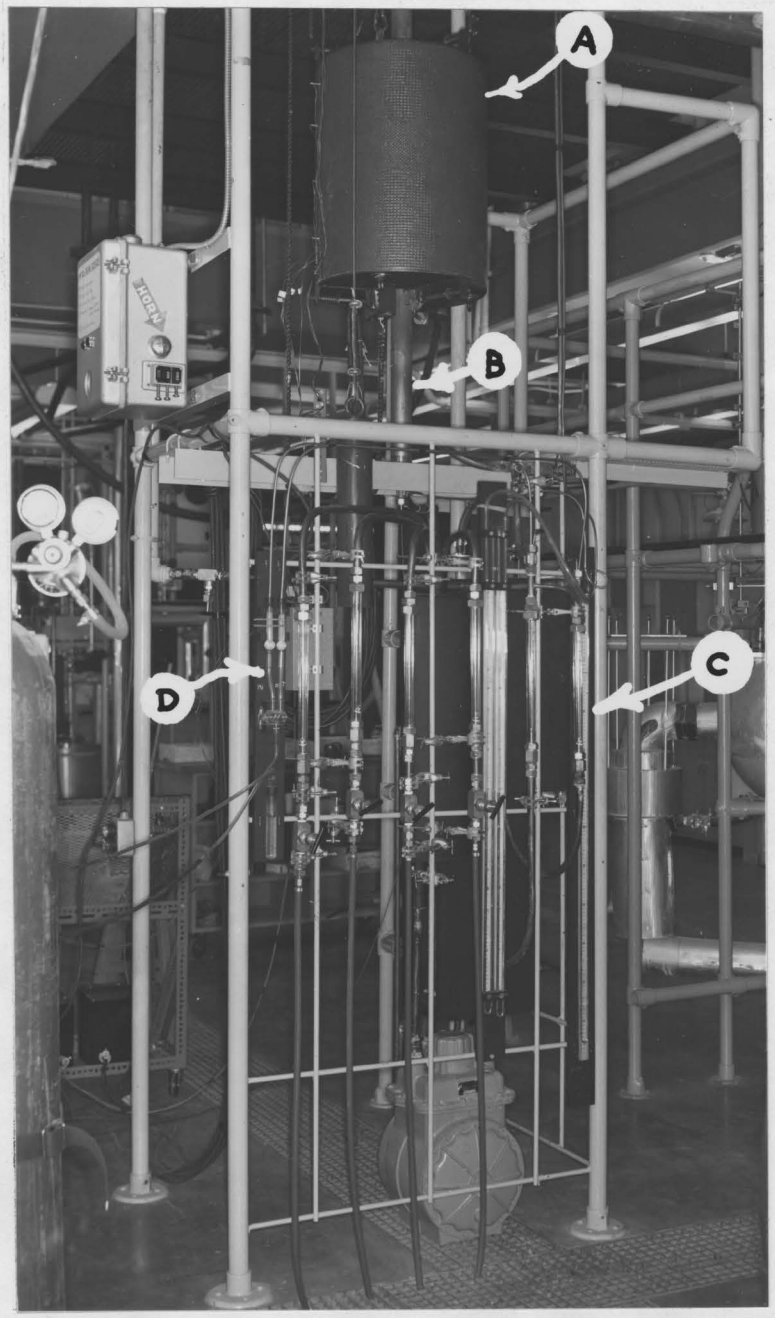

A FURNACE

B REACTION VESSEL

C FLOWMETERS

D GAS SAMPLING LINES

FIGURE 9 OVERALL VIEW OF APPARATUS

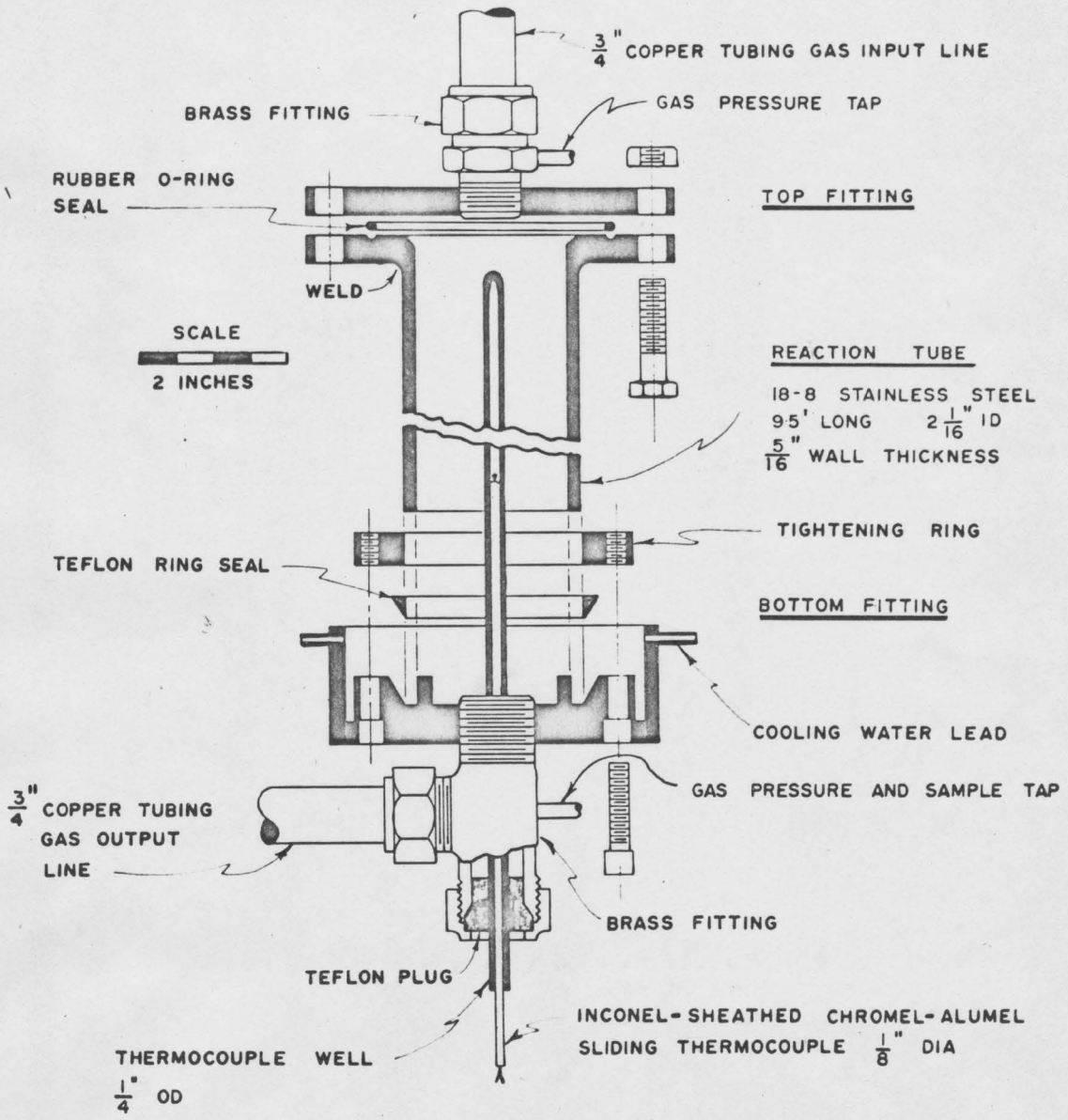

FIGURE 10 REACTION VESSEL

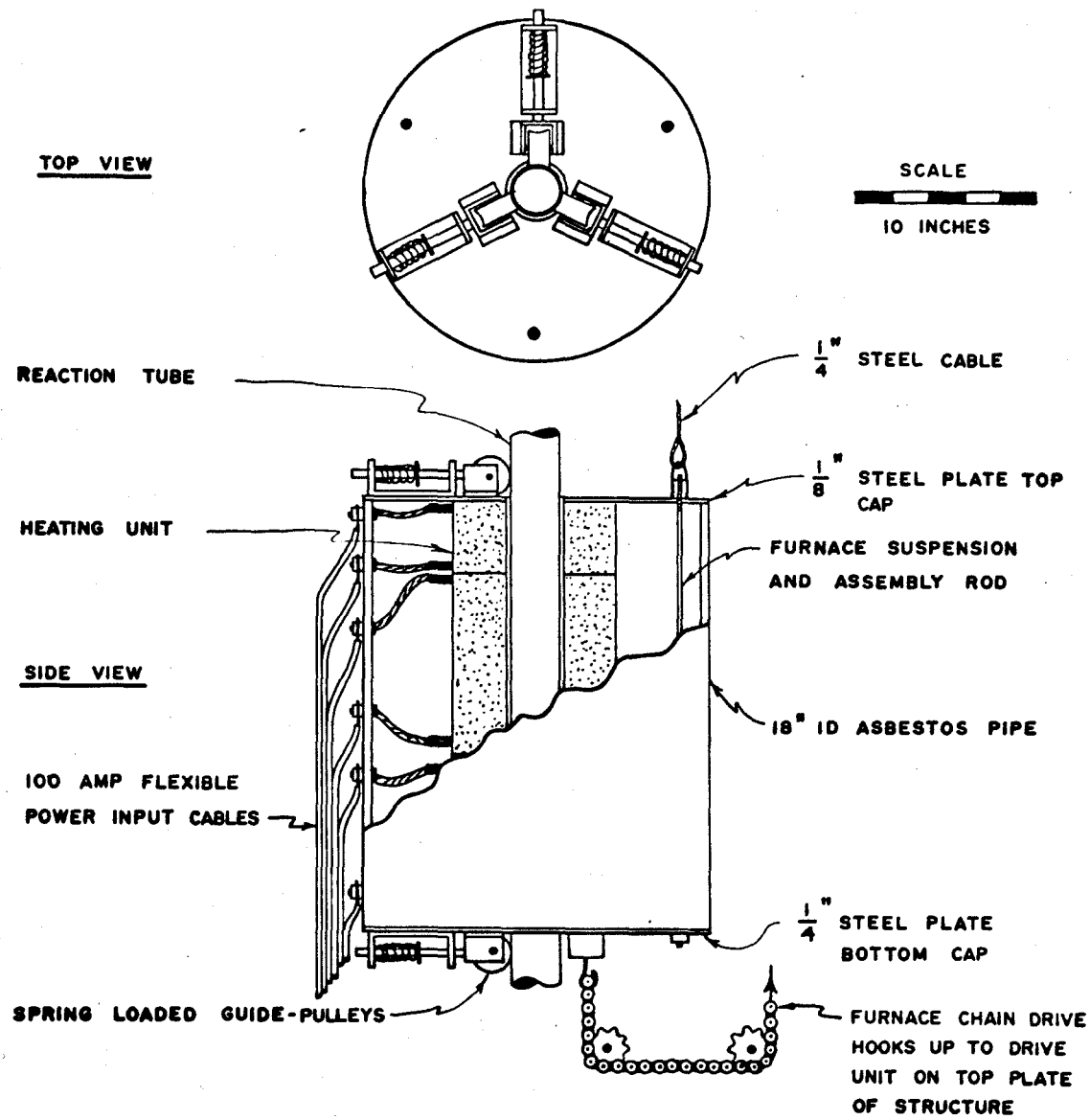

FIGURE 11 CONSTRUCTION DETAILS OF FURNACE SHELL

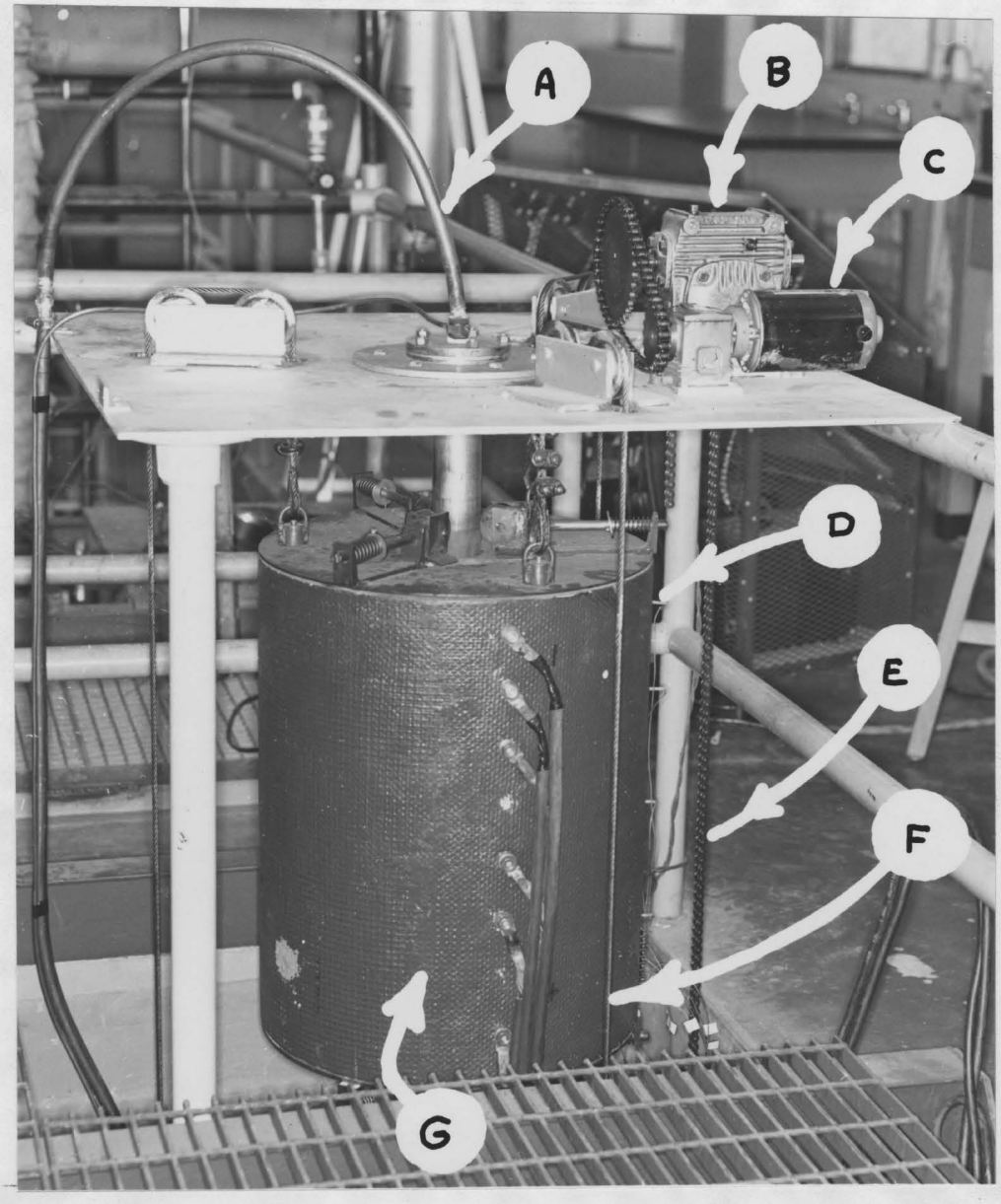

A GAS INLET TUBE
B DEMULTIPLYING DEVICE
C FURNACE MOTOR
D WINDING THERMOCOUPLE
E FURNACE DRIVE CHAIN
F FURNACE SUSPENSION CABLE
G FURNACE SHELL

FIGURE 12 CONSTRUCTION DETAILS OF APPARATUS

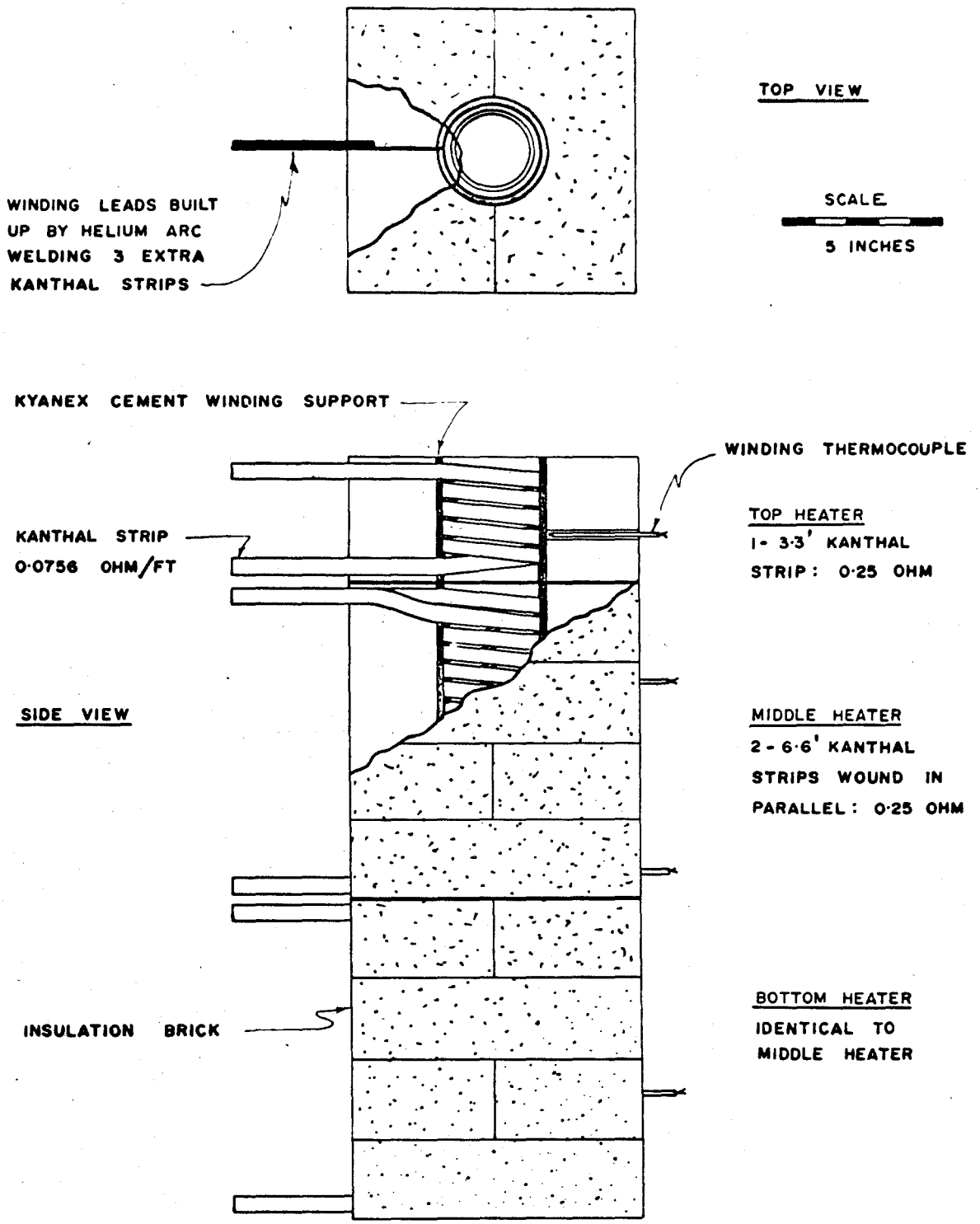

FIGURE 13 CONSTRUCTION DETAILS OF FURNACE HEATING UNIT

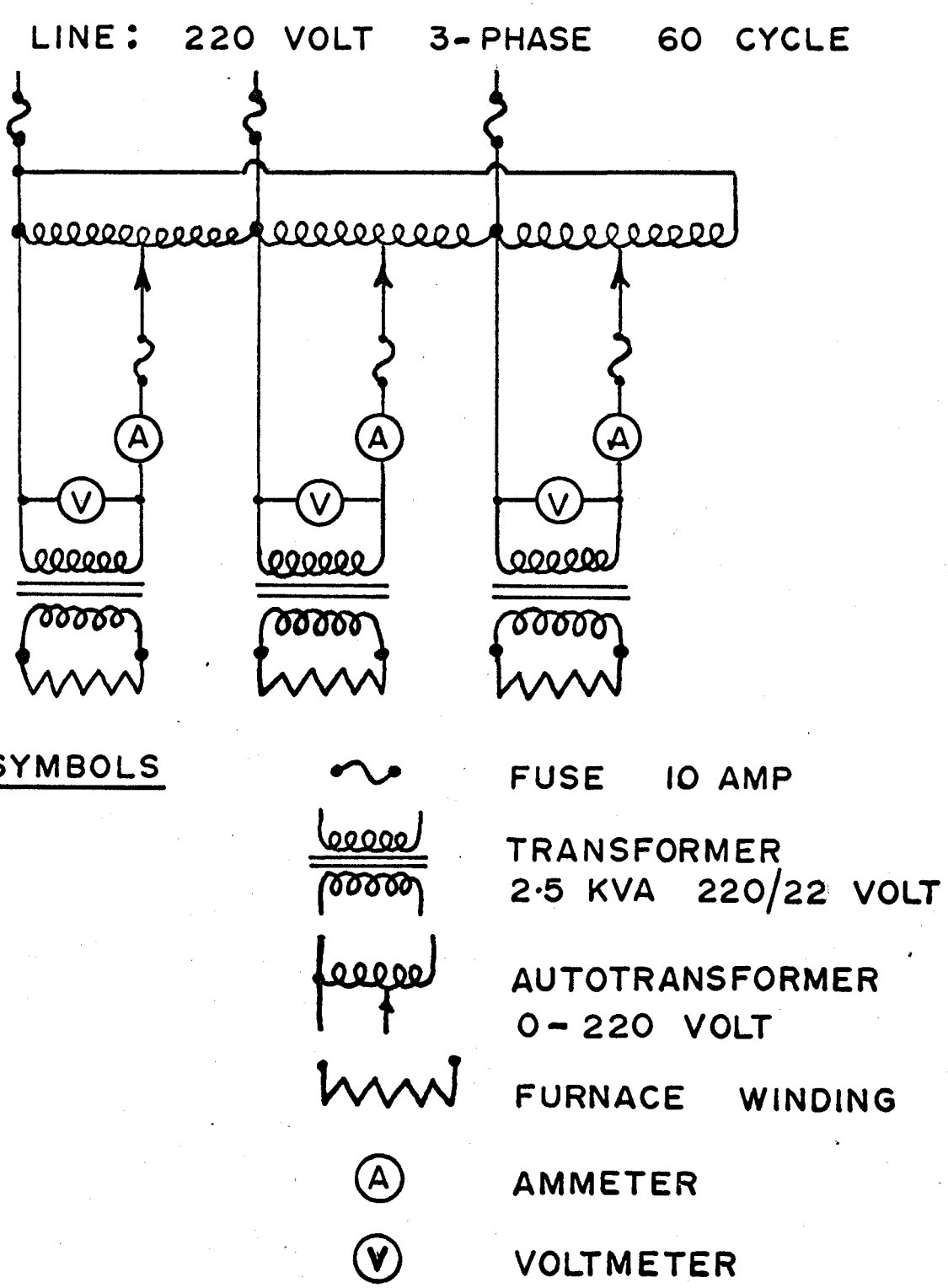

FIGURE 14 WIRING DIAGRAM OF FURNACE POWER CONTROL UNIT.

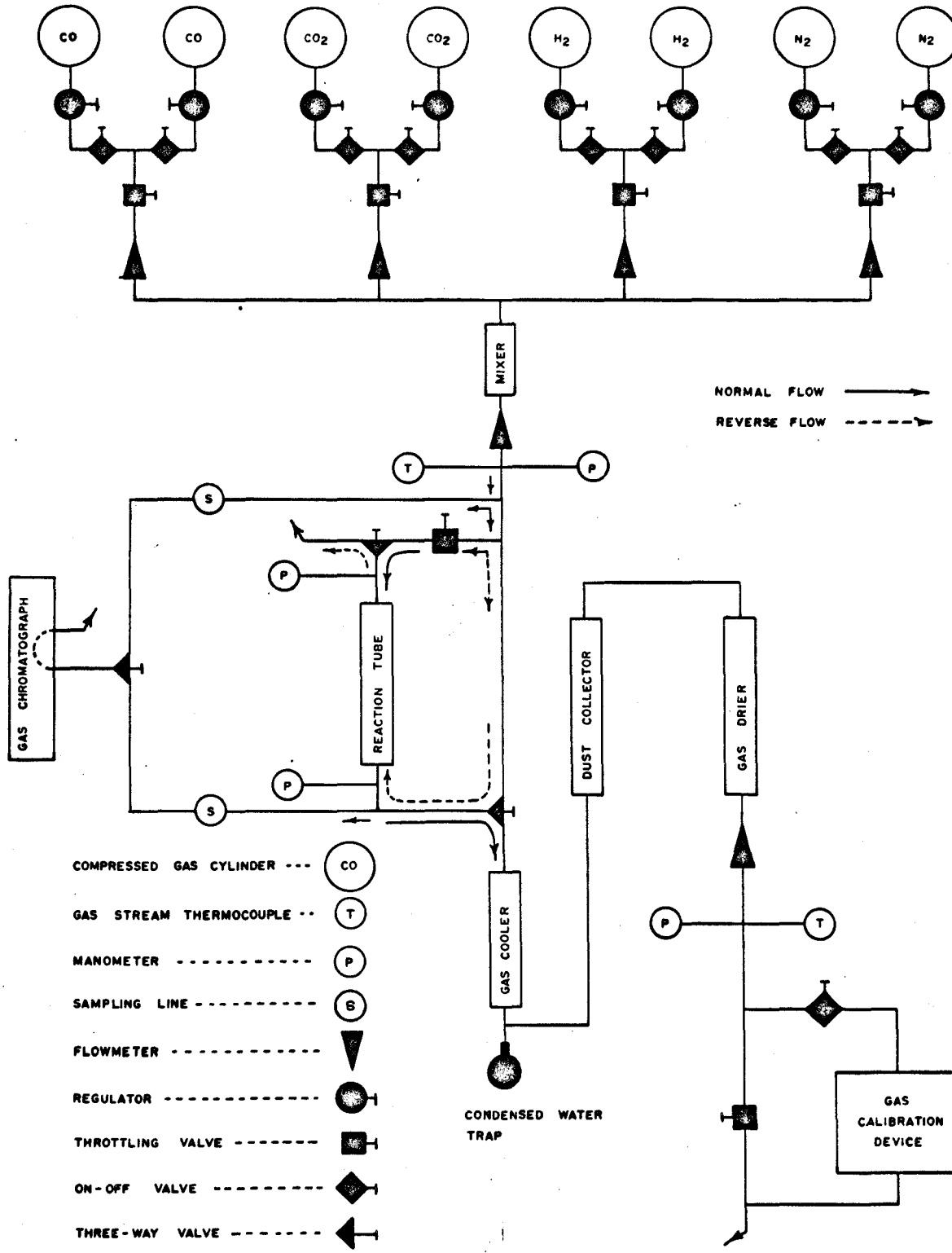

FIGURE 15 APPARATUS GAS TRAIN

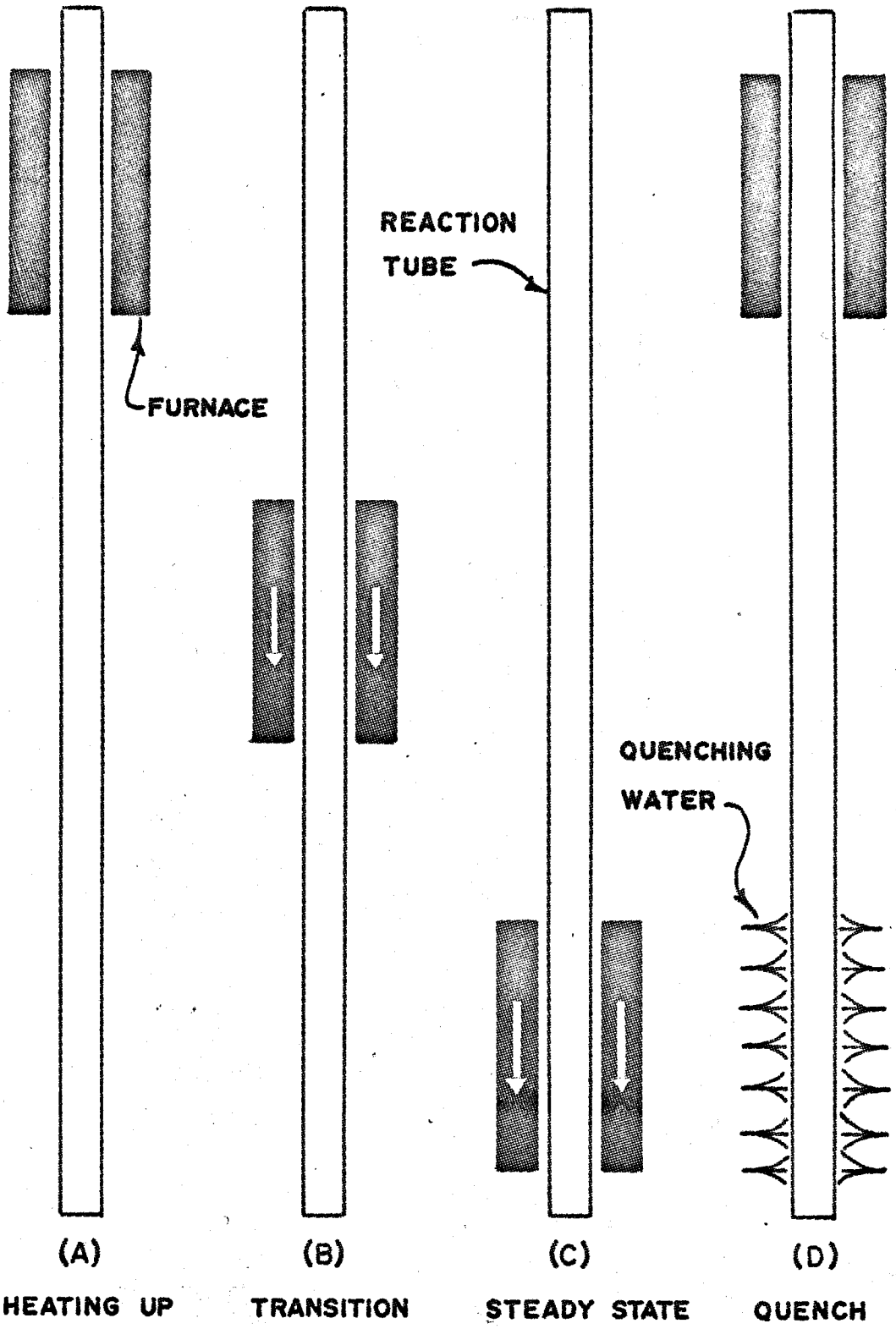

FIGURE 16 POSITION OF FURNACE AT VARIOUS STAGES OF AN EXPERIMENT

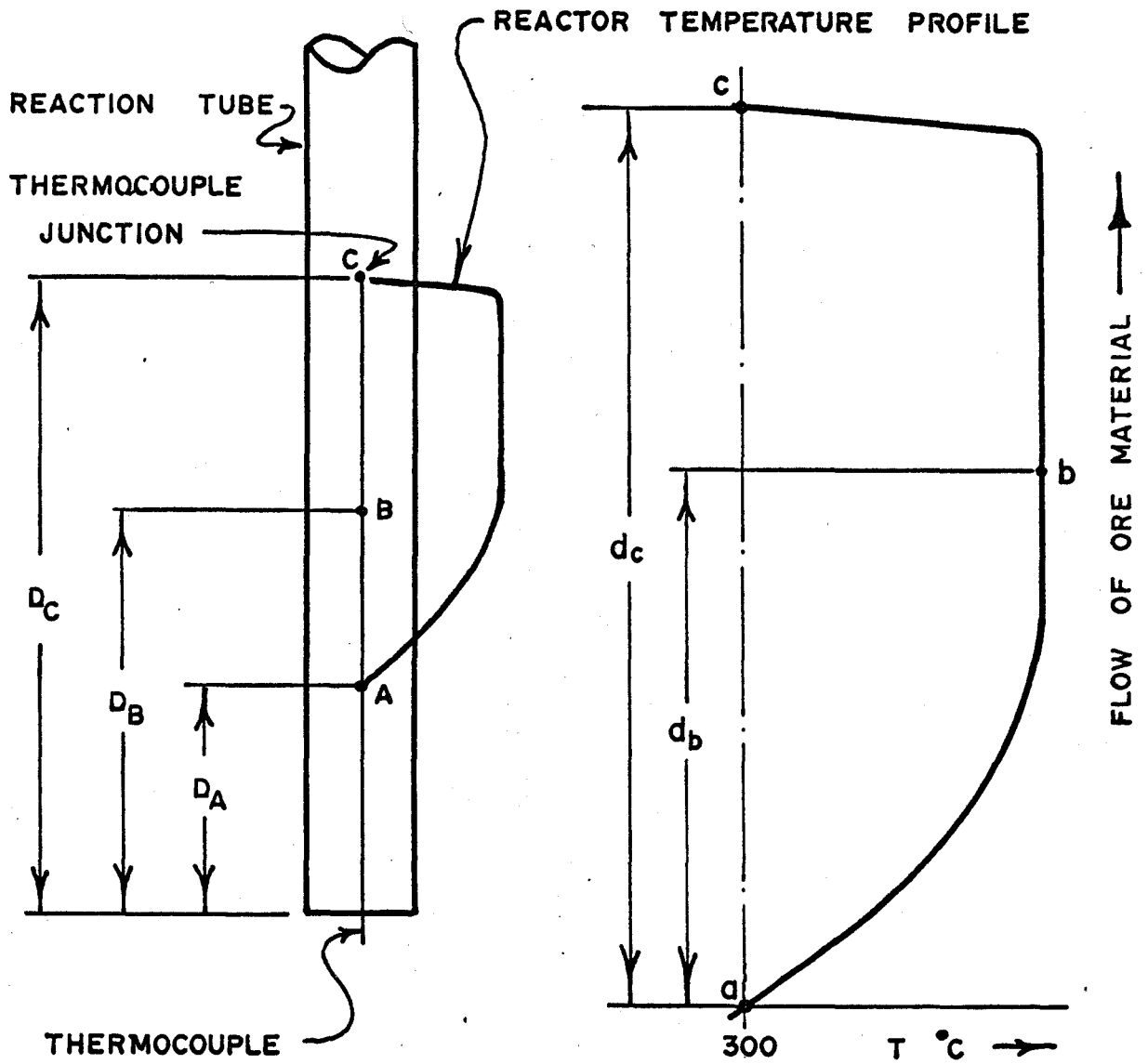

FIGURE 17 SCHEMATIC DIAGRAM ILLUSTRATING VARIOUS QUANTITIES INVOLVED IN THE CORRELATION OF O/Fe AND TEMPERATURE PROFILES

Figure 18 Oxygen Transfer Diagrams for Reduction Tests A-1, A-2, B-1, B-2, B-3 and B-4

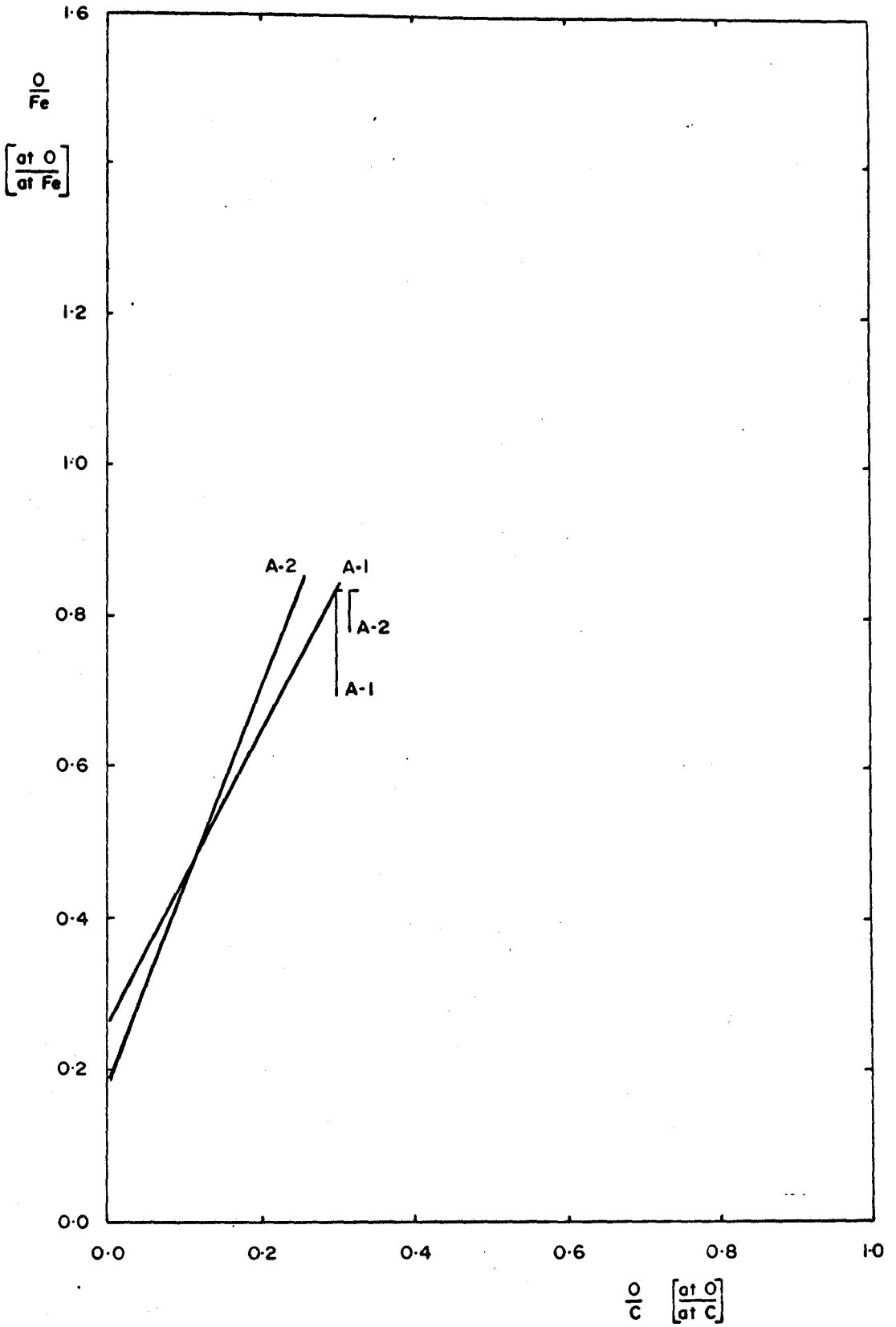
1·6
O/Fe
[at O/at Fe]
1·2
1·0
0·8
0·6
0·4
0·2
0·0
A-2
A-1
A-2
A-1
0·0
0·2
0·4
0·6
0·8
1·0
O/C [at O/at C]

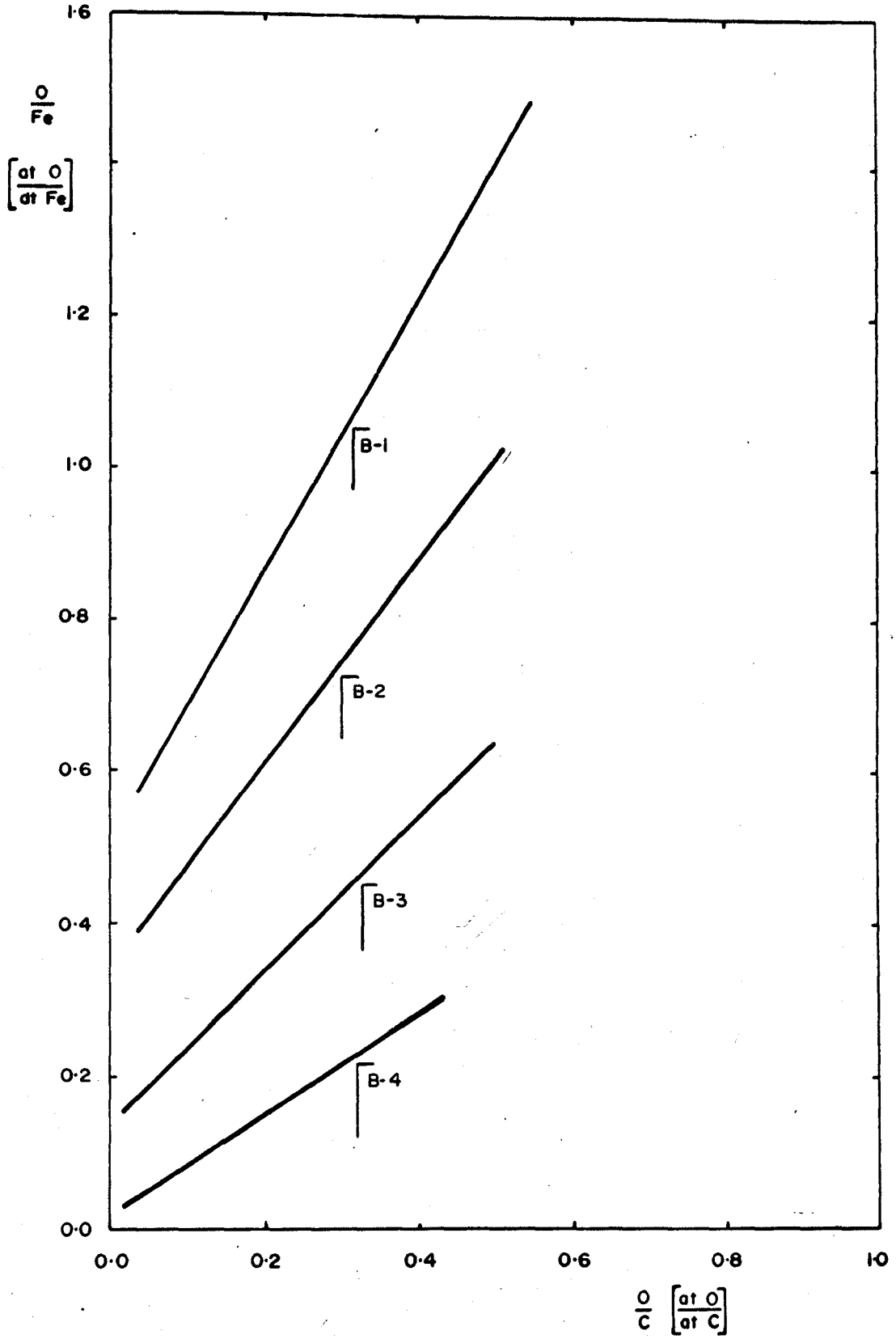
1·6
O/Fe
[at O / at Fe]
1·2
1·0
0·8
0·6
0·4
0·2
0·0
B-1
B-2
B-3
B-4
0·0
0·2
0·4
0·6
0·8
1·0
O/C [at O / at C]

Figure 19 Reduction Path Diagrams for Reduction Tests A-1, A-2, B-1, B-2, B-3 and B-4

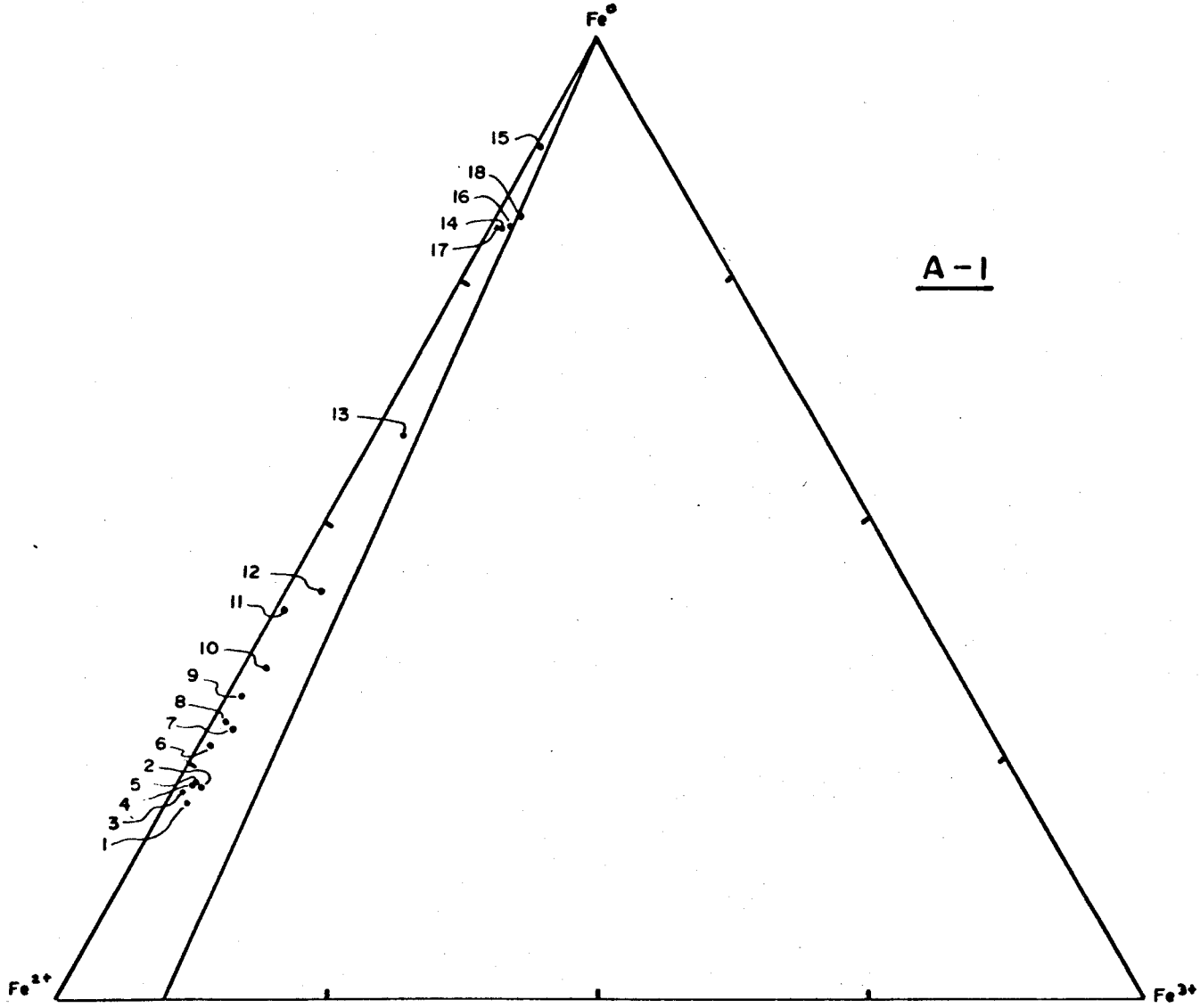

A-1

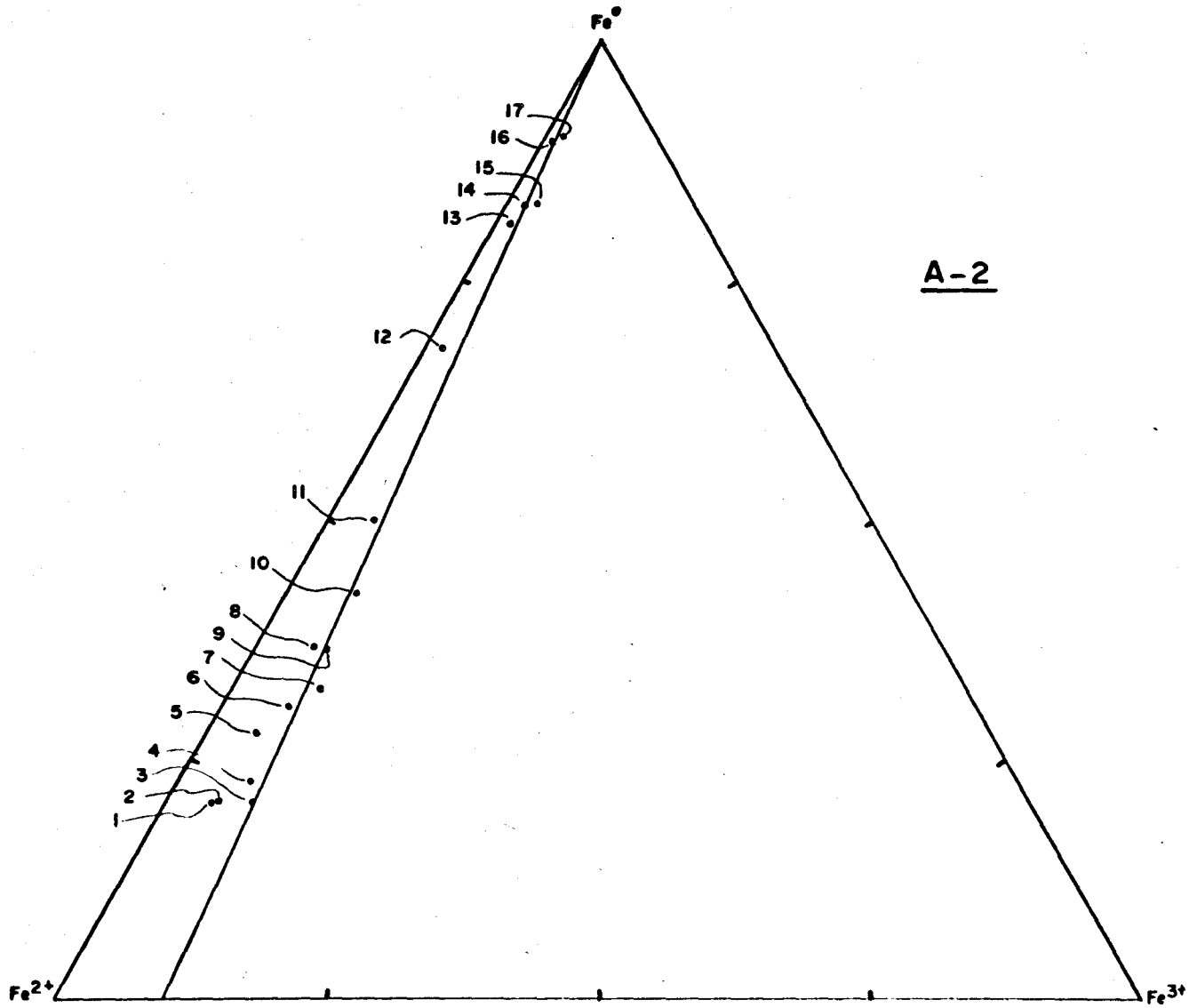

A-2

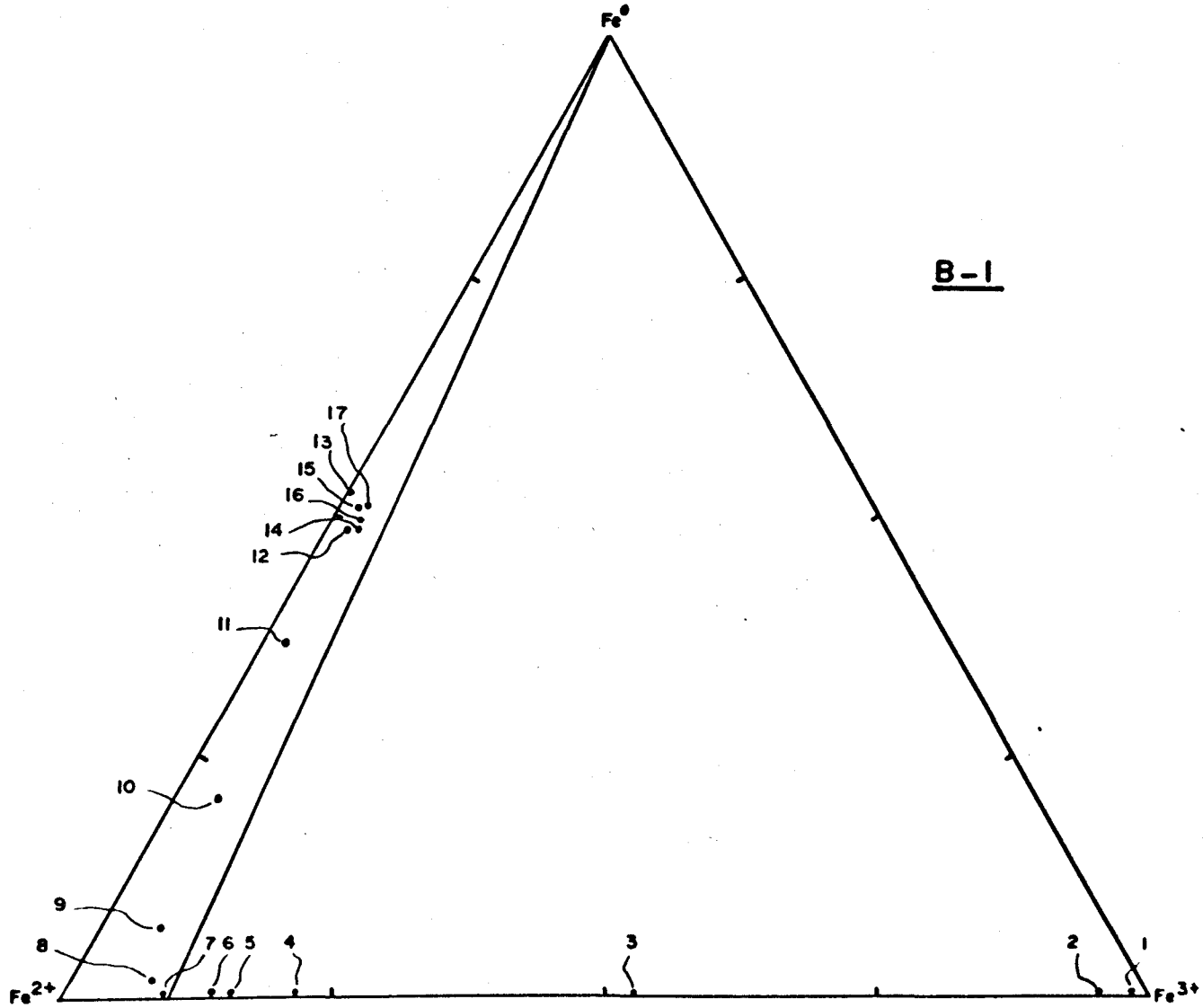
B-1
Fe°
Fe2+
Fe3+
17
13
15
16
14
12
11
10
9
8
7
6
5
4
3
2
1

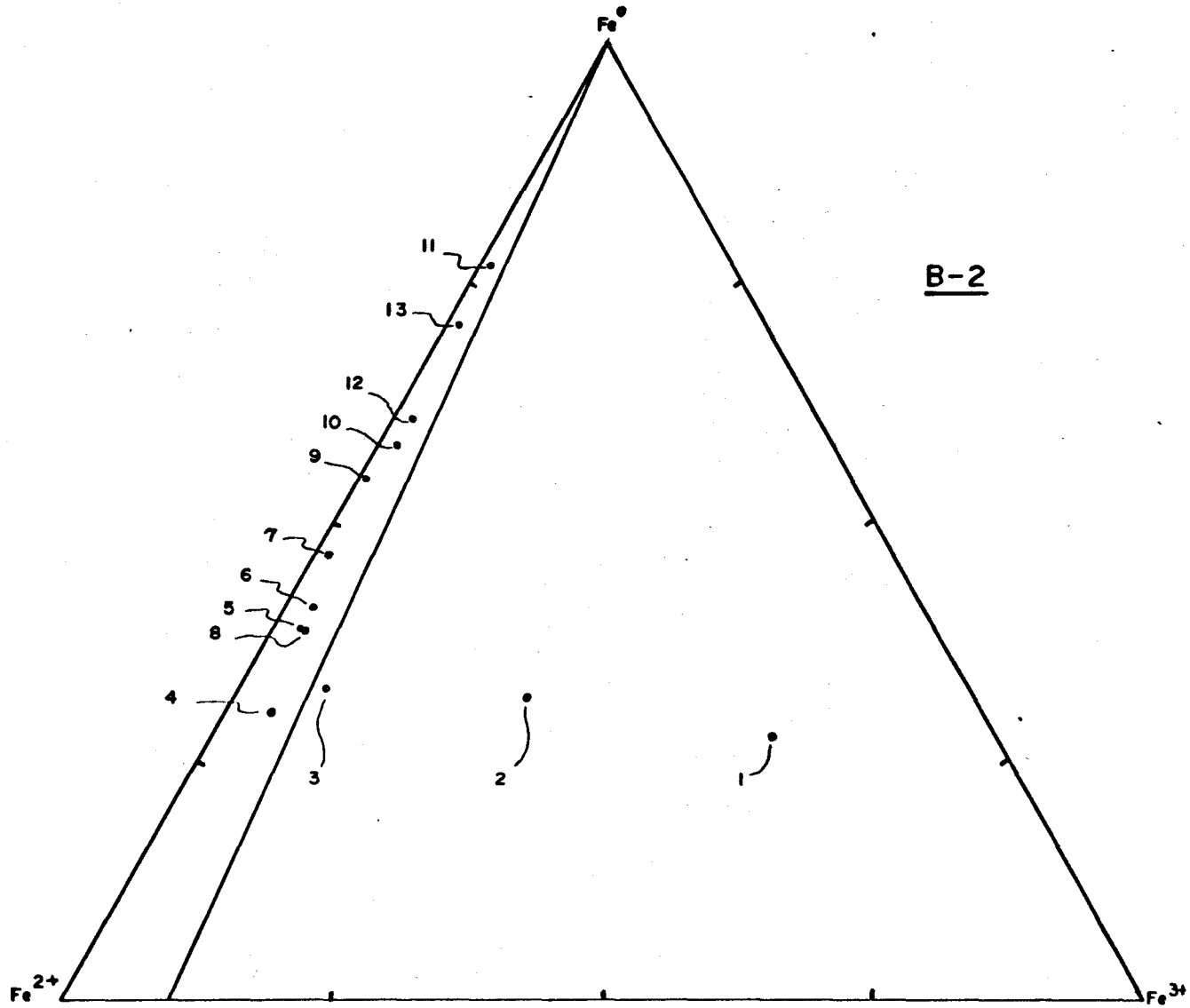

B-2

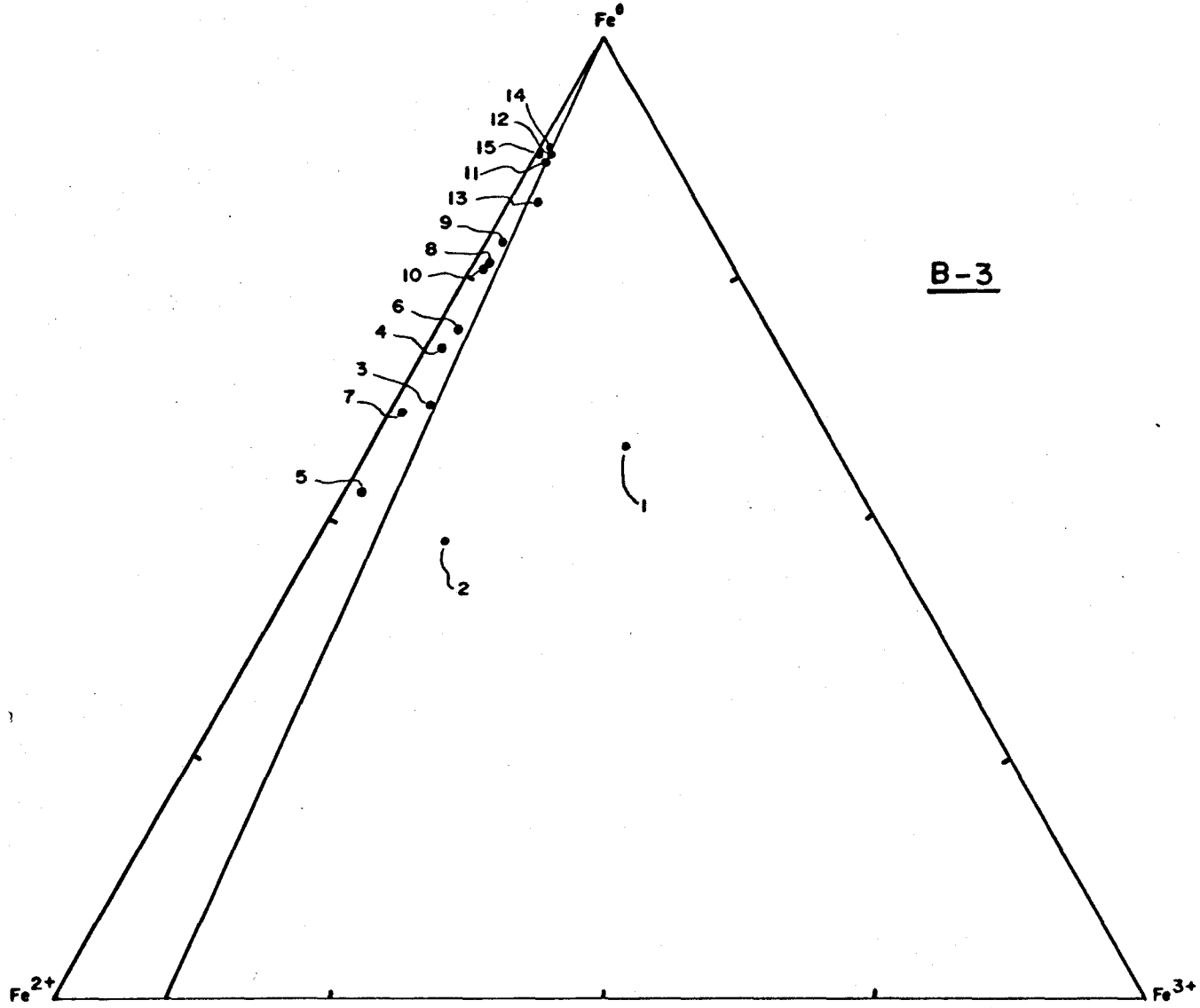

B-3

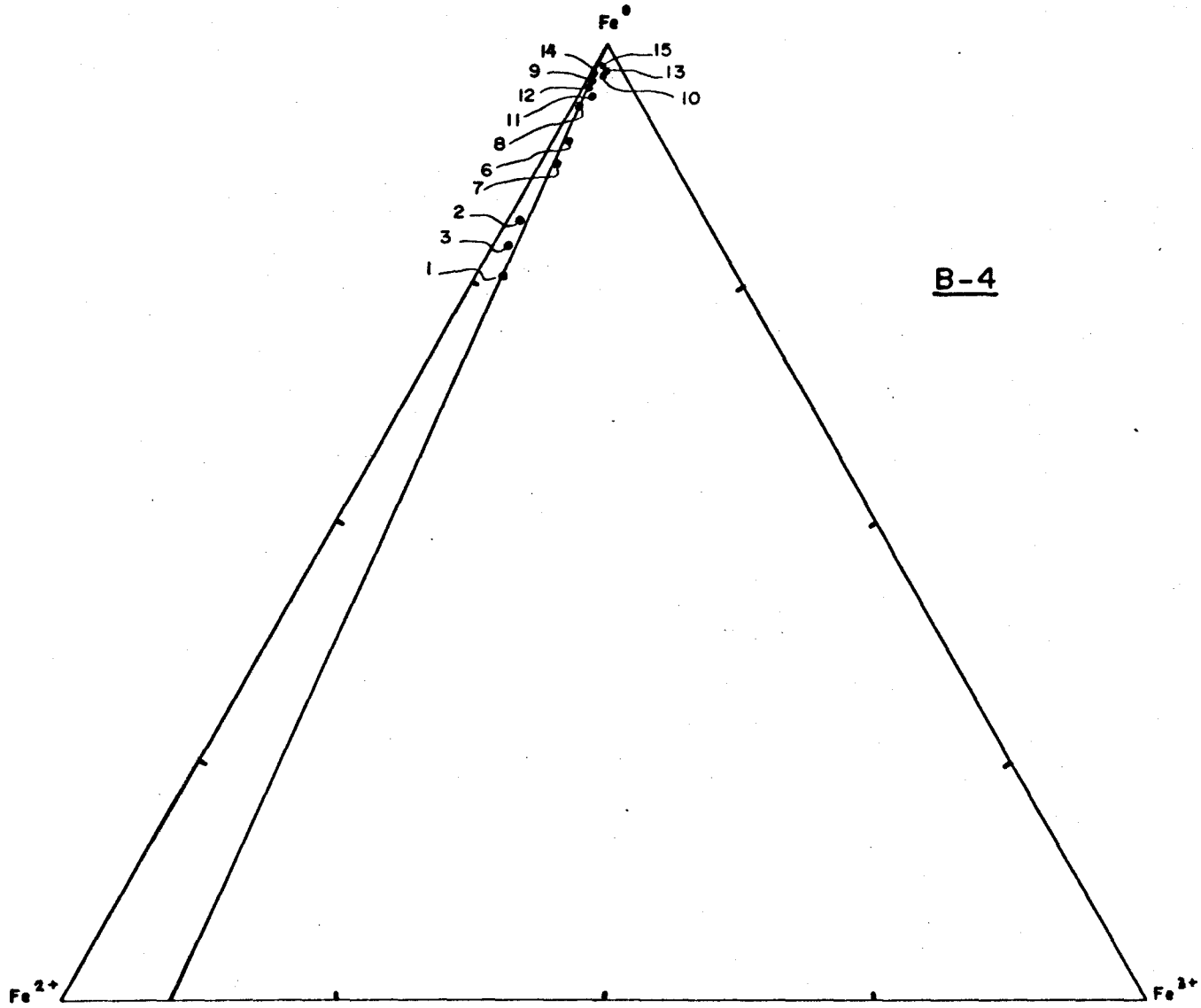

B-4

Figure 20 Residence Time Diagrams for Reductions Tests A-1, A-2, B-1, B-2, B-3 and B-4

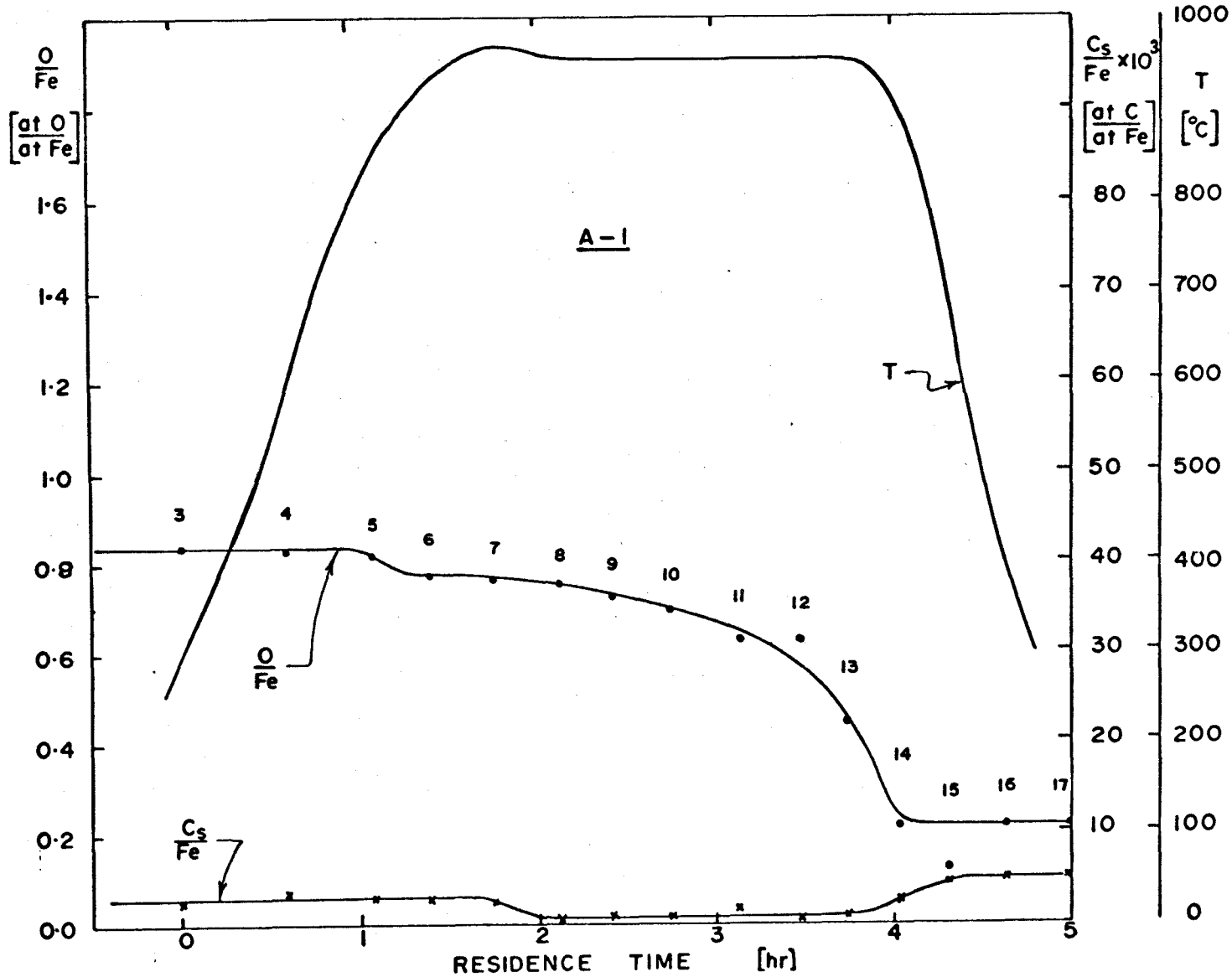

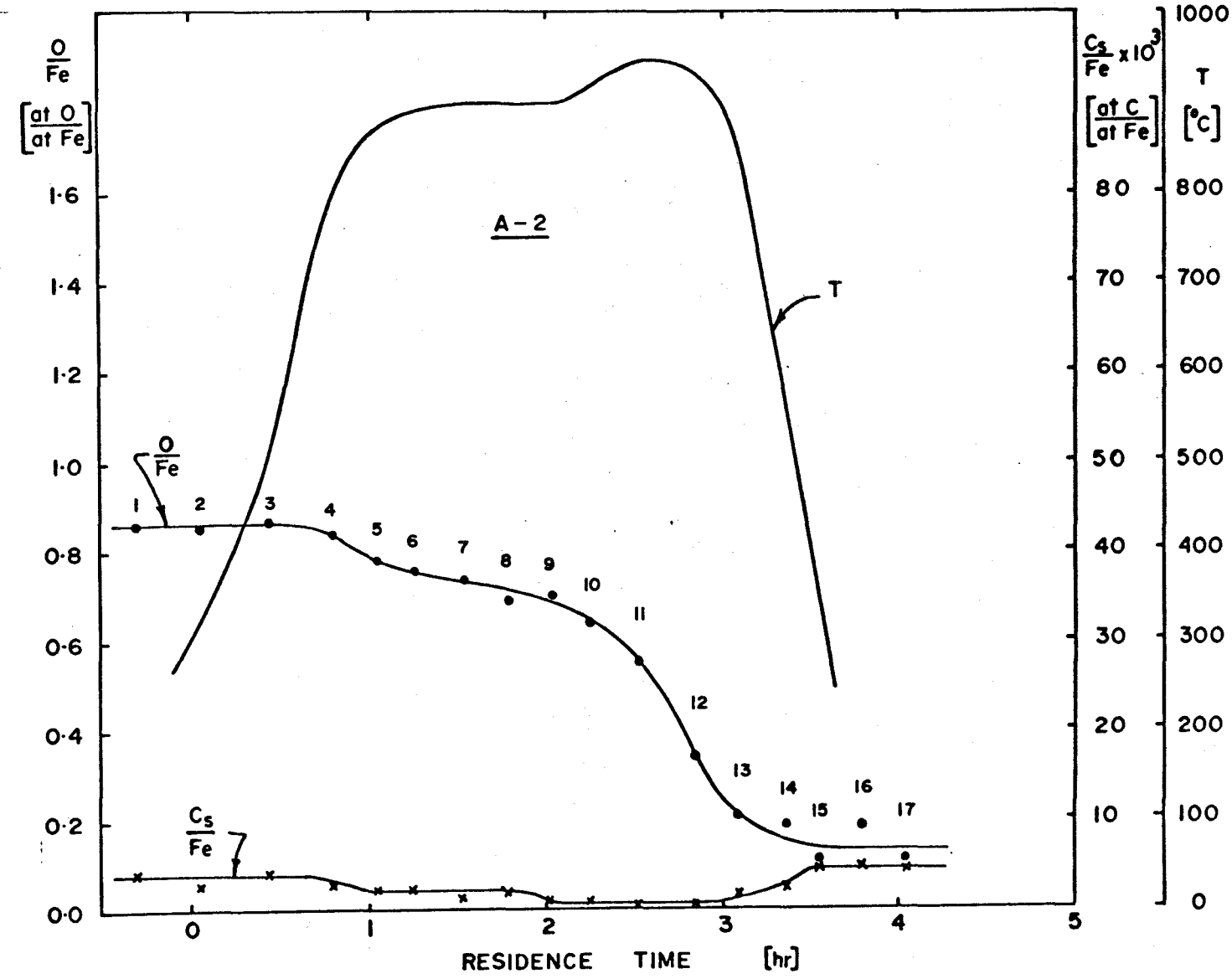
O/Fe [at O/at Fe]
Cs/Fe x10³ [at C/at Fe]
T [°C]
A-2
T
O/Fe
Cs/Fe
1·6
1·4
1·2
1·0
0·8
0·6
0·4
0·2
0·0
80
70
60
50
40
30
20
10
1000
800
700
600
500
400
300
200
100
0
1
2
3
4
5
6
7
8
9
10
11
12
13
14
15
16
17
0
1
2
3
4
5
RESIDENCE TIME [hr]

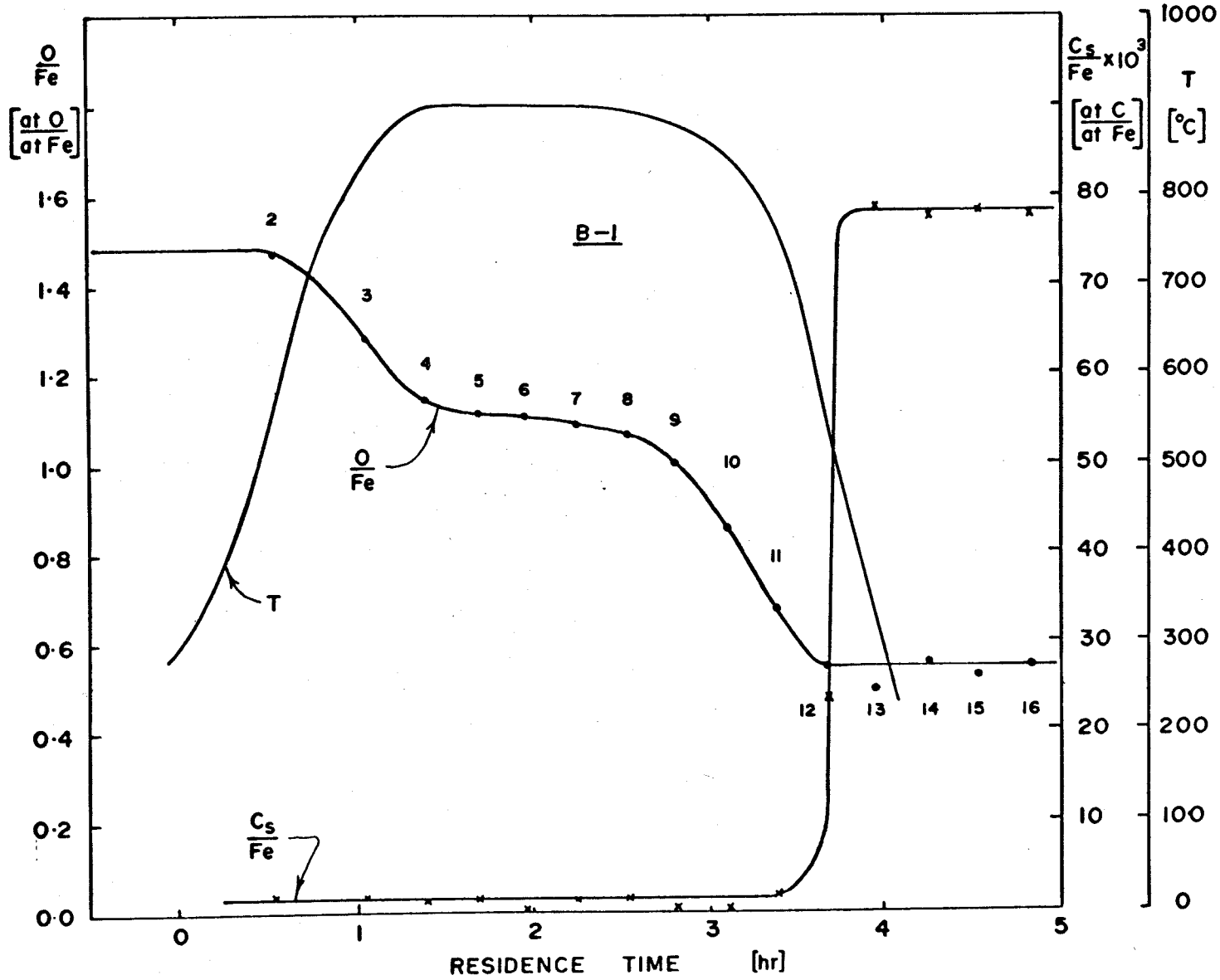
O/Fe
[at O / at Fe]
1·6
1·4
1·2
1·0
0·8
0·6
0·4
0·2
0·0
Cs/Fe x10³
[at C / at Fe]
80
70
60
50
40
30
20
10
T
[°C]
1000
800
700
600
500
400
300
200
100
0
B-I
2
3
4
5
6
7
8
9
10
11
12
13
14
15
16
O/Fe
T
Cs/Fe
0
1
2
3
4
5
RESIDENCE TIME [hr]

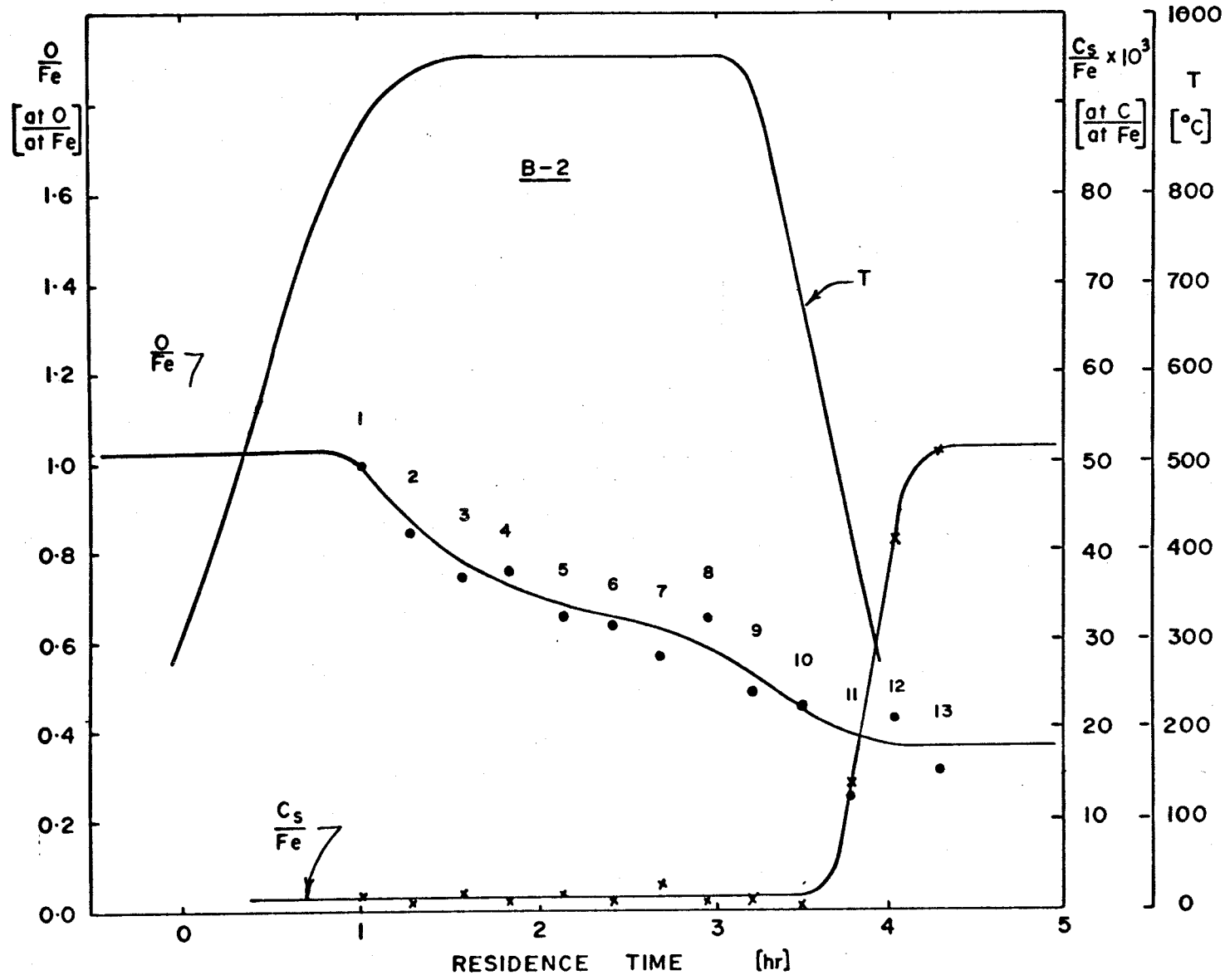
O/Fe
[at O / at Fe]
1·6
1·4
1·2
1·0
0·8
0·6
0·4
0·2
0·0
B-2
O/Fe
T
1
2
3
4
5
6
7
8
9
10
11
12
13
Cs/Fe
0
1
2
3
4
5
RESIDENCE TIME [hr]
Cs/Fe x 10³
[at C / at Fe]
80
70
60
50
40
30
20
10
T
[°C]
1600
800
700
600
500
400
300
200
100
0

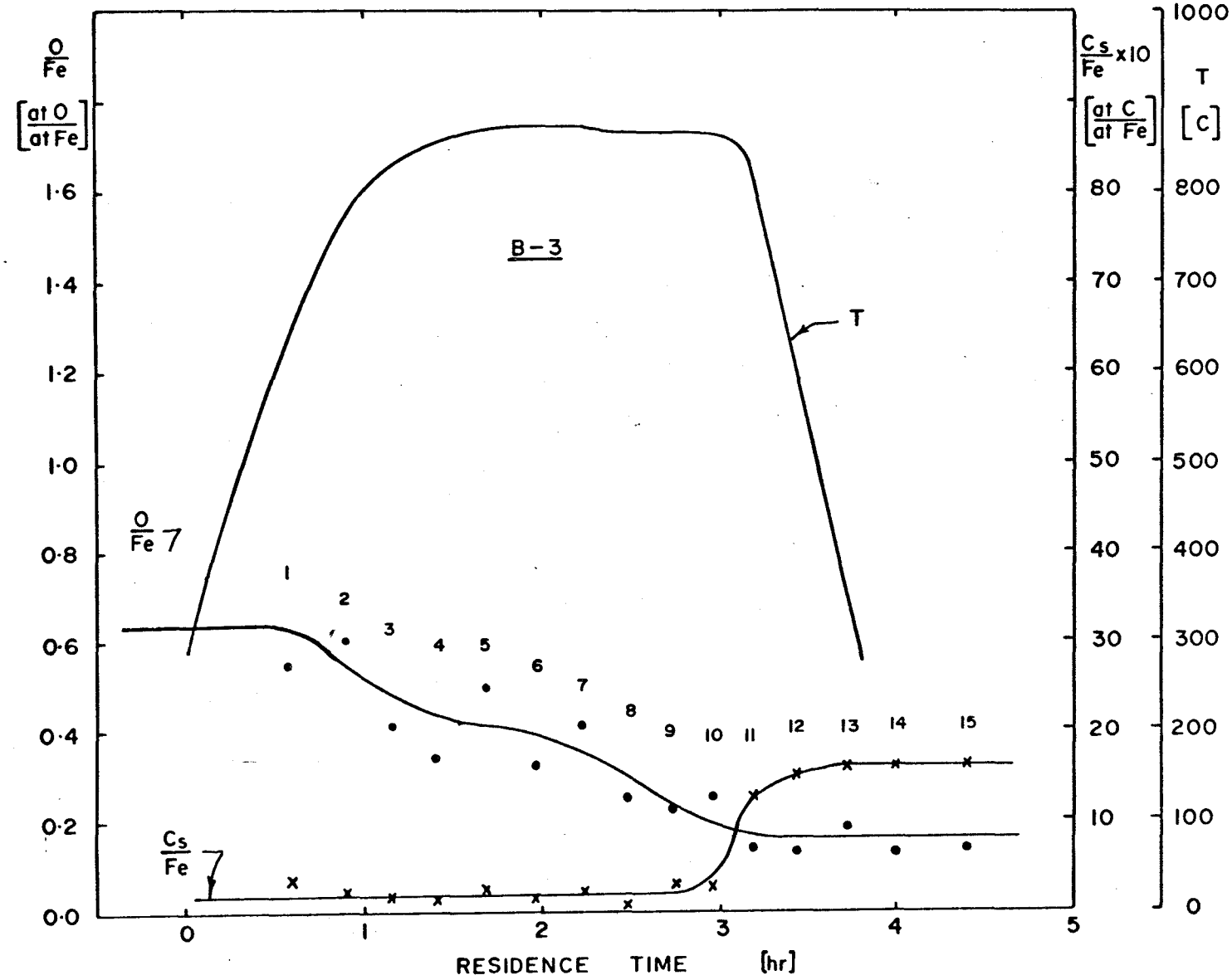
O/Fe [at O/at Fe]
Cs/Fe x10 [at C/at Fe]
T [C]
B-3
T
O/Fe 7
Cs/Fe
1
2
3
4
5
6
7
8
9
10
11
12
13
14
15
1·6
1·4
1·2
1·0
0·8
0·6
0·4
0·2
0·0
80
70
60
50
40
30
20
10
800
700
600
500
400
300
200
100
0
1000
0
1
2
3
4
5
RESIDENCE TIME [hr]

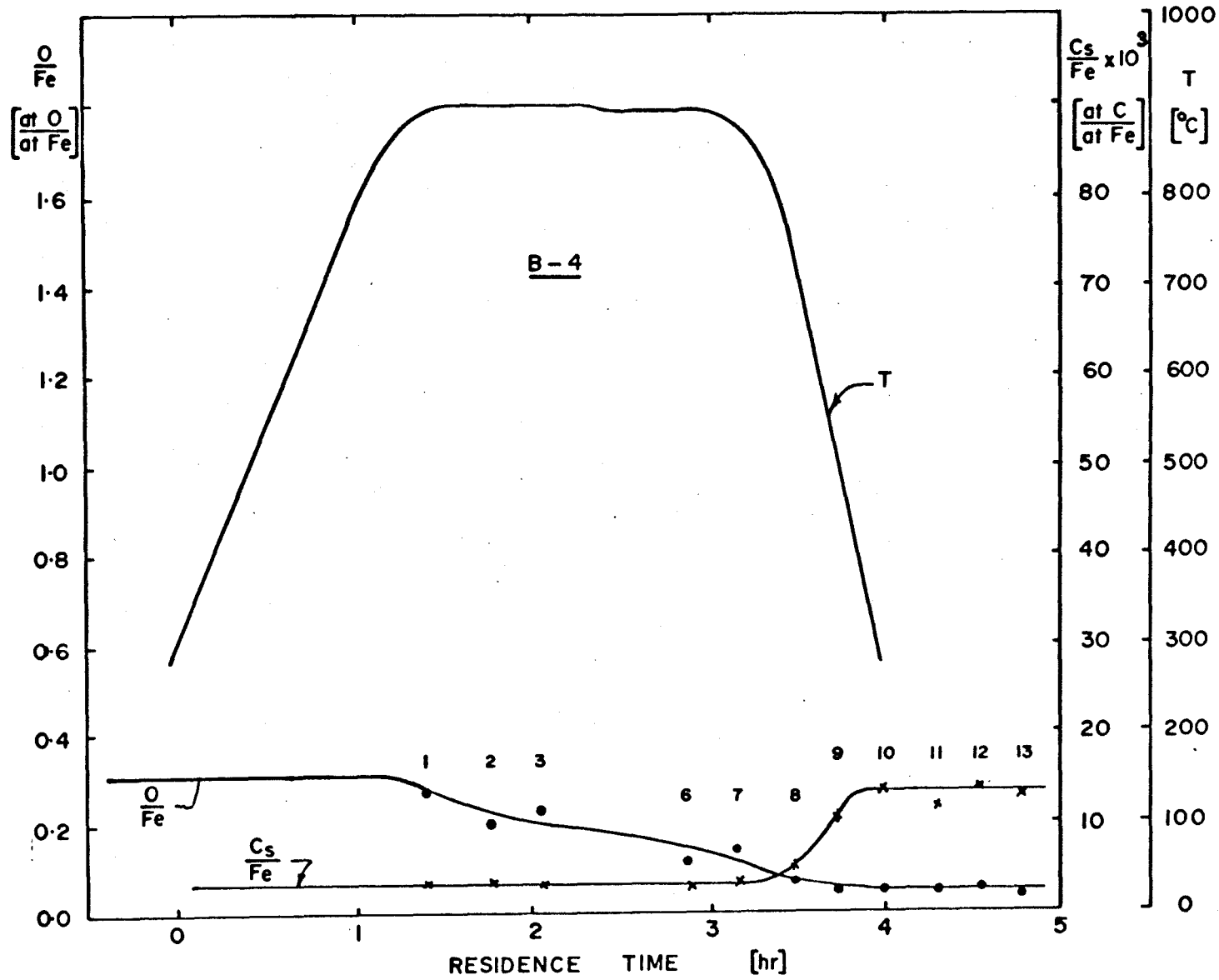
O/Fe
[at O/at Fe]
Cs/Fe x10^3
[at C/at Fe]
T
[°C]
B-4
T
O/Fe
Cs/Fe
1 2 3 6 7 8 9 10 11 12 13
0.0 0.2 0.4 0.6 0.8 1.0 1.2 1.4 1.6
10 20 30 40 50 60 70 80
100 200 300 400 500 600 700 800 1000
0 1 2 3 4 5
RESIDENCE TIME [hr]